REPORT DOCUMENTATION PAGE

Form Approved
OMB No. 0704-0188

1a. REPORT SECURITY CLASSIFICATION UNCLASSIFIED	1b. RESTRICTIVE MARKINGS

AD-A221 671

2a. SECURITY CLASSIFICATION AUTHORITY	3. DISTRIBUTION / AVAILABILITY OF REPORT
2b. DECLASSIFICATION / DOWNGRADING SCHEDULE	APPROVED FOR PUBLIC RELEASE DISTRIBUTION IS UNLIMITED

4. PERFORMING ORGANIZATION REPORT NUMBER(S)	5. MONITORING ORGANIZATION REPORT NUMBER(S) AFOSR·TR· 90-0455

6a. NAME OF PERFORMING ORGANIZATION Univ of California at Los Angeles	6b. OFFICE SYMBOL (If applicable)	7a. NAME OF MONITORING ORGANIZATION AFOSR/NA

6c. ADDRESS (City, State, and ZIP Code) Mechanical, Aerospace and Nuclear Engineering Dept Los Angeles, CA 90024-1597	7b. ADDRESS (City, State, and ZIP Code) BUILDING 410 BOLLING AFB, DC 20332-6448

8a. NAME OF FUNDING / SPONSORING ORGANIZATION AFOSR/NA	8b. OFFICE SYMBOL (If applicable) NA	9. PROCUREMENT INSTRUMENT IDENTIFICATION NUMBER AFOSR 87-0329

8c. ADDRESS (City, State, and ZIP Code) BUILDING 410 BOLLING AFB, DC 20332-6448	10. SOURCE OF FUNDING NUMBERS			
	PROGRAM ELEMENT NO. 61102F	PROJECT NO. 2307	TASK NO A2	WORK UNIT ACCESSION NO.

11. TITLE (Include Security Classification)

(U) Local and Global Resonances in Heated 2-D Jets

12. PERSONAL AUTHOR(S)
Ming Huei Yu and Peter A. Monkewitz

13a. TYPE OF REPORT Final	13b. TIME COVERED FROM 9/1/87 TO 7/31/89	14. DATE OF REPORT (Year, Month, Day) Nov 1989	15. PAGE COUNT 77

16. SUPPLEMENTARY NOTATION

17.	COSATI CODES		18. SUBJECT TERMS (Continue on reverse if necessary and identify by block number)
FIELD	GROUP	SUB-GROUP	Turbulence, Jets, Heated Jets, Global Instabilities

19. ABSTRACT (Continue on reverse if necessary and identify by block number)

The connection between local and global stability properties of free shear flows has been investigated. For 2-D inviscid jets, absolute instability was found for ratios of jet to ambient density below 0.9. Low wake heating (density) eliminates all local absolute instability. In 2-D heated jets, experiments showed that local absolute instability does lead to global instability and self-excitation at a density ratio of 0.9. The flow has been documented with Schlieren and mean velocity and temperature measurements. Theoretically, the global linear stability of a slowly diverging inviscid shear flow has been analyzed by WKB methods. Global characteristics are found, under certain assumptions, to be determined by a region where the absolute frequency of the mode with zero group velocity has a saddle.

20. DISTRIBUTION / AVAILABILITY OF ABSTRACT ☐ UNCLASSIFIED/UNLIMITED ☒ SAME AS RPT ☐ DTIC USERS	21. ABSTRACT SECURITY CLASSIFICATION UNCLASSIFIED
22a. NAME OF RESPONSIBLE INDIVIDUAL JAMES M MCMICHAEL	22b. TELEPHONE (Include Area Code) 202-767-4936 22c. OFFICE SYMBOL AFOSR/NA

DD Form 1473, JUN 86   Previous editions are obsolete.   SECURITY CLASSIFICATION OF THIS PAGE

UNIVERSITY OF CALIFORNIA, LOS ANGELES
SCHOOL OF ENGINEERING AND APPLIED SCIENCE

Final Technical Report for AFOSR Grant No. 87-0329

LOCAL AND GLOBAL RESONANCES
IN HEATED 2-D JETS

by

Ming-Huei Yu and
Peter A. Monkewitz, P.I.
Department of Mechanical, Aerospace & Nuclear
Engineering

Program Monitor: Dr. James M. McMichael

Accession For	
NTIS GRA&I	☒
DTIC TAB	☐
Un d	☐
Ju.. .	
Pr	
I	
	3
Dist	

A-1

CONTENTS

0. OVERVIEW

0.1 SUMMARY

The general theme of the research carried out under this Grant is the investigation of the connection between local and global stability properties of free shear flows. In particular, the connection between absolute instability of locally parallel mean profiles and global self-excitation has been illuminated.

On the local level, the knowledge of the stability properties of two-dimensional homogeneous and inhomogeneous (heated) jets and wakes has been expanded. For the inviscid 2-D jet absolute instability was found for ratios $S=\rho_j/\rho_\infty$ of jet ρ_j and ambient density ρ_∞ below 0.9 . For the wake the absolute instability boundary was mapped in the Reynolds number - density ratio plane. Thereby it was found that low wake density, i.e. heating, eventually eliminates all local absolute instability. These calculations were found to be entirely consistent with experiments in which the Kármán vortex street is suppressed by wake heating.

On a global level, a series of experiments with a 2-D heated jet at Reynolds numbers of 3,000-7,000 showed that the local absolute instability does lead to global instability, i.e. self-excitation at a density ratio of $S\approx0.9$. The bifurcation to global instability has been identified as a supercritical Hopf bifurcation by spectral measurements. In addition, a novel and effective way of locating the critical bifurcation parameter by auto-bicoherence measurements has been explored. In addition, the flow field has been documented by Schlieren flow visualization and mean velocity and temperature measurements.

Theoretically, the global linear stability of a slowly diverging inviscid shear flow has been analyzed by WKB methods. The analysis reveals that the global characteristics are, under certain assumptions, determined by a region in the complex x-plane (x being the streamwise direction) where the absolute frequency (the frequency of the mode with zero group velocity) has a saddle, i.e. a zero x-derivative. For this region the linearized Ginzburg-Landau equation was derived from first principles. In further work it has been used to investigate the effect of single-sensor single-actuator feedback control on the global behavior of jets and wakes.

1

0.2 PUBLICATIONS AND PRESENTATIONS FULLY OR PARTLY RELATED TO GRANT AFOSR 87-0329

Papers

Monkewitz, P.A. "The absolute and convective nature of instability in two-dimensional wakes at low Reynolds numbers". Physics of Fluids 31, 999-1006, 1988 (primary support from previous subcontract under AFOSR Grant F49620-85-C-0080).

Monkewitz, P.A. and Bechert, D.W. "Self-excited oscillations and mixing in a hot jet". Phys. Fluids 31, 2386 (Gallery of Fluid Motion), 1988 (partial support).

Monkewitz, P.A. "Self-excited oscillations in fluid systems". Part of "Physics News in 1988", Physics Today, January 1989.

Huerre, P. and Monkewitz, P.A. "Local and global instabilities in spatially-developing flows". To appear in Ann. Rev. Fluid Mech. 22, 473, 1990.

Monkewitz, P.A., Bechert, D.W., Barsikow, B. and Lehmann, B. "Self-excited oscillations and mixing in a heated round jet". To appear in J. Fluid Mech (partial support).

Yu, M.-H. Ph.D. Thesis and paper on the experimental results obtained with the 2-D hot jet. In preparation, 1989.

Yu, M.-H. and Monkewitz, P.A. "The effect of density variations on the stability of 2-dimensional jets and wakes. In preparation, 1989.

Monkewitz, P.A., Huerre, P. and Chomaz, J.M. " Global stability analysis of spatially-developing flows with application to the jet-column mode". In preparation, 1989.

Conference Proceedings

Monkewitz, P.A. "Local and global resonances in heated jets". Proc. of the AFOSR Contractors Meeting on Turbulence, June 28-30, 1988, Univ. of Southern Calif., Publ. by AFOSR.

Monkewitz, P.A. "Feedback control of global oscillations in fluid systems". AIAA paper # 89-0991, 1989.

Monkewitz, P.A. "The role of absolute and convective instability in predicting the behavior of fluid systems". Proc. of the "Forum on Chaotic Dynamics in Fluid Mechanics", ASME Fluids Engineering Spring Conf., La Jolla, Calif., July 1989. Submitted to the European J. of Mechanics B.

Conference Presentations

Monkewitz, P.A., Huerre, P. and Chomaz, J.M. "Preferred modes in jets and global instabilities". Bull. Am. Phys. Soc. 32, 2051, 1987.

Yu, M.H. and Monkewitz, P.A. "Self-excited oscillations in a low-density two-dimensional jet". Bull. Am. Phys. Soc. 33, 2246, 1988.

Yu, M.H. and Monkewitz, P.A. "Self-excited oscillations and mixing in a heated two-dimensional jet". APS/DFD Ann. Meeting 1989.

Monkewitz, P.A., Huerre, P. and Chomaz, J.M. " Global stability analysis of spatially-developing flows with application to the jet-column mode". APS/DFD Ann. Meeting 1989.

1. INTRODUCTION

1.1 PREVIOUS WORK ON VARIABLE DENSITY JETS

Jet stability problems have been investigated extensively because of its importance, e.g. its role in laminar-turbulent transition and its relation with the coherent structures in turbulent jets found by Crow and Champagne (1971). Theoretical studies, involving the effect of Mach number, Reynolds number, temperature (density) etc. on jet stability have been surveyed by Michalke (1984). However, experimental data for inhomogeneous jets have not been fully obtained to verify theoretical predictions. Recently, problems related to jet engine exhausts and to combustion have led to a renewed interest in the behavior of inhomogeneous (hot) jets which are inertia dominated, i.e. where buoyancy effects are minimal near the nozzle. The density effects on 2-D jet stability are reconsidered in this investigation, both theoretically and experimentally.

Among the studies of density effects on flow stability, Maslowe & Kelly (1971) studied stratified shear layers under the influence of gravity and illustrated that density variations can be destabilizing. Koochesfahani & Frieler (1987) studied shear layers with a wake component and found that the wake mode can become comparable or even stronger than the shear layer mode if the density of the low-speed stream is larger than that of the high-speed stream. Michalke (1970) studied spatial instability of the axisymmetric jet for various temperature ratios and Mach numbers and discovered additional instability modes later related to absolute instability by Monkewitz and Sohn (1988) who showed that a hot axisymmetric gas jet can develop a region of local absolute instability in the potential core region if the jet density is less than 0.72 times the ambient density.

The above stability analyses are based on the assumption of parallel flow where stability characteristics are independent of the streamwise coordinate. In real jets, mean flow profiles diverge with increasing streamwise coordinate. However, the parallel results can be viewed as local properties relevent to each streamwise station in the case where the mean flow variation in the streamwise direction is slow on the scale of the instability wavelength. In such cases, the effects of the small variation in streamwise direction can be included by considering higher order approximations. Crighton & Gaster (1976) used the multiple-scales method to study the stability of slowly diverging axisymmetric jet flow and obtained the streamwise development of the spatial instability amplitude. In other cases the global stability characteristics of the entire nonparallel flow field have to

be investigated. In this context the term global (linear) mode is understood to be a solution of the form $f(x, y, z) \exp(-i\omega t)$ where the vector f contains all dependent variables of the disturbance equation, linearized around a nonparallel base flow, and subject to suitable homogeneous boundary conditions.

It has been known that the behavior of homogeneous jets is sensitive to external sound, and is not only determined by the given flow parameters. However, if a flow develops self-excited (global) oscillations, forcing can become ineffective. Therefore, knowledge of the global stability characteristics of flow systems is important for a successful controller design, for instance. Monkewitz, Huerre and Chomaz (1987) considered a model problem to study the global instabilities in jet and the flow response to external forcing. Corke (1987) showed that the resonance process in jets can be suppressed or enhanced by low amplitude external forcing at the natural preferred frequency. The sensitivity of the jet to external forcing has encouraged the application of jet control by acoustic methods, see e.g. Lepicovski et al. (1988) and Ahuja (1988). Monkewitz (1989a) studied a linear nonparallel model to predict the effect of (one sensor-one actuator) feedback control with variable feedback gain and phase shift.

In addition to theoretical analyses, some experiments on the stability of variable density jet have been conducted. Sreenivasan et al. (1989) showed the absolute instability in a round Helium jet. Monkewitz et al. (1989. ref 27 and ref 28) illustrated the self-excited oscillation in a axisymmetric hot jet and the dramatic spreading of self-excited hot jet by side jets. Motivated by these studies, the purpose of this investigation is to understand the density effect on jet stability and the resonance phenomena in a 2-D hot jet.

1.2 LOCAL LINEAR STABILITY CONCEPTS

For a nonparallel flow system where mean flow profiles evolve slowly in the streamwise direction, e.g. 2-D jet/wake flow, the simplest approach for a stability analysis is to apply linear theory at a certain streamwise station, x, where the mean flow variation in the streamwise direction can be neglected, i.e. where the parallel flow assumption is made (Drazin & Reid 1981). Any disturbance quantity is expressed in normal mode form, for which the dependence on time and downstream distance x is separated out in a factor $\exp$ with x and ω the wavenumber and frequency, respectively. The distribution of any linear disturbance quantity in the transverse y-direction is then described by a system of ordinary differential equations derived from the conservation equations, with suitable boundary conditions at, say, y=0 and ∞.

The solution of this two-point boundary-value problem is only possible for certain values x and ω, the eigenvalues. The admissible values are defined by the dispersion relation $\omega = \omega(x)$, which depends on the mean flow velocity profiles $\bar{u}(y)$, density profiles $\bar{\rho}(y)$, and any other relevant flow and fluid properties at the station x. If a real wave number x is prescribed, ω assumes the role of eigenvalue and the temporal stability problem is considered. If a real frequency ω is imposed on the system, one speaks of spatial stability. The temporal case therefore describes the evolution of a spatially periodic pattern in time, while the spatial theory describes the downstream evolution of a constant-amplitude harmonic input at some x-station. In addition to the spatial and temporal cases, x and ω can be both complex, and describe the spatio-temporal behavior. Which of the theories are to be used must be decided by considering the start-up process, or more precisely the evolution of the start-up transient. For this purpose it is in fact sufficient to consider the asymptotic impulse response in the limit of large times, as discussed for instance by Huerre and Monkewitz (1985).

The asymptotic response or Green's function is conviently obtained in Fourier space, i.e. in terms of x and ω. To obtain the evolution in time and space of an impulse at say x=0 and t=0, the inverse Fourier transform must be evaluated. By applying the method of steepest descent, one finds that along each ray x/t=constant, the response is eventually dominated by the least stable mode with a wave number $x^{\times}$ and frequency $\omega^{\times} = \omega(x^{\times})$ satisfying

$$\frac{d\omega}{dx}(x^{\times}) = x/t \; ; \quad \omega^{\times} = \omega(x^{\times}). \tag{1.1}$$

Along each ray x/t=constant, the dominant mode with wave number $x^{\times}$ travels at group velocity equal to x/t and is amplified temporally at the rate of

$$\sigma_i = \omega_i^{\times} - x_i^{\times} \frac{d\omega}{dx}(x^{\times}). \tag{1.2}$$

If $\sigma_i < 0$ for all modes, the flow system is stable. Any small perturbation is suppressed as $t \to \infty$ and disappears at every x-station. If $\sigma_i > 0$ on some rays, the flow system is unstable. The evolution of an impulsive pertubation and the nature of stability can be best understood with the x-t diagram in Figure 1. The introduced disturbance is asymptotically confined between two rays on which $\sigma_i = 0$. Within the wedge-shaped region, the amplitude of the dominant mode along each ray, is amplified at the growth rate $\sigma(x^{\times}) > 0$. The largest amplification occurs on the ray associated with the mode $\omega_{i,max}^{\times}$, the most amplified temporal mode for which the growth rate σ_i is maximum. Two cases are now distinguished according to the behavior of the mode on the ray x/t=0, i.e. the mode with zero group velocity. In the case that this mode has positive growth rate as shown on Figure 1a, the wave packet travels both upstream and downstream and eventually contaminates the

whole flow region. In the other case, the growth rate of the mode with zero group velocity is less than zero, and the wave packet, although it may be amplified during traveling, is convected downstream. The flow system at any fixed space location becomes quiet eventually when t is sufficient large. This means that the response of the flow at fixed x to the impulsive perturbation is determined by the mode with zero group velocity

$$\frac{d\omega}{dx}(x^o) = 0 \; ; \; \omega^o = \omega(x^o) \tag{1.3}$$

Depending on the absolute growth rate ω_i^o, a flow system is identified as absolutely unstable if $\omega_i^o > 0$, and convectively unstable if $\omega_i^o < 0$. It is noted that this criterion is not complete and has to be supplemented by the "pinching requirement" (see Huerre & Monkewitz 1985, for instance) which mandates that the branchpoint ω^o must arise from the coalescence of a downstream and an upstream mode.

1.3 GLOBAL STABILITY CONCEPTS

In a nonparallel flow it is the global rather than the locally parallel behavior that is of practical interest. The stability analysis discussed in section 1.2 is based on the mean flow data at each x-station, viewing the flow as a parallel one. The resulting stability properties depend only parametrically on x and fail to yield a global frequency selection criterion, for instance. If, however, the computed local flow properties can be related to the observed global behavior of the actual nonparallel system, the local stability computation would provide a relatively simple guide to global behavior.

This connection between the global and local stability behavior has been investigated by Chomaz, Huerre & Redekopp (1988). From the analysis of a one-dimensional model problem, considering the streamwise development of the basic flow and neglecting its cross-stream variation, they conclude that local absolute instability is necessary but not sufficient for a global mode to become self-excited, i.e. to grow in time. They show that a system develops a self-excited response if a sufficient portion of the flow-field is absolutely unstable on a locally parallel basis, provided the nonparallelism of the base flow is not too severe. In this case the growth of a global mode is due to (local) upstream feedback by instability waves.

The relation between local and global stability calculations is also illustrated by Hannemann's numerical simulation of global behavior in a wake flow, shown in Figure 2. As shown in Figure 2b, the growth rate in the linear region and the preferred frequency of the global mode fall into the range predicted by local linear theory.

Analogous to convective and absolute instability in parallel flows, the instability characteristics of nonparallel flow systems, can be characterized as "amplifier" and "oscillator" behavior

(Monkewitz 1989).   If the flow is stable as on Figure 3a, or convectively unstable in some region as on Figure 3b, all local modes with frequency $\omega^r(x)$ defined at each x by equation (1.3) and consequently all global modes are time-damped, provided the system contains no additional global pressure feedback or active control loop.   In other words, a flow system corresponding to Figure 3b behaves as an "amplifier" that spatially amplifies selected external disturbances with a nonzero signal to noise ratio, but reverts to an undisturbed state if the excitation is turned off.   On the other hand, if a system, starting from the undisturbed state, only needs an initial impulse to develop time-growing oscillations at any fixed location, it is self-excited and termed an "oscillator".   Following the initial exponential growth of the disturbance, the system in many cases settles into a limit cycle behavior, e.g. the Kármán vortex street in the case of a wake base-flow. This final nonlinear state generally represents a global response which is intrinsic to the system and frequently independent of the nature of the initial impulse.

2. THE LOCAL LINEAR STABILITY OF VARIABLE DENSITY 2-D JETS AND WAKES

2.1 MEAN FLOW

For the present investigation, local stability calculations have been carried out for a two-parameter family of velocity profiles already used by Monkewitz & Nguyen (1987). It is defined by equation (2.1) in nondimensional form, using the jet half-width $y_{1/2}^{*}$ and the average velocity $\bar{u}_{ave}^{*}$ as characteristic length and velocity.

$$\bar{u}(y) = 1 - \Lambda + 2\Lambda F(y), \tag{2.1}$$

$$\Lambda \equiv \frac{\bar{u}^{*}(y=0) - \bar{u}^{*}(y=\infty)}{\bar{u}^{*}(y=0) + \bar{u}^{*}(y=\infty)}$$

$$F(y) = [1 + \sinh^{2N}(y \sinh^{-1}1)]^{-1}$$

where Λ is the velocity ratio. $\Lambda = +1$ corresponds to a jet with zero ambient velocity. N is the shape parameter which controls the ratio of mixing layer thickness to jet half-width. For large N, i.e. thin shear layers, the nondimensional maximum-slope thickness is well approximate by the relation $\delta_{\omega} \sim \sqrt{2} [N \sinh^{-1}1]^{-1}$. The temperature profile is assumed to have the same shape as the velocity profile by the Busemann-Crocco relationship at zero Mach number. The normalized temperature profile is then given in terms of the normalized velocity profile $F(y)$ and the density ratio $S = \rho_c/\rho_\infty$.

$$\bar{T}(y) = 1 + (\frac{1}{S} - 1)F(y). \tag{2.2}$$

The viscosity is related to temperature by

$$\bar{\mu} = \bar{T}^{3/2} \frac{1 + C/\bar{T}_{\infty}^{*}}{\bar{T} + C/\bar{T}_{\infty}^{*}}$$

where $\bar{T}_{\infty}^{*}$ is ambient temperature and C is a constant. Between the jet exit and the asymptotic region, N is chosen such as to yield the 2-dimensional shear layer spreading rates measured by Brown & Roshko (1974) in the region where the jet shear layers are thin compared with the jet width.

9

2.2 DISTURBANCE EQUATIONS

Michalke (1970) and Monkewitz & Sohn (1988) carried out the linear stability analysis of the axisymmetric, inhomogeneous inviscid jet. The development of the stability analysis in this section is similar to theirs, except that 2-D viscous flow is being considered.

In addition to parallel flow, several simplifying assumptions are made. First, nonlinear terms are neglected which limits the analysis to the small amplitude regime. Second, the mean flow is considered to be "quasi-laminar". That is, the interaction of the large scale instability wave with small scale turbulence is neglected as discussed explicitly by Strange & Crighton (1983). Third, buoyancy is neglected in the near-field potential core region where inertial forces dominate. Fourth, the fluid is assumed to be a calorically perfect gas without heat sources.

Furthermore, only 2-D disturbances are considered in this section since they are more unstable at zero Mach number than 3-D disturbances by Squire's transformation (1933).

The equations of motion of a heat-conducting viscous fluid can be found in text books (e.g. Batchelor 1967). The equations for 2-D flow in Cartesian coordinates are as follows.

The equation of continuity is

$$\frac{\partial \rho^*}{\partial t^*} + \frac{\partial (\rho^* u^*)}{\partial x^*} + \frac{\partial (\rho^* v^*)}{\partial y^*} = 0 \tag{2.3}$$

The equations of motion are the Navier-Stokes equations. With the further assumptions of no body force and Stokes' relation $\lambda = -2/3\ \mu$, the momentum equations in x- and y-directions are

$$\rho^* \frac{\partial u^*}{\partial t^*} + \rho^* u^* \frac{\partial u^*}{\partial x^*} + \rho^* v^* \frac{\partial u^*}{\partial y^*} = -\frac{\partial p^*}{\partial x^*} + \frac{\partial}{\partial x^*}[2\mu \frac{\partial u^*}{\partial x^*}$$

$$-\frac{2}{3}\mu(\frac{\partial u^*}{\partial x^*} + \frac{\partial v^*}{\partial y^*})] + \frac{\partial}{\partial y^*}[\mu(\frac{\partial u^*}{\partial y^*} + \frac{\partial v^*}{\partial x^*})] \tag{2.4}$$

and

$$\rho^* \frac{\partial v^*}{\partial t^*} + \rho^* u^* \frac{\partial v^*}{\partial x^*} + \rho^* v^* \frac{\partial v^*}{\partial y^*} = -\frac{\partial p^*}{\partial y^*} + \frac{\partial}{\partial y^*}[2\mu \frac{\partial v^*}{\partial y^*}$$

$$-\frac{2}{3}\mu(\frac{\partial u^*}{\partial x^*} + \frac{\partial v^*}{\partial y^*})] + \frac{\partial}{\partial x^*}[\mu(\frac{\partial u^*}{\partial y^*} + \frac{\partial v^*}{\partial x^*})] \tag{2.5}$$

10

The energy equation for a calorically perfect gas is

$$\rho C_p \left(\frac{\partial T^*}{\partial t^*} + u^* \frac{\partial T^*}{\partial x^*} + v^* \frac{\partial T^*}{\partial y^*} \right) = \frac{\partial}{\partial x^*} \left(\kappa \frac{\partial T^*}{\partial x^*} \right) + \frac{\partial}{\partial y^*} \left(\kappa \frac{\partial T^*}{\partial y^*} \right) + \frac{Dp^*}{Dt^*}$$

$$+ 2\mu \left[\left(\frac{\partial u^*}{\partial x^*} \right)^2 + \left(\frac{\partial v^*}{\partial y^*} \right)^2 \right] - \frac{2}{3} \mu \left(\frac{\partial u^*}{\partial x^*} + \frac{\partial v^*}{\partial y^*} \right)^2 \tag{2.6}$$

The equation of state is

$$p^* = \rho^* R T^* \tag{2.7}$$

Here we denote a dimensional variable by an asterisk superscript.

The dependent variables are decomposed into mean values and small perturbations in the form,

$$q = \bar{q} + q',$$

and all equations are linearized around the mean values (basic state). Furthermore, assuming constant Prandtl number and introducing $\bar{\mu}_\infty^*$, $\bar{\kappa}_\infty^*$, $\bar{\rho}_\infty^*$, $\bar{u}_{ave}^*$, $\bar{\rho}_\infty^* \bar{u}_{ave}^{*2}$, $\bar{T}_\infty^*$ and $y_{1/2}^*$ as characteristic viscosity, conductivity, density, velocity, pressure, temperature and length respectively, the disturbance equations are obtained in dimensionless form as follows,

$$\frac{1}{\bar{\rho}} \frac{\partial \rho'}{\partial t} + \left(\frac{\partial u'}{\partial x} + \frac{\partial v'}{\partial y} \right) + \frac{1}{\bar{\rho}} \frac{d\bar{\rho}}{dy} v' + \frac{\bar{u}}{\bar{\rho}} \frac{\partial \rho'}{\partial x} = 0 \tag{2.8}$$

$$\bar{\rho} \frac{\partial u'}{\partial t} + \bar{\rho} \bar{u} \frac{\partial u'}{\partial x} + \bar{\rho} v' \frac{\partial \bar{u}}{\partial y} = - \frac{\partial p'}{\partial x} + \frac{1}{R_e} \left[2\bar{\mu} \frac{\partial^2 u'}{\partial x^2} - \frac{2\bar{\mu}}{3} \frac{\partial}{\partial x} \left(\frac{\partial u'}{\partial x} + \frac{\partial v'}{\partial y} \right) \right.$$

$$+ \bar{\mu} \frac{\partial}{\partial y} \left(\frac{\partial u'}{\partial y} + \frac{\partial v'}{\partial x} \right) + \frac{d\bar{u}}{dy} \left(\frac{d\bar{\mu}_T}{dy} T' + \bar{\mu}_T \frac{\partial T'}{\partial y} \right)$$

$$+ \frac{d\bar{\mu}}{dy} \left(\frac{\partial u'}{\partial y} + \frac{\partial v'}{\partial x} \right) + \bar{\mu}_T \frac{d^2 \bar{u}}{dy^2} T' \right] \tag{2.9}$$

$$\bar{\rho} \frac{\partial v'}{\partial t} + \bar{\rho} \bar{u} \frac{\partial v'}{\partial x} = - \frac{\partial p'}{\partial y} + \frac{1}{R_e} \left[\bar{\mu} \frac{\partial}{\partial x} \left(\frac{\partial u'}{\partial y} + \frac{\partial v'}{\partial x} \right) + 2\bar{\mu} \frac{\partial}{\partial y} \left(\frac{\partial v'}{\partial y} \right) - \frac{2\bar{\mu}}{3} \frac{\partial}{\partial y} \left(\frac{\partial u'}{\partial x} + \frac{\partial v'}{\partial y} \right) \right.$$

$$+ \bar{\mu}_T \frac{d\bar{u}}{dy} \frac{\partial T'}{\partial x} + 2 \frac{d\bar{\mu}}{dy} \frac{\partial v'}{\partial y} - \frac{2}{3} \frac{d\bar{\mu}}{dy} \left(\frac{\partial u'}{\partial x} + \frac{\partial v'}{\partial y} \right) \right] \tag{2.10}$$

11

$$\bar{\rho}\left(\frac{\partial T'}{\partial t} + \bar{u}\frac{\partial T'}{\partial x} + \frac{\partial \bar{T}}{\partial y}v'\right) = \frac{1}{R_e P_r}\left(\bar{\kappa}\frac{\partial^2 T'}{\partial x^2} + \bar{\kappa}\frac{\partial^2 T'}{\partial y^2} + \frac{d\bar{\kappa}}{dy}\frac{\partial T'}{dy} + \bar{\kappa}_T\frac{d^2\bar{T}}{dy^2}T'\right.$$

$$\left. + \bar{\kappa}_T\frac{d\bar{T}}{dy}\frac{\partial T'}{\partial y} + \frac{d\bar{\kappa}_T}{dy}\frac{d\bar{T}}{dy}T'\right) + (\gamma-1)M_\infty^2\left(\frac{\partial p'}{\partial t} + \bar{u}\frac{\partial p'}{\partial x}\right)$$

$$+ \frac{(\gamma-1)M_\infty^2}{R_e}\left[2\bar{u}\frac{\partial \bar{u}}{\partial y}\left(\frac{\partial u'}{\partial y} + \frac{\partial v'}{\partial x}\right) + \bar{\mu}_T\left(\frac{d\bar{u}}{dy}\right)^2\right] \qquad (2.11.a)$$

$$p'\gamma M_\infty^2 = \frac{\rho'}{\bar{\rho}} + \frac{T'}{\bar{T}} \qquad (2.12.b)$$

where $R_e = \dfrac{\bar{\rho}_\infty \bar{u}_{ave} y_{1/2}}{\mu_\infty}$, $P_r = \dfrac{C_p \mu_\infty}{\kappa_\infty}$, $M_\infty^2 = \dfrac{\bar{u}_{ave}^2}{\gamma R \bar{T}_\infty}$ and $(\ )_T = \dfrac{d(\ )}{dT}$.

In case of incompressible flow, M_∞ is zero. The equations (2.11.a) and (2.12.a) can be reduced to

$$\bar{\rho}\left(\frac{\partial T'}{\partial t} + \bar{u}\frac{\partial T'}{\partial x} + \frac{d\bar{T}}{dy}v'\right) = \frac{1}{R_e P_r}\left(\bar{\kappa}\frac{\partial^2 T'}{\partial x^2} + \bar{\kappa}\frac{\partial^2 T'}{\partial y^2} + \frac{d\bar{\kappa}}{dy}\frac{\partial T'}{dy} + \bar{\kappa}_T\frac{d^2\bar{T}}{dy^2}T'\right.$$

$$\left. + \bar{\kappa}_T\frac{d\bar{T}}{dy}\frac{\partial T'}{\partial y} + \frac{d\bar{\kappa}_T}{dy}\frac{d\bar{T}}{dy}T'\right) \qquad (2.11)$$

$$0 = \frac{\rho'}{\bar{\rho}} + \frac{T'}{\bar{T}} \qquad (2.12)$$

Now, we have five equations for five unknown disturbance quantities ρ', u', v', p' and T', with coefficients given by the basic flow. For uniform mean pressure and an ideal gas, we have $\bar{\rho} = 1/\bar{T}$. The solution of the system of equations is now sought in the form of normal modes, i.e. the disturbance quantities are expressed in the form

$$q'(x,y,t) = \tilde{q}(y)\, e^{i(\alpha x - \omega t)}.$$

With

$$\frac{\partial q'}{\partial t} = -i\omega \tilde{q}(y)\, e^{i(\alpha x - \omega t)}$$

and

$$\frac{\partial q'}{\partial x} = i\alpha \tilde{q}(y)\, e^{i(\alpha x - \omega t)},$$

12

equations (2.8)-(2.12) become a system of ordinary differential equations for the $\tilde{q}(y)$'s:

$$i\alpha\overline{T}(\overline{u} - \frac{\omega}{\alpha})\tilde{\rho} + i\alpha\tilde{u} + \tilde{v}_y - \frac{\overline{T}_y}{\overline{T}}\tilde{v} = 0 \qquad (2.13)$$

$$\frac{1}{\overline{T}}[i\alpha(\overline{u} - \frac{\omega}{\alpha})\tilde{u} + \overline{u}_y\tilde{v}] = -i\alpha\tilde{p} + \frac{1}{R_e}[\overline{\mu}(\tilde{u}_{yy} - \frac{4}{3}\alpha^2\tilde{u} + \frac{i\alpha}{3}\tilde{v}_y)$$

$$+ \overline{\mu}_T(\overline{u}_{yy}\tilde{T} + \overline{T}_y\tilde{u}_y + i\alpha\overline{T}_y\tilde{v} + \overline{u}_y\tilde{T}_y) + \overline{\mu}_{TT}\overline{T}_y\overline{u}_y] \qquad (2.14)$$

$$\frac{1}{\overline{T}}(\overline{u} - \frac{\omega}{\alpha})\tilde{v} = \frac{-1}{i\alpha}\tilde{p}_y + \frac{1}{i\alpha R_e}[\overline{\mu}(\frac{4}{3}\tilde{v}_{yy} - \alpha^2\tilde{v} + \frac{i\alpha}{3}\tilde{u}_y) + \overline{\mu}_y(i\alpha\overline{u}_y\tilde{T} + \frac{4}{3}\overline{T}_y\tilde{v}_y - \frac{2i\alpha}{3}\overline{T}_y\tilde{u})] \quad (2.15)$$

$$\frac{1}{\overline{T}}[i\alpha(\overline{u} - \frac{\omega}{\alpha})\tilde{T} + \overline{T}_y\tilde{v}] = \frac{1}{R_e P_r}[\overline{\mu}(\tilde{T}_{yy} - \alpha^2\tilde{T}) + \overline{\mu}_T(2\overline{T}_y\tilde{T}_y + \overline{T}_{yy}\tilde{T}) + \overline{\mu}_{yy}(\overline{T}_y)^2\tilde{T}] \qquad (2.16)$$

$$\frac{\tilde{\rho}}{\overline{\rho}} + \frac{\tilde{T}}{\overline{T}} = 0 \qquad (2.17)$$

where $(\ )_y = \dfrac{d(\ )}{dy}$

relating $\tilde{\rho}$ to $\tilde{T}$ by the state equation and rearranging equations such that the highest order differentiation term for each variable is moved to the left-hand side, we have the following equations.

$$\frac{d\tilde{v}}{dy} = -i\alpha\tilde{u} + \frac{1}{\overline{T}}[i\alpha(\overline{u} - \frac{\omega}{\alpha})\tilde{T} + \overline{T}_y\tilde{v}] \qquad (2.18)$$

$$\frac{d\tilde{u}_y}{dy} = \alpha^2\tilde{u} - \frac{i\alpha}{3\overline{T}}[i\alpha(\overline{u} - \frac{\omega}{\alpha})\tilde{T} + \overline{T}_y\tilde{v}] - \frac{\overline{\mu}_T}{\overline{\mu}}[\overline{u}_{yy}\tilde{T} + \overline{T}_y\tilde{u}_y + i\alpha\overline{T}_y\tilde{v} + \overline{u}_y\tilde{T}_y]$$

$$- \frac{\overline{\mu}_{TT}}{\overline{\mu}}\overline{T}_y\overline{u}_y\tilde{T} + \frac{i\alpha R_e}{\overline{\mu}}\tilde{p} + \frac{R_e}{\overline{\mu}\,\overline{T}}[i\alpha(\overline{u} - \frac{\omega}{\alpha})\tilde{u} + \overline{u}_y\tilde{v}] \qquad (2.19)$$

$$\frac{d\tilde{p}}{dy} = \frac{-i\alpha}{\overline{T}}(\overline{u} - \frac{\omega}{\alpha})\tilde{v} - \frac{\overline{\mu}}{R_e}\{i\alpha\tilde{u}_y + \frac{4}{3}\frac{\overline{T}_y}{\overline{T}}i\alpha\tilde{u} - (\frac{4}{3}\frac{\overline{T}_{yy}}{\overline{T}} - \alpha^2)\tilde{v} - \frac{4i\alpha}{3\overline{T}}[(\overline{u} - \frac{\omega}{\alpha})\tilde{T}_y + \overline{u}_y\tilde{T}]\}$$

13

$$+ \frac{\bar{\mu}_T}{R_e}\{\bar{u}_y i\alpha \tilde{T} + \frac{4}{3}\frac{\overline{T}_y}{\overline{T}}[i\alpha(\bar{u} - \frac{\omega}{\alpha})\tilde{T} + \overline{T}_y\tilde{v}] - 2\overline{T}_y i\alpha\tilde{u}\} \qquad (2.20)$$

$$\frac{d\tilde{T}_y}{dy} = \alpha^2\tilde{T} - \frac{\bar{\mu}_T}{\bar{\mu}}(2\overline{T}_y\tilde{T}_y + \overline{T}_{yy}\tilde{T}) - \frac{\bar{\mu}_{TT}}{\bar{\mu}}(\overline{T}_y)^2\tilde{T}$$

$$+ \frac{R_e P_r}{\bar{\mu}\overline{T}}[i\alpha(\bar{u} - \frac{\omega}{\alpha})\tilde{T} + \overline{T}_y\tilde{v}] \qquad (2.21)$$

The result is the system of five coupled first-order ordinary differential equations for $\tilde{\rho}$, $\tilde{u}$, $\tilde{v}$, $\tilde{p}$ and $\tilde{T}$ which, together with the boundary conditions, represents an eigenvalue problem with either the wavenumber α or the frequency ω playing the role of eigenvalue.

2.3   BOUNDARY CONDITIONS

Boundary conditions are specified by the requirement that the perturbation can't be felt in the the far-field region, i.e. $|y| \to \infty$, and that the disturbance distributions, $\tilde{u}(y)$, $\tilde{v}(y)$, $\tilde{p}(y)$ and $\tilde{T}(y)$ are even or odd functions of y for a symmetric base flow. When $y \to +\infty$, $\bar{\rho} = \bar{\rho}_\infty = 1$ and $\bar{u} = \bar{u}_\infty$, and the disturbance equations become of constant coefficient type. When substituting for the disturbance quantities $[\tilde{u}, \tilde{v}, \tilde{p}, \tilde{T},] = [C_1, C_2, C_3, C_4]\, e^{By}$, where C_i and B are constants, three exponentially decaying solutions are found, representing asymptotic solutions when $y \to +\infty$

$$\begin{bmatrix} \tilde{v} \\ \tilde{u} \\ \tilde{u}_y \\ \tilde{p} \\ \tilde{T} \\ \tilde{T}_y \end{bmatrix} \sim \begin{bmatrix} 1 \\ -i \\ i\alpha \\ i(\bar{u}_\infty - \frac{\omega}{\alpha}) \\ 0 \\ 0 \end{bmatrix} e^{-\alpha y} \qquad (2.22a)$$

$$
\begin{bmatrix} \tilde{v} \\ \tilde{u} \\ \tilde{u}_y \\ \tilde{p} \\ \tilde{T} \\ \tilde{T}_y \end{bmatrix} \sim \begin{bmatrix} 1 \\ -i\beta/\alpha \\ i\beta^2/\alpha \\ 0 \\ 0 \\ 0 \end{bmatrix} e^{-\beta y}
\tag{2.22b}
$$

$$
\begin{bmatrix} \tilde{v} \\ \tilde{u} \\ \tilde{u}_y \\ \tilde{p} \\ \tilde{T} \\ \tilde{T}_y \end{bmatrix} \sim \begin{bmatrix} 1 \\ -i\dfrac{\alpha}{\zeta} \\ i\alpha \\ (1-\dfrac{4}{3}P_r)\dfrac{i\alpha}{\zeta}(\bar{u}_\infty - \dfrac{\omega}{\alpha}) \\ P_r\dfrac{R_e}{\zeta} \\ P_r R_e \end{bmatrix} e^{-\zeta y}
\tag{2.22c}
$$

where $\beta = \sqrt{R_e i\alpha(\bar{u}_\infty - \dfrac{\omega}{\alpha}) + \alpha^2}$, $Real(\beta) > 0$

and $\zeta = \sqrt{P_r R_e i\alpha(\bar{u}_\infty - \dfrac{\omega}{\alpha}) + \alpha^2}$, $Real(\zeta) > 0$

The boundary conditions at y=0 are as follows. For the sinuous (odd) mode $\tilde{u} = 0 \quad \tilde{p} = 0 \quad \tilde{T} = 0$, for the varicose (even) mode $\tilde{v} = 0 \quad \tilde{u}_y = 0 \quad \tilde{T}_y = 0$.

In case of infinite Reynolds number, the disturbance equations (2.13)-(2.17) can be reduced to the simple form,

$$
\frac{d\tilde{p}^2}{dy^2} - (\frac{1}{\bar{\rho}}\frac{d\bar{\rho}}{dy} + \frac{2}{\bar{u} - \omega/\alpha}\frac{d\bar{u}}{dy})\frac{d\tilde{p}}{dy} - \alpha^2\tilde{p} = 0,
\tag{2.23}
$$

with boundary conditions at $y \to +\infty$

$$
\begin{bmatrix} \tilde{p} \\ \tilde{p}_y \end{bmatrix} \sim \begin{bmatrix} 1 \\ -\alpha \end{bmatrix} e^{-\alpha y},
\tag{2.24}
$$

and at y=0, $\tilde{p} = 0$ for the sinuous mode and $\tilde{p}_y = 0$ for the varicose mode.

15

2.4 THE NUMERICAL METHOD

To determinate the stability character for the given base flow, the dispersion relation is found numerically. The branch point ω^o, defined by (1.3), is found by two steps, following the numerical approach used by Sohn (1986). First, eigenvalues are found by a standard shooting procedure. For the numerical integration a standard 4th-5th order Runge-Kutta-Fehlberg scheme with stepsize control was used. Following Monkewitz (1978), solutions were kept linearly independent by pseudo-orthogonalization during integration. Then, to search for the branch point ω^o, two eigenvalues ω_1 and ω_2 associated with the corresponding wavenumbers, $x_1^-(\omega_1)$ and $x_2^-(\omega_2)$, are used as initial guesses to predict the branch point ω^o by extrapolation, using the relation

$$x^{\pm} - x^o = \pm\, C_S(\omega - \omega^o)^{1/2} + C_L(\omega - \omega^o) + \ldots ,\qquad(2.25)$$

which is obtained directly from the Taylor expansion of the dispersion relation around the branch point ω^o (see definition (1.3)).

$$\omega = \omega^o + \frac{1}{2}(x - x^o)^2 \frac{d^2\omega}{dx^2}(x^o).\qquad(2.26)$$

Using equation (2.25) and two initial frequency guesses ω_1, ω_2 with four corresponding x_1^- and x_2^-, ω^o, x^o, C_S and C_L are determined. A new frequency $\omega_3 = (\omega_2 + \omega^o)/2$ is chosen instead of ω_1 as new initial guess and the procedure is repeated until the last two branch point extrapolations are equal to within the required convergence criterion.

2.5 RESULTS OF LOCAL STABILITY CALCULATIONS FOR HEATED JETS AND WAKES

For the calculations parameters R_r, P_r, S, Λ and N have to be specified. For jet flows calculations have been carried out at infinite Reynolds number, because in the region of interest $R_r > 10^3$ the quantitative differences between inviscid and viscous calculation found by Morris (1983) for axisymmetric jets are relatively small and do not justify the considerable increase of computation associated with finite Reynolds numbers. Furthermore, for a two-dimensional jet into stagnant fluid, the velocity ratio, Λ defined by equation (2.1) is equal to 1, and the Prandtl number is assumed to be constant $P_r = 0.71$. Hence, only the parameters S and N are varied systematically in the jet. Finally, based on the calculations, the sinuous mode is more stable than the varicose mode in jet flows. Therefore the following study concentrates on the latter.

The complex branch points ω^o as function of N are shown in Figure 5 for varying density ratio S. The corresponding complex saddle points, x^o are documented in Figure 6. From the absolute growth rate,

16

ω_i^o, it follows that local absolute instability first occurs for S=0.9 and a mean flow profile with N=5. For S lower than 0.9, local absolute stability occurs in an interval of N. Hence, according to Chomaz, Huerre and Redekopp's model study, mentioned in section 1.3, the 2-D hot jet has the potential for global instability when the density ratio S<0.9.

To complete the stability analysis for 2-D flows with non-uniform density, calculations were also carried out for 2-D wake flows at low Reynolds numbers, where Kármán vortices have been successfully suppressed by heating the wake, as in Strykowski's experiment (1986). In the wake case, the more unstable sinuous modes are of primary interest. The absolute instability boundary, where $\omega_i^o = 0$, plotted in the $S - N^{-1}$ plane is shown on Figure 7 for wake model profiles with reverse flow ($\Lambda = -1.25$) and with zero mean velocity on the centerline ($\Lambda = -1$), under the assumption of constant viscosity. It is shown that for the homogeneous wake S=1, local absolute instability occurs in a certain interval of N, which corresponds to the "oscillator" behavior in the homogeneous 2-D wake, i.e. Kármán vortex shedding. The absolute growth rates are reduced by decreasing S and all local absolute instability is eventually eliminated when the density ratio is sufficiently low, depending on R_e and Λ. As in the homogeneous case one finds that, while viscosity decreases the size of the absolutely unstable region for a given density ratio, reverse flow increases it. The latter seems to have a more significant effect on the instability of wake flows.

To see how much heating is necessary to suppress the global Kármán mode, more calculations were carried out to search for the critical density ratio corresponding to zero growth rate $\omega_i^o = 0$ which defines the boundary between absolute and convective instability. Also considered were some fluid property effects other than density effects on the jet stability. As heating is an easy way to create a non-uniform density flow in the lab, the effect of mean temperature variation on fluid properties, such as viscosity and heat conduction coefficient were studied. For example, the viscosity μ and specific C_p of air at ambient pressure will increase 19.8% and 0.56%, respectively, from a temperature of $20^\circ C$ to $100^\circ C$ with the Prandtl number decreasing 1.26%. The variation of viscosity is comparable with the density decrease, 21.5% in the same temperature range. To examine whether the viscosity variation contributes significantly to the stability behavior of the flow, stability calculations are also carried out without the assumption of constant viscosity. For this Sutherland formula for $\bar{\mu}(\bar{T})$ (Section 2.1) was used and C_p and P_r were assumed to be constants. The boundary, where the maximum grow rate ω_i^o is zero for all N, is plotted on the S-R plane in Figure 8 for two values of Λ. Below the curves, modes with zero group velocity have negative growth rates $\omega_i^o < 0$ for all N, and the flow system is convectively unstable. In other words absolute instability is suppressed by heating. The variable viscosity effect is shown to be relatively small compared to the density effect. On the same figure

the S required to suppress Kármán vortex shedding (Berger & Schumm, 1988) is also indicated. For this, the relation between $R^{(D)}$ based on the cylinder diameter and the profile Reynolds number R, as well as the Λ_{min} has been estimated according to Monkewitz (1988). The experiment again confirms the scenario of Chomaz Huerre & Redekopp in which global stability is guaranteed if the flow is everywhere convectively unstable.

3. EXPERIMENTS ON A 2-D HOT JET

3.1 FACILITY AND INSTRUMENTATION

Facility

The facility used to produce a two dimensional hot jet with aspect ratio of 20:1 is shown on Figure 9. A variable speed blower connected to a long duct delivers air into an acoustic filter, which is lined with fiberglass to eliminate acoustic noise. The cold and quiet air then passes through a 6.5 KW heater packed with aluminum wool, which makes air velocity and temperature distribution more uniform. A two-dimensional divergent-convergent settling chamber is acoustically lined with 1" thick fiberglass and a layer of steel wool is installed in the middle of the chamber to reduce turbulence and further smooth the temperature distribution. A piece of honeycomb and several screens are then installed to straighten the flow and eliminate large eddies. A final 10:1 contraction with smooth Formica as inside surface and fiberglass as outside insulation provides a nozzle of 15mm x 300mm, pointing vertically up. The streamwise direction is denoted by x, the definition of the y and z coordinates is indicated on Figure 9.

Two plexiglass plates, good for photography, are fixed on both sides of the nozzle , parallel to the x-y plane, to prevent the jet spreading in the z-direction at the two ends, thus improving the 2-D characteristics of the jet. The hot air is forced out of the room by an exhaust fan.

Acoustic noise level

Great care was taken to quiet the facility. In addition to the use of fiberglass in the settling chamber and the acoustic filter, the level of acoustic noise in the laboratory was minimized by carrying out the experiments at night with no traffic in or around the building, by switching off the exhaust fan during data acquisition, and by moving the blower and the electronic equipment with cooling fans out of the room into the hallway. The resulting RMS turbulence level in the nozzle exit plane of the unheated jet was determined with a constant temperature hotwire and found to be less than 0.06% for a jet velocity of 4.46m/s. The streamwise velocity spectrum recorded at $x/H=0$ and $y/H=0$ in the potential core is shown on Figure 10(a). The pressure spectra of the background noise with the jet turned off is shown on Figure 10(b) to document the dominant noise frequencies, originating mainly from the building the air conditioning and ventilation system.

Instrumentation

For the experiments the facility was instrumented as follows. The operating parameters, jet temperatures and velocities, were obtained from a chromel-Alumel (K-Type) thermocouple probe with a junction of 2 mm diameter and a MKS pressure transducer type 398HD with a total head probe of 1 mm diameter. The thermocouple and pitot/pressure transducer were also used to calibrate a DANTEC hotwire anemometer in constant current and constant temperature mode for local turbulent temperature and velocity measurements, respectively. The probe had a $5\mu m$ platinum-plated tungsten wire with a working length of 1.25 mm. In constant current mode, the resistance of the wire is measured which depends on temperature only. Hence temperature information can be detected in this set-up without being affected by velocity fluctuation. In constant temperature mode, an overheat ratio of 0.8 was set for velocity measurements in the homogeneous jet. The mean data were obtained by a DANTEC mean value unit Type 56N22 with integration time up to 1000 seconds. The fluctuating data were collected by a HP 3400A RMS voltmeter and/or a HP 3582A Spectrum Analyzer, which was connected to a X-Y recorder. The near-field pressure outside the jet was monitored by a 1/2" B&K microphone fitted with a standard protective cap to shield it from the entrainment flow.

Flow visualization was carried out with Schlieren optics shown on Figure 11. This system was based on two spherical mirrors of 6 inches diameter and 60 inches focal length. A XENON (Model 437B) 20ns spark gap and a 2mm diameter pinhole were combined to provide the light source. The photographs were taken with an Iris instead of the knife edge to obtain equal sensitivity in all directions.

Operating range

Limited by the temperature tolerance of the fabrication material, plywood, the experiments have been carried out with jet temperatures ranging from ambient, which was always close to $20^{\circ}C$, to $130^{\circ}C$. The facility can provide a hot jet with density ratios down to 0.72. Under such conditions, a Reynolds number of about 7000 can be attained, with a corresponding Froude number, defined as $SU_j^2[H(1-S)g]^{-1}$, of about 2900, at which buoyancy forces can be neglected in the near field of the hot jet.

Symmetry of the mean flow

The mean velocity and temperature profiles in the nozzle plane are documented to show the quality of the 2-D hot jet facility. The mean temperature variation along the z-direction, excluding the boundary layer region, in the range of $-6.7 < z/H < 6.7$ is less than 3% of the temperature difference between jet centerline and ambient, $\Delta T = T_j - T_{ambient}$, for q=0.79 mmH_2O as shown on Figure 12. Temperature distribution in the y-direction are quite symmetric around y=0 and are almost duplicated at the stations of z/H=-6.7, 0, +6.7, with the var-

iation less than 5% of ΔT, as illustrated in Figure 13. The thermal boundary layer thickness, defined by $\Delta T/(dT/dy)_{max}$, is about 0.14 jet widths. The velocity profiles in the z-direction are uniform except for some deviations on both ends as shown in Figure 14. The velocity profiles in the y-direction are shown in Figure 15 for the cold jet, illustrating the symmetry during the flow development. The initial momentum thickness for the cold jet was measured to be $\frac{\theta}{H} = \frac{1.14}{\sqrt{R_e}}$ demonstrating laminar initial conditions.

3.2 FLOW VISUALIZATION

To visualize the 2-D heated jet, the Schlieren optical system was aligned such that the light beams in the test section were parallel to the z-axis of the jet, as shown on Figure 11, with the receiving lens focusing at the z=0 plane.

The Schlieren images in Figure 16 show the qualitative difference of the vortex structure in the near-field of a slightly heated jet with S=0.90 and a hot jet with S=0.73 where $S=\rho_j/\rho_\infty$ is the ratio of jet and ambient density. In the former case, vortices evolve gradually in the shear layers from small wavy structures to larger and larger vortex pairs by vortex pairing. In the hot jet, on the other hand, large vortex-pair structures form immediately after an initial, virtually undisturbed jet region. Furthermore, different Schlieren images under the same hot jet condition were observed as shown in Figure 15(d)-15(f). These large vortex structures were found to be quite symmetric about the jet center line, corresponding to the varicose instability mode. The observations were repeated for other hot jet condition as shown in Figure 17. These findings suggest that the hot jet column is self-excited in contrast to the slightly heated or cold jet. Before proceeding to a quantitative examination of the jet oscillations by spectral measurements, side-view Schlieren are shown on Figure 18 to document the 2-D characteristics of the vortex pairs near the nozzle. It shows that the hot jet oscillations under consideration remain 2-D up to approximately x/H=4, where 3-D disturbances seem to become important. This observation implies that the first vortex pair is essentially 2-D since it forms at x/H less than 4.

3.3 SPECTRAL DATA IN THE NEAR-FIELD

3.3.1 Velocity and temperature spectra

To characterize the jet behavior, three fluctuating quantities -velocity, temperature and pressure- are examined in the frequency domain.

In the Reynolds number range we study, $4,000 < R_e < 7,000$, the near-field sound pressure level of the jet is about the same as the acoustic noise of the enviroment. Near-field pressure spectra detected by the microphone therefore do not have a good signal to noise ratio. However, it provides a reference of noise frequencies. On the other hand, the hot wire is less sensitive to acoustic noise and consequently has a better signal to noise ratio, but it is sensitive to both velocity and temperature fluctuations which exist in a nonhomogeneous hot jet flow. For a hot jet, the combined use of velocity and temperature signals is necessary.

The selection of measurement locations

Samples of velocity, temperature and pressure spectra in the entrainment region are shown on Figure 19. Figure 19(a) illustrates the uniformity of the temperature of the hot jet in the entrainment region (outside the jet shear layers) with a turbulent intensity less than 0.06% of ΔT. Therefore, the spectral data in the entrainment region obtained by the H.W. probe in constant temperature mode is due to velocity fluctuations. At the same location as the temperature spectra, velocity spectra of the hot jet are shown on Figure 19(b). The dominant frequencies, i.e. the peaks on the spectra, are the same as the ones measured by microphone and shown on Figure 19(c), but do not correspond to the peaks of the external noise spectra on Figure 10(b). Since velocity spectra have a better signal to noise ratio than pressure spectra in our operating range, mainly velocity data are collected in the entrainment region. In the shear layers of the hot jet both temperature and velocity fluctuations are comparable. Therefore the hot-wire was operated in constant current mode such as to sense only temperature.

Velocity and temperature spectra in the hot jet

The near-field velocity spectra of the cold and hot jet, shown on Figure 20, were obtained with the hot-wire probe inserted in the entrainment region outside but close to the shear layers (see for instance the hot-wire probe location in Figure 17c). As shown by these velocity spectra, a cold jet has a broad band spectrum while the hot jet spectra are line-dominated with a substantial harmonics content, which suggests an oscillator behavior. The temperature spectra in the shear layer, shown on Figure 21, also display the change from the broad band spectrum of a slightly heated jet to the line-dominated spectrum of the hot jet with S<0.9. With the latter spectra , the hot jet is reminiscent of cylinder wakes which display a limit cycle oscillation. However it is clear from the flow visualization that the hot-jet oscillation is dominated by the even (varicose) mode, in contrast to the odd (sinuous) mode in wake flows. That is in agreement with the predictions of linear stability theory. Also, as predicted by linear theory, lower density has opposite effects in wake and jet flows. The present experiment has shown that heating the jet promotes oscil-

22

lations, while large vortices in wake flows are suppressed by heating the wake as in Strykowski's experiment (section 2.5).

The self-excited nature of the jet oscillation

The dominant frequencies in an oscillating hot jet, i.e. the peak values in the spectra, are the same at varying locations in the near-field under the same flow conditions, but different from those of the noise spectrum detected by a sensitive microphone when the jet flow is turned off. This indicates that the dominant modes are not due to the amplification of ambient noise. Furthermore, the quiet spectrum right after the nozzle, already shown on Figure 10a, eliminates the possibility of acoustic cavity resonances in the settling chamber. Therefore, it is concluded that the nature of the oscillation is intrinsic and self-excited for density ratios $S \leq 0.9$, as opposed to the convective nature in a cold jet. Hence, all the spectra for $S \leq 0.9$ correspond to a nonlinear stable saturation state, i.e. limit cycle.

3.3.2 The Dominant Strouhal Numbers

The Strouhal number dominating the near-field spectrum close to the nozzle is plotted on Figure 22 for all cases during the present experiments in which line-dominated spectra were observed. They were all found to be in the range of 0.12 to 0.33, which is consistent with the stability calculations in Chapter 2 : Figure 5 gives in the region of absolute instability a typical value of $\omega_r^o \approx 1.4$ for the absolute frequency, which corresponds to a Strouhal number $St = fH/U_j \approx 0.22$. This supports the notion that the observed strong oscillations are related to absolute instability, i.e. to feedback by upstream vorticity waves.

3.3.3 The character of the bifurcation to self-excited oscillations

As already shown in Figure 21, the broad band spectra become line-dominated with decreasing density ratio. When the normalized amplitude of the dominant spectral line is plotted as function of density ratio, a Hopf bifurcation is found as illustrated in Figure 23. The similarities to the global behavior of the cylinder wake, as investigated by Provansal, Mathis and Boyer (1987) and others, become apparent. According to Landau's theory, in the small region close to the critical control parameter (density ratio S in this case), the amplitude of an unstable system, can be described by equation(3.1) in the case of zero forcing

$$\frac{d|A|}{dt} = C_1|A| - C_2|A|^3 \tag{3.1}$$

where the temporal growth rate C_1 is to leading order proportional to $(S_{crit} - S)$. For $C_2 > 0$, the cubic nonlinearity limits the amplitude, and the saturated amplitude, A_{sat}, is found to depend on S as

$$A_{sat} \propto (S_{crit} - S)^{1/2}; \quad S \leq S_{crit} \tag{3.2}$$

The data in Figure 23 for the lowest frequency peak f_o have been fitted with this relationship, leading to $S_{crit} = 0.92$.

For a self-excited hot jet, the maximum (with respect to the y-direction) amplitude of the dominant spectral lines f_o and $2f_o$ at different streamwise locations is documented in Figure 24. At x/H=3, the energy of f_o reaches a maximum, marking the approximate point where the first strong vortex pair is observed.

3.4 NONLINEAR PHASE LOCKING

3.4.1 Introduction and definition of bicoherence

In section 3.3, the power (or amplitude) spectrum has been used to analyze the frequency content of the velocity and temperature fluctuations in a hot jet. If the fluctuating signal in the time domain is a superposition of normal modes, with phases varying independently, the power spectrum describes the signal completely (Knisely & Rockwell, 1981). However, if a spectral component with frequency f_m is a product of nonlinear coupling between two frequencies f_l and f_k, then the power spectrum can't provide sufficient information about this nonlinear interaction. For this the bispectrum and its normalized form, the bicoherence spectrum, have been useful tools. Hasselman, Munk & McDonald (1963) used bispectrum estimates to study geophysical flow. Kim & Powers (1979) analyzed and interpreted plasma fluctuation data by the bispectral analysis technique. Lii, Rosenblatt & Van Atta (1976) used the bispectral estimates to show the direction of energy transfer between the frequency components of the velocity field. Knisely & Rockwell (1981) applied bispectral estimates to study non-linear flow in an impinging shear layer. Miksad et al. (1982,1983) used bicoherence spectral measurements to investigate the nonlinear interactions in a laminar 2-D wake during transition to turbulence. Corke (1987) studied nonlinear phase locking in an axisymmetric homogeneous jet by examining the cross-bicoherence between the unsteady pressure at the lip and velocity fluctuations at different streamwise locations.

To define bicoherence, it is necessary to recall the definition of bispectrum and the Fouier transform of a real and stationary signal. If a fluctuating signal in the time domain, e.g. the temperature fluctuation measured at a point in a mean-steady hot jet, has a discrete Fourier representation

$$x(t) = \sum_{m=-N}^{N} X_m e^{-i2\pi f_m t}$$

24

$$X_m = \lim_{T \to \infty} \frac{1}{T} \int_{-\frac{T}{2}}^{\frac{T}{2}} x(t)\, e^{i2\pi f_m t} dt$$

where X_m is the complex Fourier amplitude at frequency f_m and has the relation $X_{-m} = X_m^*$ (* indicates complex conjugate). $f_m = m/T$ and T is the record length of $x(t)$. The bispectrum for any two frequencies f_k and f_l is defined as (Kim & Powers, 1979)

$$B(f_k, f_l) = E[X_k X_l X_{k+l}^*]$$

Here $E[\ ]$ denotes an expected value. Physically, the bispectrum measures the production of a third wave with frequency f_m from the coupling interaction of the primary waves at f_k and f_l. The wave frequencies (f_k, f_l, f_m) must satisfy the resonance condition $f_m = f_k + f_l$. The bicoherence spectrum is a normalized version of the bispectrum and is defined as

$$b^2(f_k, f_l) = \frac{|B(f_k, f_l)|^2}{E[|X_k X_l|^2]E[|X_{k+l}|^2]} \qquad (3.3)$$

where $|\ |$ denotes the modulus. The bicoherence spectrum is bounded by $0 \le b^2(f_k, f_l) \le 1$. If three spectral components at frequencies f_k, f_l, f_m are coupled to one another, a phase lock exists and the bicoherence $b(f_k, f_l)$ yields a nonzero value. If these three spectral components are independent of one another, $b(f_k, f_l)$ is close to zero.

3.4.2 Data acquisition and processing for bicoherence

The temperature signal of a heated jet, obtained by a DANTEC hot-wire anemometer in constant current mode, as described in section 3.1 was fed into a low-pass filter (KROHN-HITE Model 330A) with 250 Hz cutoff frequency. This analog signal was then amplified and sampled with a 12-bit analog-to-digital converter (MetraByte's DASH-16) at a sample rate of 600 samples per second, and recorded on a IBM PC-AT compatible. Each record contained 81920 samples of the temperature signal corresponding to 135.53 seconds of real time. To estimate bicoherence, each record was divided into 80 consecutive blocks of 1024 samples. Each block was then fast Fourier transformed with $\Delta f = 0.586$Hz resolution (Oppenheim & Schafer, 1975). The 80 spectra, each consisting of 1024 complex numbers corresponding to the amplitude and phase for frequencies between -300 Hz and +300 Hz at intervals of Δf, were stored in memory and the bicoherence was evaluated from each spectrum according to definition (3.3). The average amplitude spectrum was also calculated to find the dominant frequencies and to compare with the results obtained by the HP spectral Analyzer. The samples are shown on Figure 25 which is to be compared with Figure 21a.

The domain of bicoherence spectrum, $b(f_k, f_l)$, is limited by the Nyquist criterion. The absolute values of f_l, f_k and $f_l + f_k$ should be smaller than or equal to the Nyquist frequency f_N. It is noted that, due to the symmetry of the bicoherence $b(f_k, f_l) = b(f_l, f_k)$ and $X_{-m} = X_m^*$ for the Fourier amplitude, it is only necessary to calculate the bicoherence

25

in a triangular domain given by $0 \leq f_k \leq \frac{f_N}{2}$, $f_k \leq f_l \leq f_N - f_k$. If we are only interested in the coherence of a particular frequency, e.g. the dominant frequency f_0 in hot jets, with other frequencies, then only $b(f_0, f)$ needs to be calculated.

3.4.3 Test of the bicoherence computation

To test the bicoherence estimator described previously, we generated a test signal which involves three oscillators with frequencies f_1, f_2 and $f_3 = f_1 + f_2$

$$x(t) = A_1 \cos(2\pi f_1 t + \theta_1) + A_2 \cos(2\pi f_2 t + \theta_2) + A_3 \cos(2\pi f_3 t + \theta_3) \qquad (3.4)$$

where the amplitudes A_1, A_2 and A_3 were chosen to be close to the peak amplitudes found in the hot spectrum as shown in Figure 25a, i.e. $f_1 \approx f_0$, $f_2 \approx 2f_0$ and $f_3 \approx 3f_0$ (see Figure 26a). First, the effect of phase-locking was verified by computing $b^2(f_1, f)$ for $\theta_3 = \theta_1 + \theta_2$ (with θ_1 and θ_2 random) which yields $b^2(f_1, f_2) = 1$ (Figure 26b), and also for all three phases radom (Figure 26c) which yields a $b^2(f_1, f_2)$ near zero. .

To test the effect of signal-to-noise ratio on the bicoherence estimates, the phase-locked signal of Figure 26 was superimposed with the noisy temperature fluctuation in the slightly heated jet of Figure 25. The decrease of $b(f_1, f_2)$ from 1 to 0.88 indicates that the maximum bicoherence depends on the signal-to-noise ratio of the data as pointed out by Corke (1987).

3.4.4 Results from bicoherence estimates

Phase locking in hot jets

The bicoherence of the dominant frequency f_0 with other frequencies in the hot jet at several streamwise locations is shown in Figure 28. The peaks of $b^2(f_0, f_0)$ and $b^2(f_0, 2f_0)$ indicate the phase lock between the primary harmonics f_0 and $2f_0$ when x > 1.5 approximately. On the other hand, in a slightly heated jet, where the amplitude spectrum has no obvious dominant frequency, f_0 of the hot jet is still used for the $b^2(f_0, f)$ calculation since the dominant frequency is almost independent of the density ratio if the total head remains constant, as shown in Figure 21(a). The bicoherence $b^2(f_0, f)$ of a slightly heated jet at different streamwise location is shown in Figure 29. The much lower values of $b^2(f_0, f)$, close to zero indicate the lack of phase coherence between f_0 and other frequencies.

Bicoherence as a function of streamwise location

In Figure 30 we show the distribution of bicoherence $b^2(f_0, f_0)$ and $b^2(f_0, 2f_0)$ in the hot jet along the streamwise direction. It is noted that no phase locking appears at x/H close to zero, which is probably due to a low signal to noise ratio in this region of low oscillation amplitude, while the maximum bicoherence is found around x/H = 2.5.

Bicoherence versus density ratio

In Figure 31 the bicoherence $b^2(f_0, f)$ of the hot jet is shown for different density ratios. If $b^2(f_0, f_0)$ and $b^2(f_0, 2f_0)$ are plotted versus density ratio, again a critical value of S=0.9 is obtained below which phase locking occurs, in good agreement with Figure 23.

3.5   MEAN FLOW DATA

Mean velocity and temperature profiles of an oscillating hot jet are shown on Figure 33 and Figure 34, respectively. For x/H = 4,6, intermediate plateaus appear in the shear layers at the location of the large mixed vortex cores. This is further evidence for the highly organized nature of the large vortex-pair structures implied by the near field-spectra and the flow visualization. The center-line velocities of the self-excited hot jet and cold jet are shown in Figure 35. The earlier decay for the self-excited hot jet indicates enhanced mixing in comparison with the cold jet at same Reynolds number.

4. FURTHER INVESTIGATIONS

4.1 GLOBAL LINEAR STABILITY ANALYSIS OF NONPARALLEL FLOWS
(WITH P. HUERRE AND J.M. CHOMAZ)

The stability of spatially developing free shear flows, such as jets and wakes, is studied under the assumption that the streamwise development of the base flow, characterized for instance by its the local momentum thickness $\theta(x)$, is "slow" on the scale of a typical instability wavelength λ, that is

$$\epsilon \simeq \lambda/[d(\ln\theta)/dx] \ll 1 . \qquad (4.1)$$

To simplify matters, we consider only doubly-infinite, two-dimensional, incompressible, and inviscid base flows without boundaries and seek time-periodic perturbations thereof - henceforth termed global modes - which vanish at infinity in all directions. Of particular interest are systems which exhibit supercritical (Hopf) bifurcations to global oscillations, which, in general, entails local absolute instability over a finite x-interval. To simplify further, it is assumed that at each x-station the local dispersion relation $k(\omega)$ has only one square-root branch point $\omega_o(x)$ or, in other words, that it has only two branches: an "upstream" branch k^- and a "downstream" branch k^+.

For _infinitesimal (linear) disturbances_, P. Huerre, J.M. Chomaz and this author have demonstrated (paper in preparation) that the eigen-frequencies $\omega_{G,n}$ of the most amplified global modes are determined by the connection of the "upstream" and "downstream" waves through a double turning point region around the complex location x_t, defined by

$$d\omega_o/dx(x_t)=0 , \qquad (4.2)$$

which, loosely speaking, may be viewed as a "wavemaker". It is thereby assumed that ω_o has only one saddle point x_t, which means that the absolute growth rate ω_{oi} has a simple maximum on the real x-axis, and that the flow contains only one interval (of the real x-axis) of absolute instability (i.e. $\omega_{oi}>0$). Local stability calculations show that this latter assumption is justified in jets and bluff-body wakes which are of primary interest here. Since this linear analysis has not been published yet, it is briefly described. The starting point is the Euler equation, linearized around the mean stream function $\Psi_o(y,X)$, where $X=\epsilon x$ is the slow scale characteristic of the mean flow development. Following

Crighton and Gaster (1976), the instability waves far up- and downstream are given by the WKB approximations

$$\Psi^{\pm} = A^{\pm}(X) \ \Phi(y;X) \ \exp\left[\frac{i}{e} \int k^{\pm}dX - i\omega_G t\right] \ .$$
(4.3)

The branches $\pm$ are selected such as to satisfy the boundary conditions at $|x|\rightarrow\infty$. With the definitions adopted here, the appropriate subdominant branches far up- and downstream are k^- and k^+ respectively. Moving on to the problem of connecting the two waves, and determining the eigenvalue ω_G, one finds that the WKB approximation breaks down at potential matching locations where the group velocity is zero, i.e. where $\omega_G=\omega_o(x)$ and $k^-=k^+$. For the assumed structure of $\omega_o(x)$ with one saddle point at x_t the two pairs of curves in the complex x-plane $\omega_{or}=$const. and $\omega_{oi}=$const. only intersect at x_t if $\omega_o=\omega_t$, where $\omega_o(x_t)=\omega_t$. As in quantum-mechanical scattering problems, this point x_t is a second order turning point of the "inner" problem which allows the connection between the upstream and downstream waves for eigenvalues

$$\omega_G \sim \omega_t + O(\epsilon) \ .$$
(4.4)

Therefore, a global mode can only become self-excited (time-amplified) if $\omega_{t,i}>0$. By analyzing the neighborhood of the saddle point at x_t, Chomaz et al. (1989) show that the "hills" must be arranged as on Figure 36. This means that, if $\omega_{t,i}>0$, there must be a region of absolute instability with $\omega_{o,i}>0$ on the physical, real x-axis. To analyze the inner region the streamwise coordinate is appropriately rescaled as

$$\xi = e^{1/2}(x-x_t) = \epsilon^{-1/2}(X-X_t) \ .$$
(4.5)

Because the basic flow is parallel on the scale ξ, one finds that the transverse structure of the disturbance Ψ is frozen and given by $\Phi(y;\xi=0)$, thus leading to

$$\Psi = A(\xi,\tau) \ \Phi(y;\xi=0) \ \exp[ik(\omega_t)x - i\omega_t t] \ ; \ \tau=\epsilon t \ .$$
(4.6)

Expansion of the basic flow $\Psi_o(y,X)$ in a Taylor series around X_t then yields, by the method of multiple scales, for the amplitude $A(\xi,\tau)$ a linearized Ginzburg-Landau equation with variable coefficients,

$$\frac{\partial A}{\partial \tau} + C_2 \frac{\partial^2 A}{\partial \xi^2} + C_1 \xi \frac{\partial A}{\partial \xi} + (C_{00}+C_{02}\xi^2) \ A = F(\xi,\tau) \ ,$$
(4.7)

where a forcing term F has been added for later reference (F=0 for free global modes), and the C_n are complex constants obtained from solvability conditions, i.e. given as y-integrals over functions of $\Psi_o(y;X)$ and $\Phi(y;X)$ and their derivatives. In Fourier-space this equation (4.7) corresponds to the dispersion relation

$$\omega_2 - \delta\omega = (\omega_{kk}/2)\,\kappa^2 + \omega_{kx}\,\kappa\,\xi + (\omega_{xx}/2)\,\xi^2\ ;$$

$$\omega_2 = \epsilon^{-1}(\omega-\omega_t)\ ;\ \kappa = \epsilon^{-1/2}(k-k_t)\ , \tag{4.8}$$

where $\delta\omega$ is a genuine nonparallel frequency correction, and ω_{kk}, ω_{kx} and ω_{xx} are complex coefficients related to the C_n by

$$C_{00} = i\,\delta\omega$$

$$C_{02} = i\,(\omega_{xx}/2)$$

$$C_1 = \omega_{kx} \tag{4.9}$$

$$C_2 = -i\,(\omega_{kk}/2)\ .$$

In terms of the rescaled absolute frequency ω_{2o} and corresponding wave number κ_o, equation (4.8) is

$$\omega_2 - \omega_{2o}(\xi) = (\omega_{kk}/2)[\kappa - \kappa_o(\xi)]^2\ ; \tag{4.10a}$$

$$\omega_{2o}(\xi) = (1/2)[\omega_{xx}-(\omega^2_{kx}/\omega_{kk})]\,\xi^2 \equiv (\omega_{oxx}/2)\,\xi^2\ ; \tag{4.10b}$$

$$\kappa_o(\xi) = -(\omega_{kx}/\omega_{kk})\,\xi \equiv k_{ox}\,\xi\ . \tag{4.10c}$$

With $A\propto\exp(i\omega_2\tau)$ the solution of (4.7) is given in terms of Hermite polynomials He_n and the "remainder" of the eigenvalue ω_2 is determined such as to ensure the asymptotic match to the "outer" solutions $\Psi^{\pm}$.

$$A_n(\xi) = \exp\{(\xi^2/2)[ik_{ox}-(\omega_{oxx}/\omega_{kk})^{1/2}]\}\ He_n[(4\omega_{oxx}/\omega_{kk})^{1/4}\xi]$$

$$\omega_{2n} = \delta\omega - (i/2)\omega_{kk}k_{ox} + (\omega_{oxx}\omega_{kk})^{1/2}[n+(1/2)] \tag{4.11}$$

30

4.2 FEEDBACK CONTROL OF GLOBAL OSCILLATIONS

In a further investigation, the equation (4.7), valid in the turning point region around x_t, has been used as a model to study the effect of the simplest possible, _nonlocal feedback control_ on the evolution of global modes (Monkewitz, AIAA paper no. 89-0991, 1989). For this, the forcing term in (4.7) was specified as:

$$F(\xi,\tau) = G\ \delta(\xi-\xi_f)\ A(\xi=\xi_s,\tau)\ ,\qquad\qquad(4.12)$$

where the delta function $\delta(\xi-\xi_f)$ describes a localized actuator at ξ_f, $A(\xi=\xi_s,\tau)$ is the wave amplitude measured by a sensor at ξ_s, and G is a fixed (complex) feedback gain. Without going into the specifics, which can be found in the paper, the main results can be summarized as follows:

When the control (4.12) is applied to a globally stable system, it is not surprising that feedback can be destabilizing. What is interesting, however, is that, for the particular jet flow considered in the paper, it is in general not the least-damped mode, but some higher mode that is destabilized by feedback. It appears from experiments of Berger (1964) that this feature is also a property of other, quite different systems, such as the cylinder wake.

When attempting to use this simple control for the stabilization of a globally unstable system, one finds that this is only possible near the onset of global instability. The reason is that the requirements of a minimum gain to stabilize the unstable "fundamental" mode, and of staying below the critical gain, at which some higher mode is destabilized, quickly become incompatible. This behavior is in complete qualitative agreement with the experiments by Berger (1964) in the wake of an oblong cylinder.

REFERENCES

Ahuja, K.K. (1988) *Acoustic control of a coanda jet,* Bull. Am. Phys. Soc., Vol. 33, 1988, p. 2296.

Batchelor, G.K. (1967) *An introduction to fluid dynamics,* Cambridge University Press.

Berger, E. & Schumm, M. (1988) *Untersuchungen der Instabilitaetsmechanismen in Nachlauf von Zylindern* Contractor report Be 343/18-1, Technical University, Berlin

Brown, G.L. & Roshko, A. (1974) *On density effects and large structure in turbulent mixing layers,* J. Fluid Mech., Vol 64, pp. 775-816.

Chomaz, J.M., Huerre, P. & Redekopp, L.G. (1988) *Bifurcations to local and global modes in spatially developing flows,* Vol. 60, No. 1, Physical Review Letters 4 Jan. 1988.

Corke, T.C. (1987) *Measurements of resonant phase locking in unstable axisymmetric jets and boundary layers,* In: *Nonlinear wave interactions in fluids,* (ed. Miksad, R.W. Akylas, T.R. & Herbert, T.), pp. 37-65. ASME publication AMD, Vol. 87.

Crighton, D.G. & Gaster, M. (1976) *Stability of slowly diverging jet flow,* J. Fluid Mech. Vol. 77, Part 2, pp. 397-413.

Crow, S.C. & Champagne, F.H. (1971) *Orderly structure in jet turbulence,* J. Fluid Mech., 48, pp. 547-591.

Drazin, P.G. & Reid, W.H. (1981) *Hydradynamic stability,* Cambridge University Press, London.

Hasselman, K., Munk, W & McDonald G. (1963) *Bispectrum of ocean wave,* In: *Proceeding of symposium on time series analysis,* (edited by M. Rosenblatt) John Wiley, New York, pp. 125-139.

Huerre, P. & Monkewitz, P.A. (1985) *Absolute and convective instabilities in free shear layers,* J. Fluid Mech., Vol. 159.

Kim, Y, C. & Powers, E. J. (1979) *Digital bispectral analysis and its application to nonlinear wave interactions,* IEEE Trans. Plasma Sci. PS-7, 120-131.

Knisely, C. & Rockwell, D. (1981) *Self-sustained low-frequency components in an impinging shear layer,* J. of Fluid Mech., 116, pp. 157-187.

Koochesfhani, M.M. & Frieler, C.E. (1987) *Instability of nonuniform density free shear layers with a wake profile,* AIAA Paper 87-0047.

Lepicovski, J., Ahuja, K.K., Brown, W.H., Salikuddin, M. & Morris, P.J. (1988) *Acoustically excited heated jets,* NASA CR 4129, Part I-III.

Lii, K. S., Rosenblatt, M. & Van Atta, C. (1976) *Bispectral measurements in turbulence,* J. Fluid Mech., 77, PP.45-62.

Maslowe, S.A. & Kelly, R.E. (1971) *Inviscid instability of an unbounded heterogeneous shear layer,* J. Fluid Mech., 48, pp. 405-415.

Michalke, A. (1970) *A note in the spatial jet-instability of the compressible cylindrical vortex sheet,* DFVLR Tech. Rep. 70-50.

Michalke, Alfons (1984) *Survey on jet instability theory* Prog. Aerospace Sci. Vol 21, pp.159-199.

Miksad, R. W., Jones, F. L., Kim, Y. C. & Khadra, L. (1982) *Experiments on the role of amplitude and phase modulations during transition to turbulence,* J. Fluid Mech., 123, pp.1-29.

Miksad, R., Jones, F. & Powers, E. (1983) *Measurements of nonlinear interactions during natural transition of a symmetric wake,* Phys. Fluids, 26, 6, pp.1402-1409.

Monkewitz, M.A. (1978) *Analytic psedoorthogonalization methods for linear two-point boundary value problems illustrated by the orr-sommerfeld equation,* J. of Applied Math. Vol. 29..

Monkewitz, P.A. (1988) *The absolute and convective nature of instability in two-dimensional wakes at low Reynolds number,* Phys. Fluids 31 (5)

Monkewitz, P.A. (1989) *Feedback control of global oscillations in fluid systems,* AIAA-89-0991.

Monkewitz, P.A. (1989) *The role of absolute and convective instability in predicting the behavior of fluid systems,* ASME conference La Jolla, Ca. July.

Monkewitz, P.A., Bechert, D.W., Barsikow, B., & Lehmann, B. (1989) *Self-excited oscillations and mixing in a heated round jet,* To appear in JFM.

Monkewitz, P.A., Huerre, P. & Chomaz, J.M. (1987) *Preferred modes in jets and global instabilities, Bull. Am. Phys. Soc. 32, p. 2051.*

Monkewitz. P.A., Lehman, B., Barsikow, B., & Bechert, D.W. (1989) *The spreading of self-excited hot jet by side jets,* Phys. Fluids A 1 (3), p. 446.

Monkewitz, P.A. & Nguyen, L. (1987) *Absolute instability in the near-wake of two-dimensional bluff bodies,* J. of Fluids and Structures.

Monkewitz, P.A. & Sohn K.D. (1988) *Absolute instability in hot jets,* AIAA Journal, Vol. 26, No. 8.

Morris, P.J. (1983) *Viscous stability of compressible axisymmetric jets,* AIAA J. 21, 1983, pp. 481-482.

Oppenheim, A. V. & Schafer, R. W. (1975) *Digital signal processing,* Prentice-Hall Inc, Englewood Cliffs, New Jersey.

Provansal, L., Mathis, C., & Boyer, L. *Benard-von Karman instability: transient and forced regimes,* J. Fluid Mech., 182, pp. 1-22.

Sohn, Kiho David (1986) *Absolute instability in hot jets,* MS Thesis UCLA

Squire, H.B. (1933) *On the stability of three-dimensional disturbances of viscous flow between parallel walls.* Proc. Roy. Soc. A 142, pp. 621-628.

Sreenivasan, K.R., Raghu, S. & Kyle, D. (1989) *Absolute instability in variable density round jets,* To appear in Experiments in Fluids.

Strange, P.J.R. & Crighton, D.G. 1983 *Spinning modes on axisymmetric jets. Part 1.* J. Fluid Mech., 134, 1983, pp. 231-245.

Strykowski, P.J. (1986) *The control of absolutely and convectively unstable shear flows,* Ph.D. Thesis, Yale University.
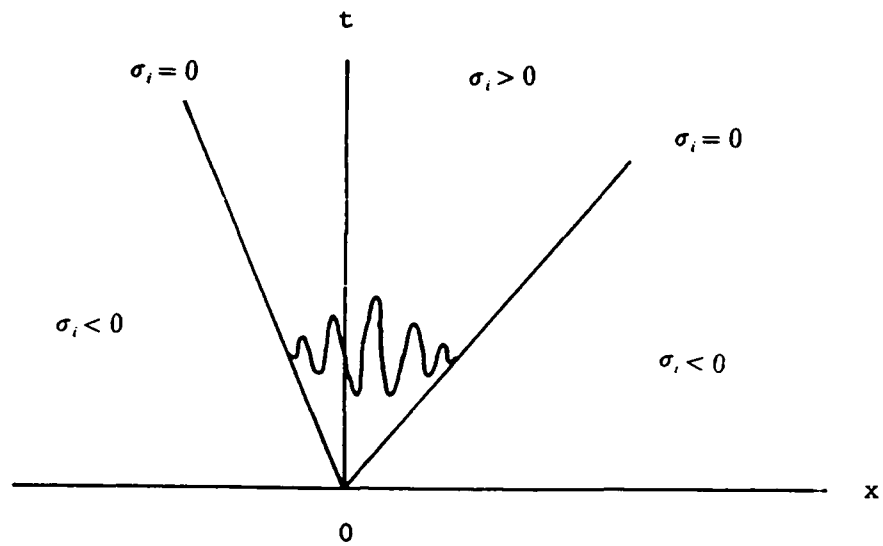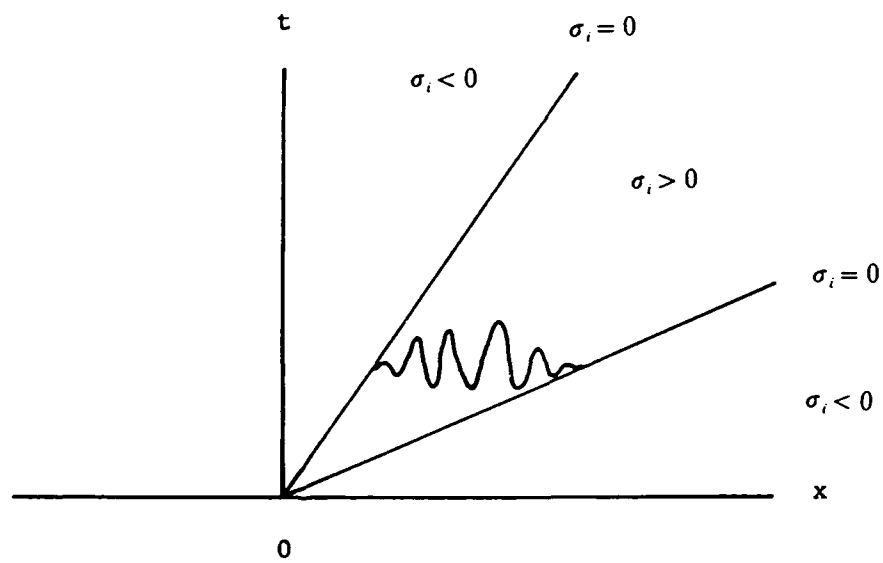
Figure 1   Sketch of typical impulse response for (a) Absolutely
            unstable flow (b) Convectively unstable flow. (from
            Monkewitz, 1989)

35
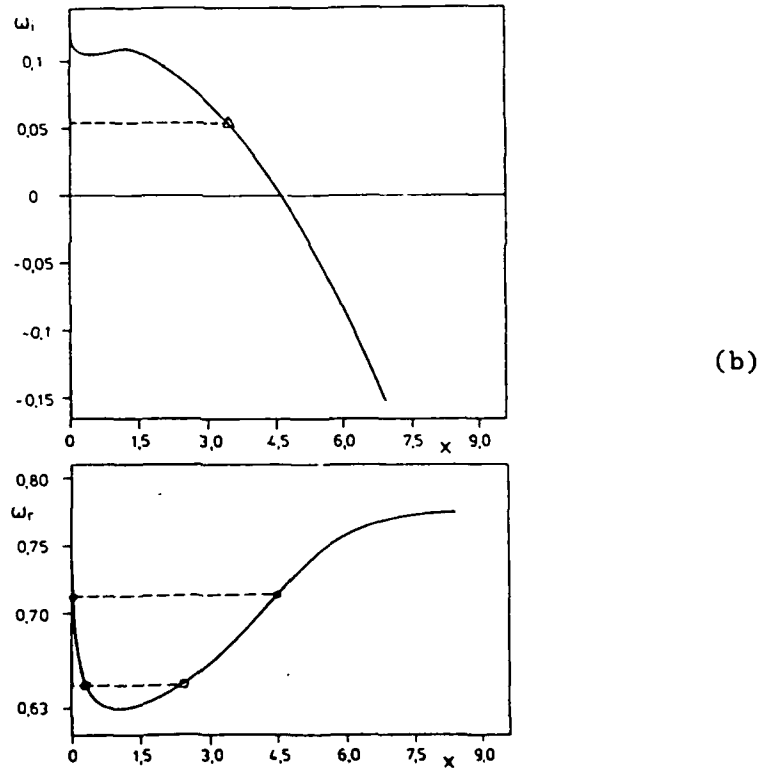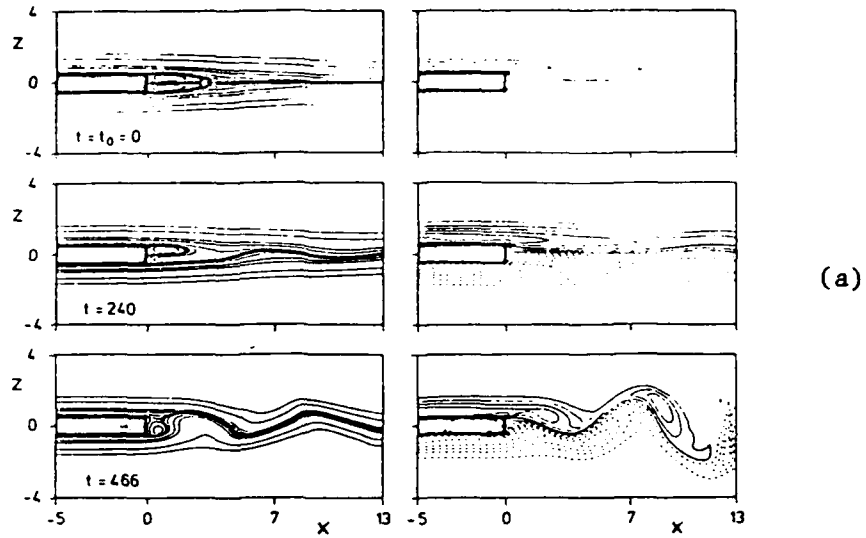
Figure 2   Local and global stability calculations by Hannemann (1988)
for wake flow, (a) numerical simulation of wake flow used
to calculate stability characters, (b) the growth rate ω_i
and frequency ω_r calculated by local linear theory (——) and
global simulation (-----). O global frequency in nonlinear
state, □ global frequency in linear regime.
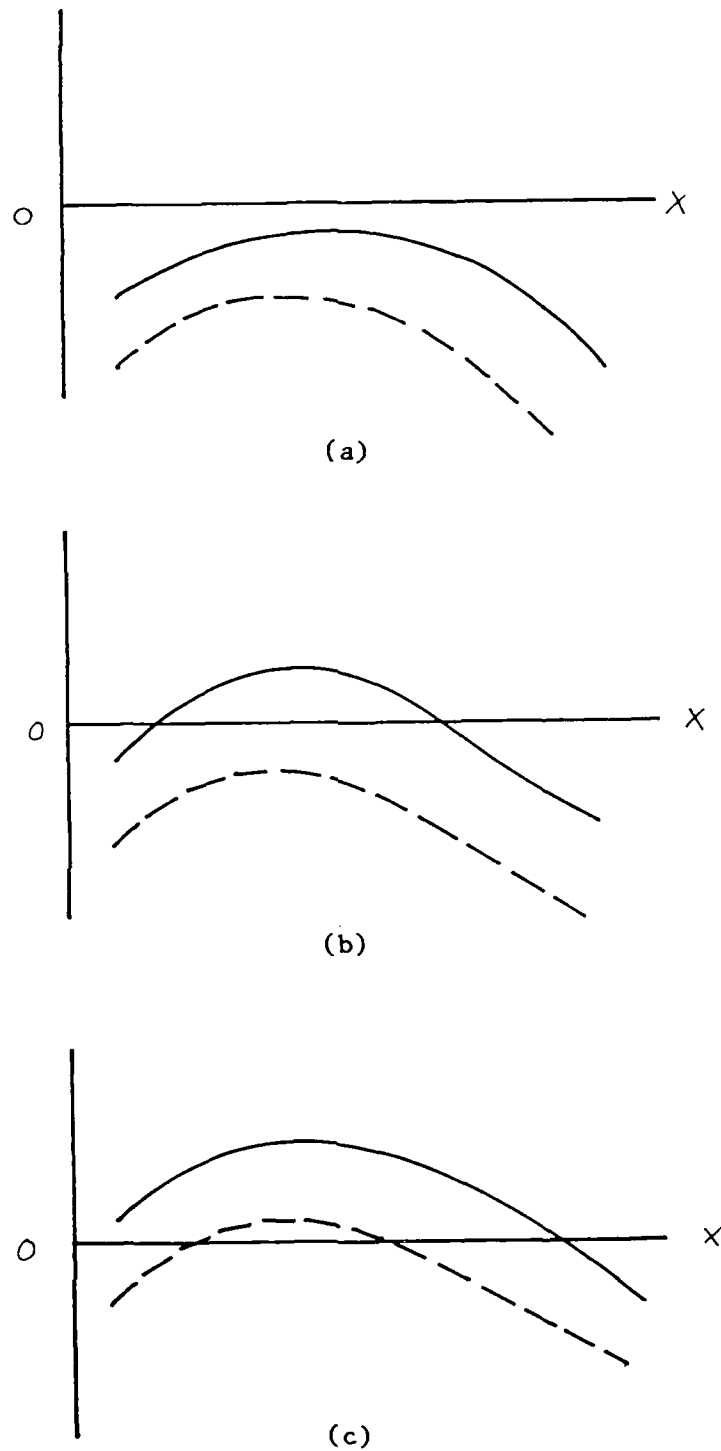
Figure 3   Sketch of the typical x-dependence of the local maximum
temporal growth rate $\omega^o_{i,max}$ (——) and the local absolute growth
rate ω^o_i (-----) in free shear flows for the case of: (a)
uniform local stability; (b) local convective instability;
(c) local absolute instability.
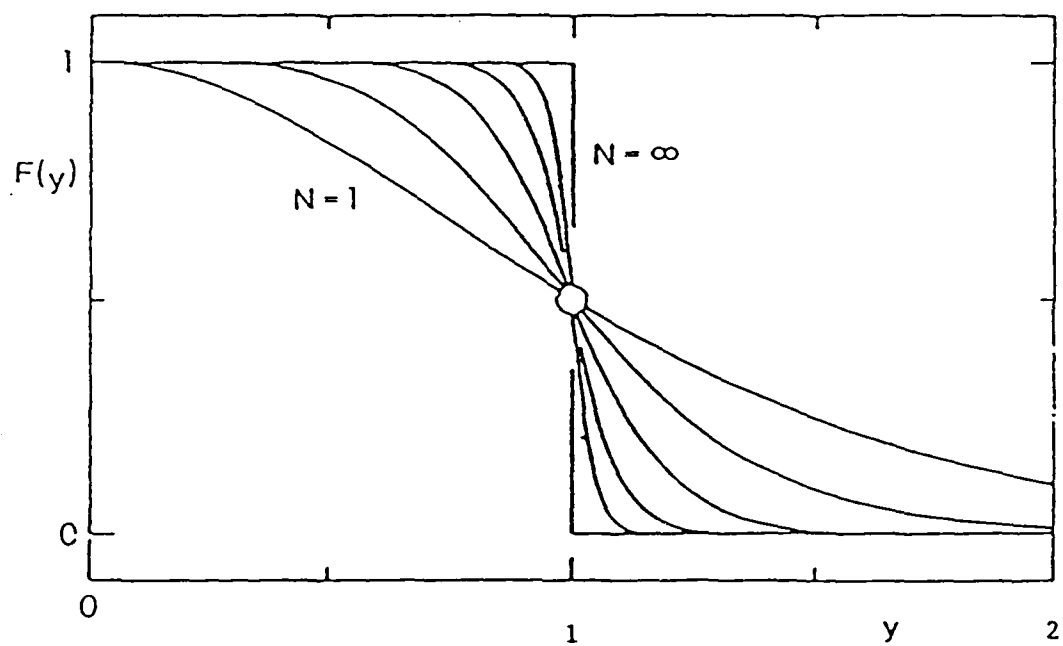
Figure 4   The family of mean velocity profile (2.1)
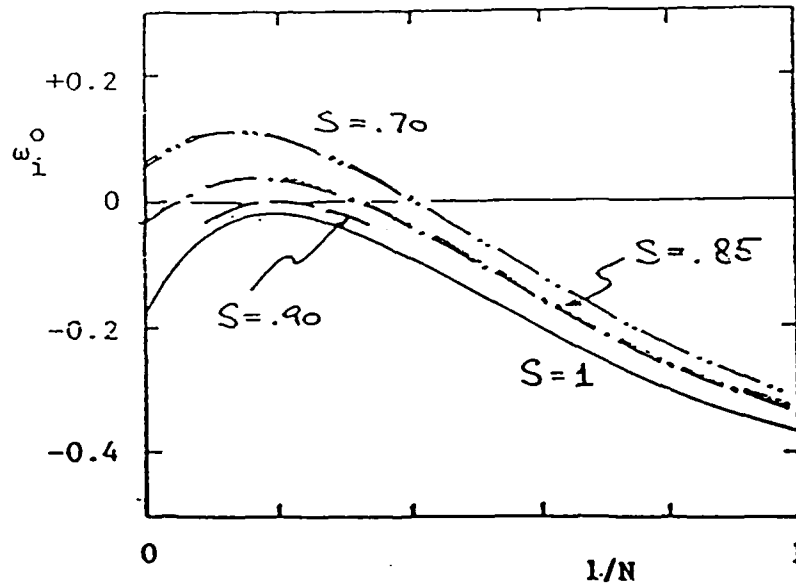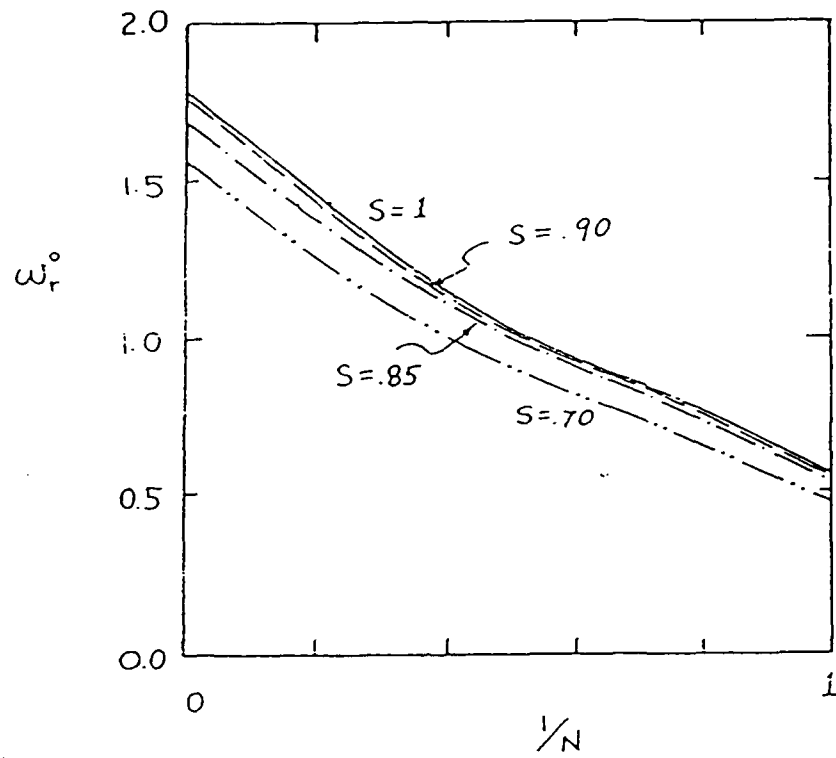
Figure 5   Branch point ω^o as a function of N^{-1} for the jet model
profiles defined in section 2.1, $\Lambda = 1$, S=1, 0.9, 0.85 and
0.7

39
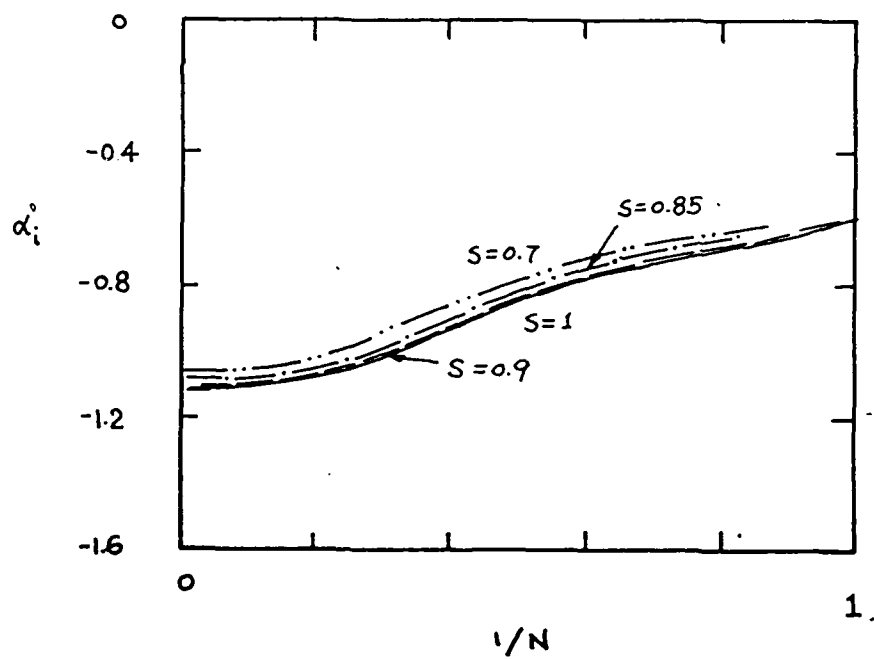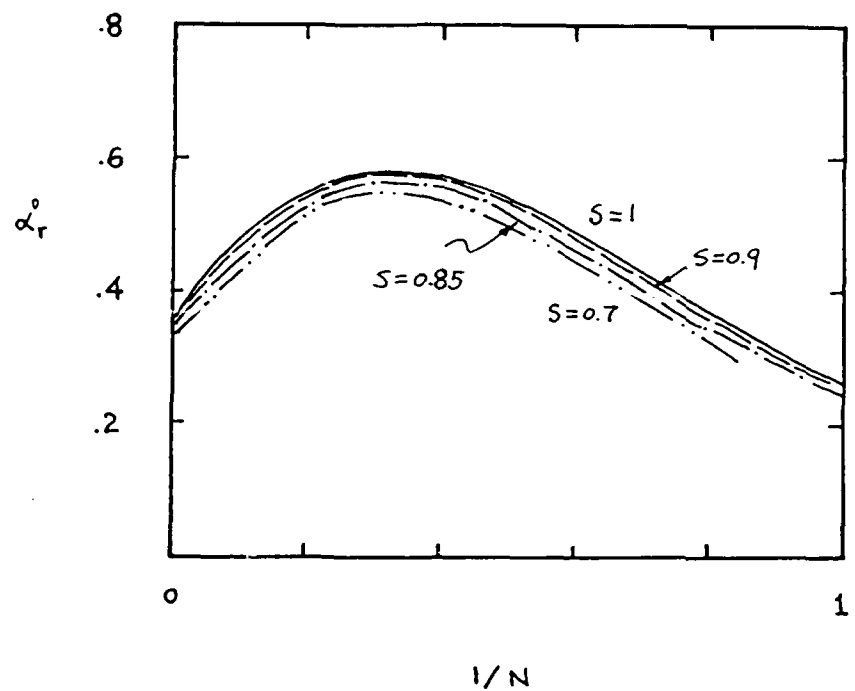
Figure 6   The saddle points α° corresponding to the ω° of figure 5.
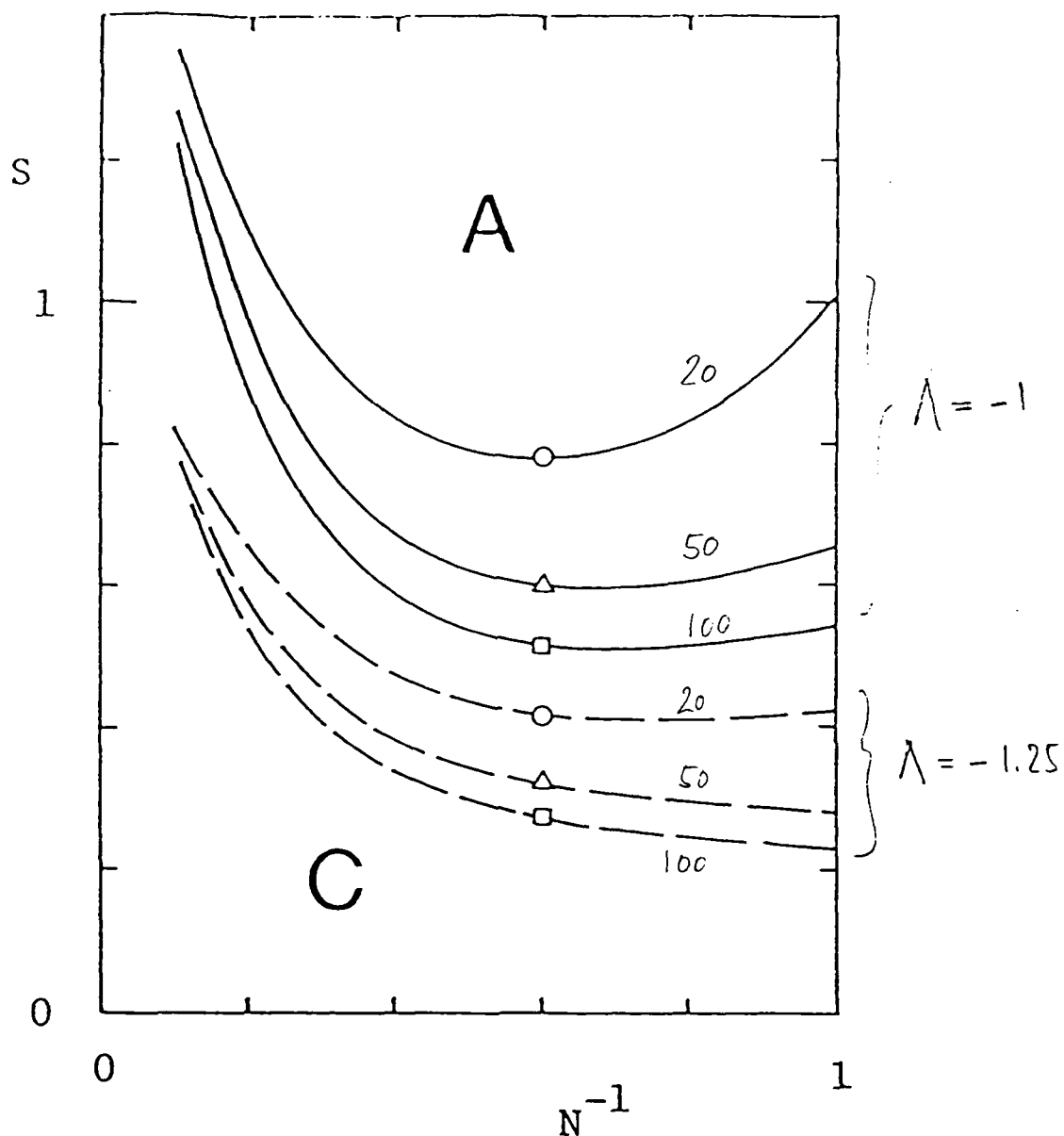
Figure 7   Absolute instability boundary of the wake model profile and
            mean density variation in the $S - N^{-1}$ plane, for Reynolds
            numbers of 20 ($\bigcirc$), 50 ($\triangle$), 100 ($\square$), and velocity ratio
            $\Lambda = -1$ (———) and $\Lambda = -1.25$ (-----)   with viscosity $\mu =$ constant.
            The regions of absolute and convective instability are
            marked by A and C, respectively.
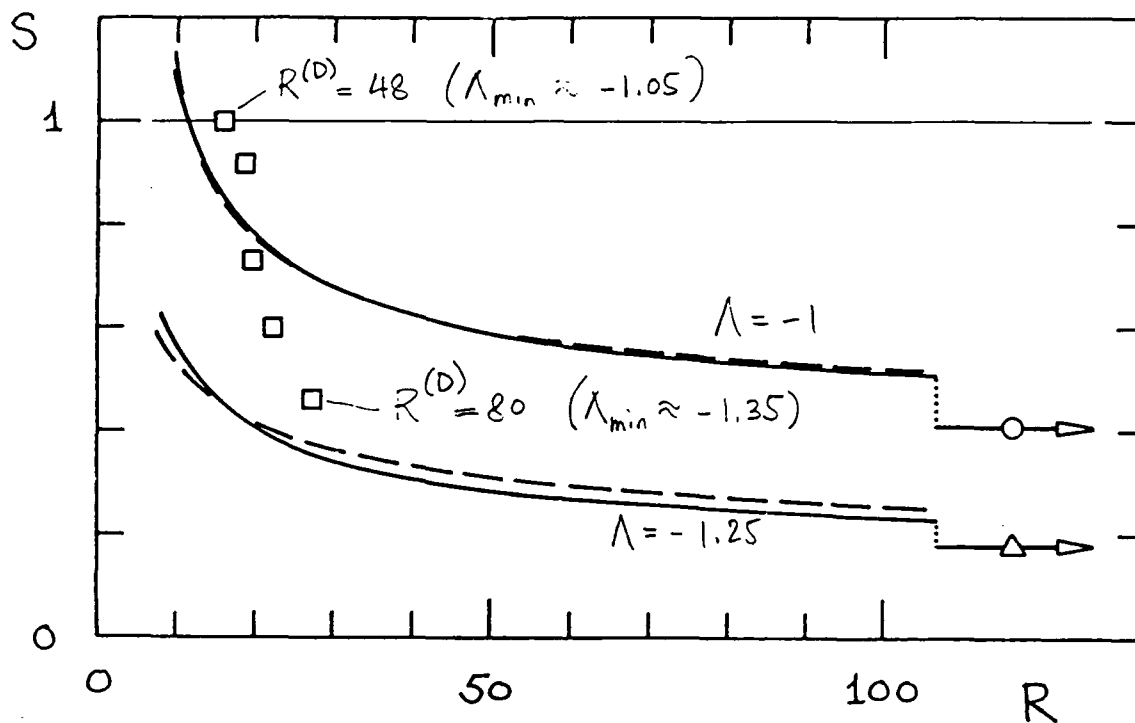
Figure 8   Absolute instability boundary of the variable density wake
in the S-R plane, for $\Lambda = -1$ (O) and $\Lambda = -1.25$ ($\triangle$), with
$\mu = \mu_\infty$ = constant (——), and $\mu = \mu(T)$ (-----). Experimental global
instability boundary ($\square$) from Berger & Schumm, 1988.

NOZZLE 1.5×30 cm

10:1 CONTRACTION

SCREEN
HONEYCOMB

FIBER
GLASS

120×120×60 cm BOX

STEEL WOOL

ALUMINUM WOOL

HEATER

MUFFLER   BLOWER

AIR FLOW ←

X
Z
Y
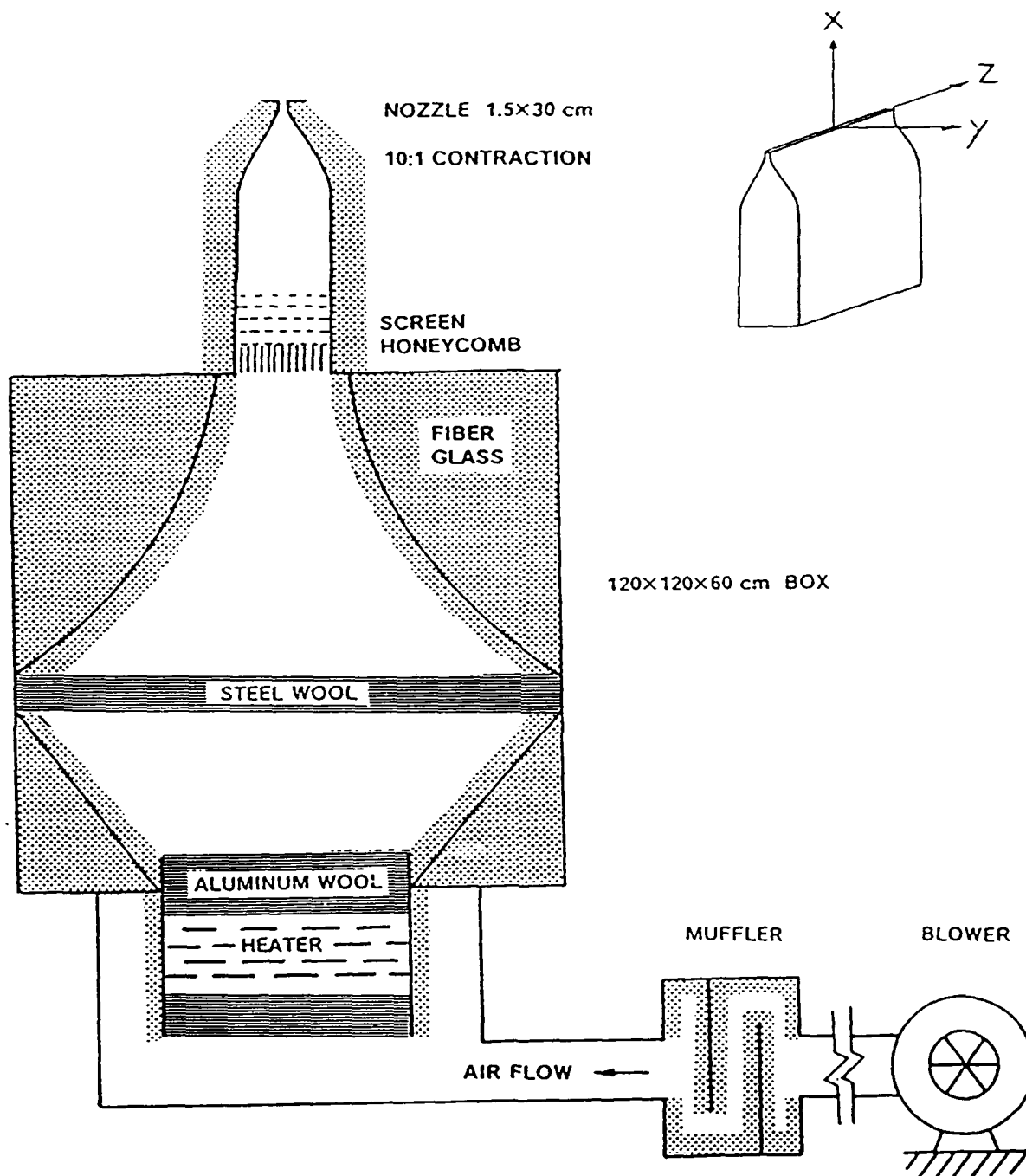
Figure 9   The heated 2-D jet facility.

$\dfrac{u'}{U_j}$

10 dB/div

0.06 % →

0   500 Hz

(a)

p'

(rel. dB)

10 dB/div

0   500 Hz

(b)
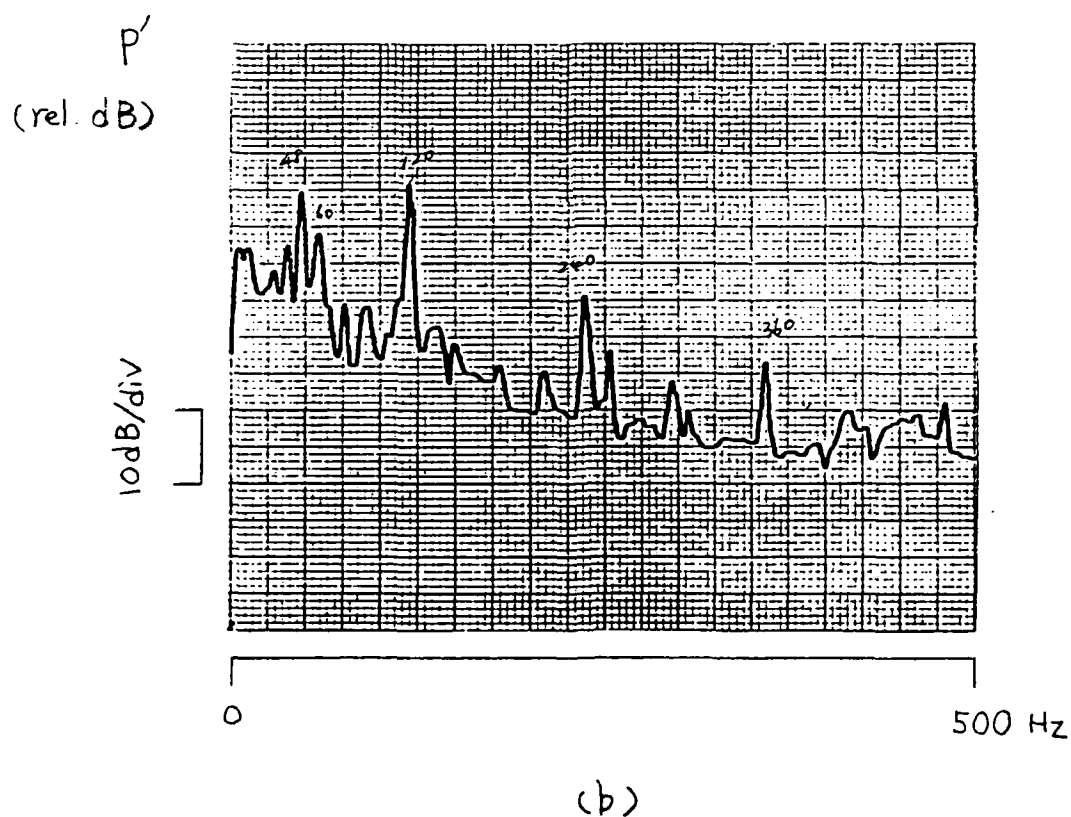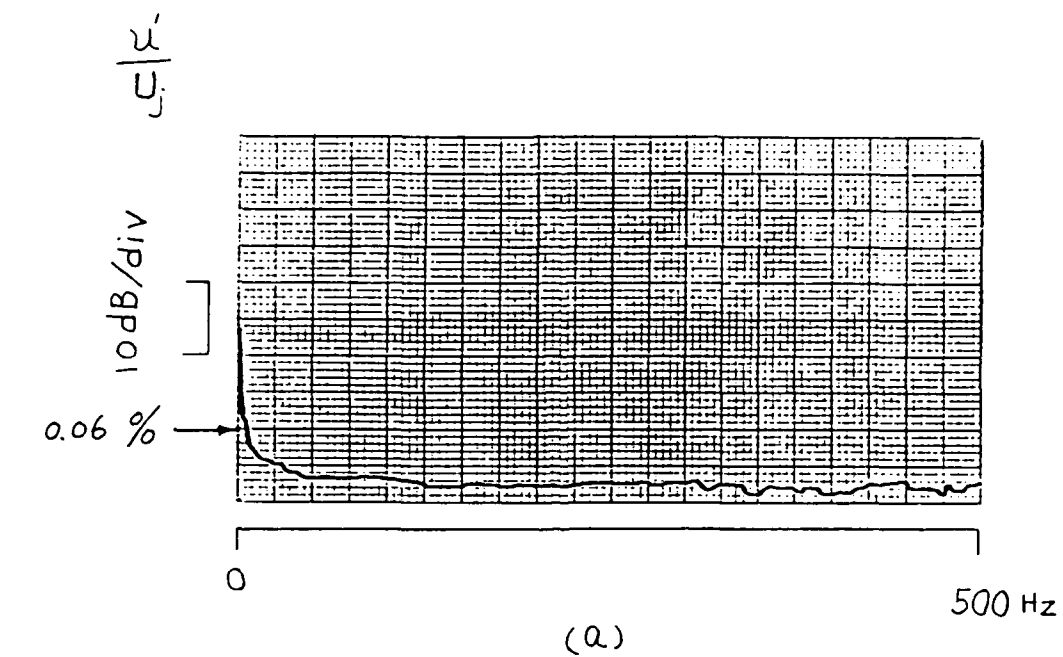
Figure 10   (a) The level of turbulent intensity of the 2-D jet facility at x=y=z=0 for q=1.25 mmH_2O, and (b) the acoustic pressure spectrum of the background noise with the jet turned off (microphone at x/H ~ 2, y/H ~ 1.3)

44

SPARK
20 ns

PINHOLE
$\phi = 2$ mm

2-D JET NOZZLE
ASPECT RATIO 20:1

150 mm SPHERICAL MIRROR

IRIS

CAMERA
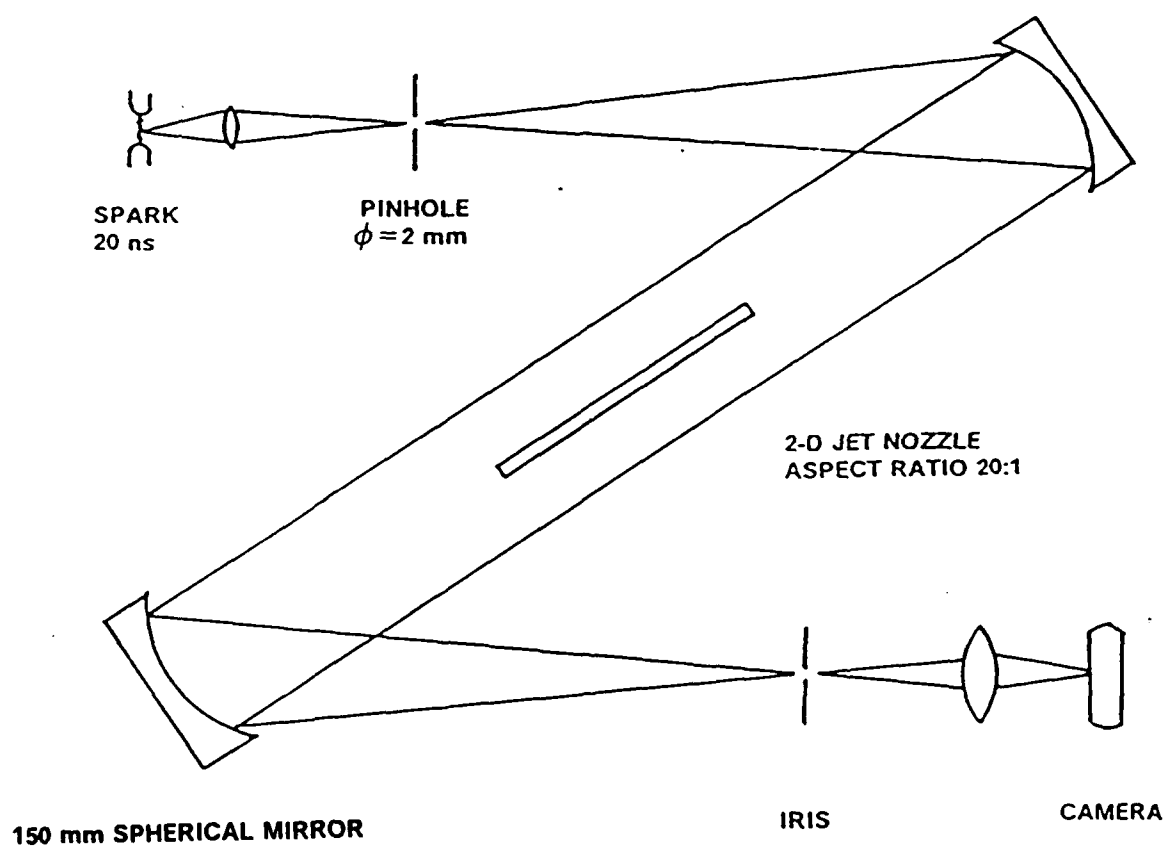
Figure 11   The Schlieren system
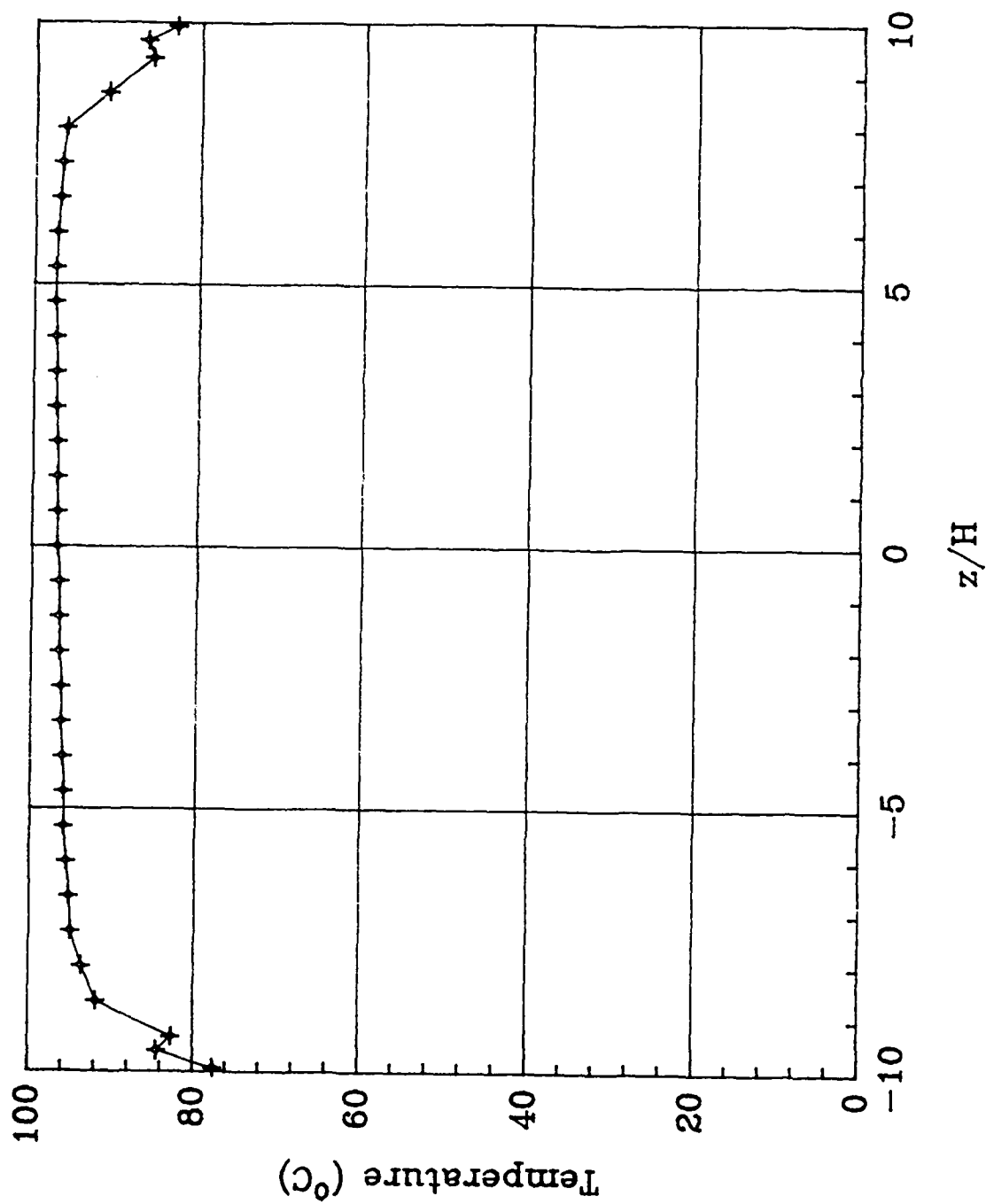
Figure 12   Mean temperature profile $\overline{T}(z)$ at x=y=0 for q=0.79 mmH_2O

46
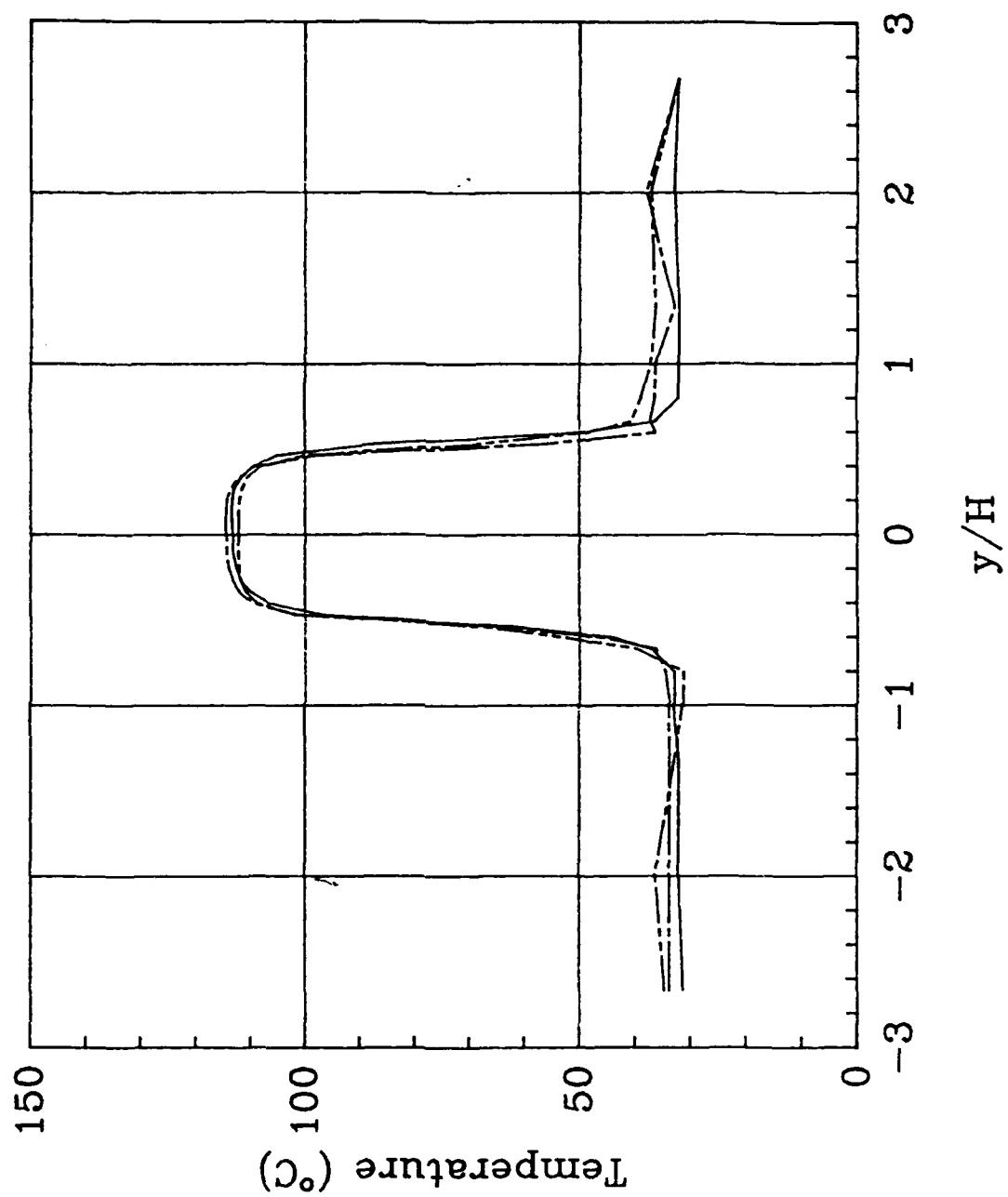
Figure 13 $\overline{T}(y)$ at x=0, z/H=-6.7 (— — —),   z/H=0 (——),   z/H=6.7 (— – —),   q=0.75 mmH_2O .
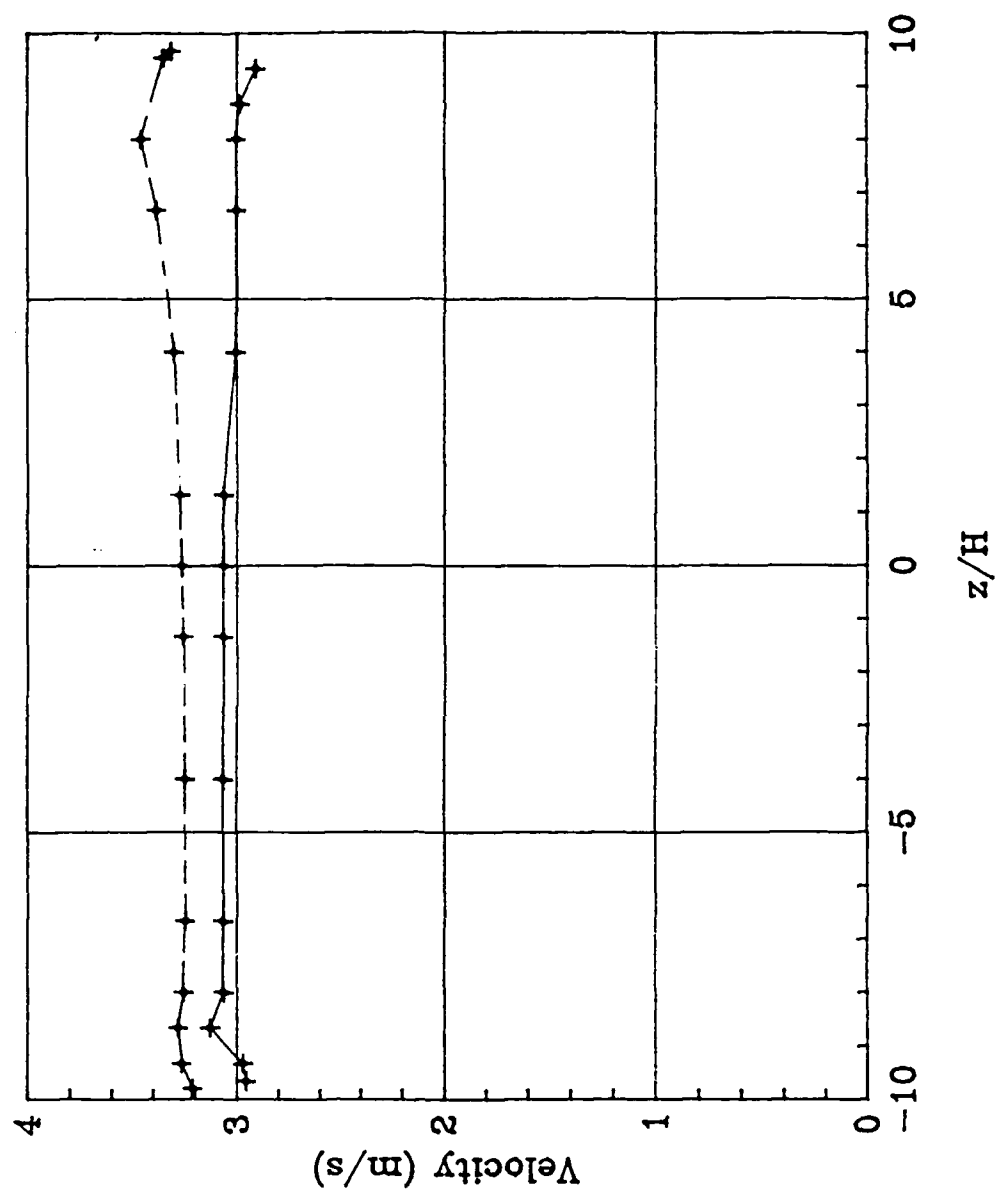
Figure 14 $\overline{V}(z)$ at y=0, q=0.75 mmH_2O,   S=1,   x/H=0 (——) ,   x/H=8
(— —) .
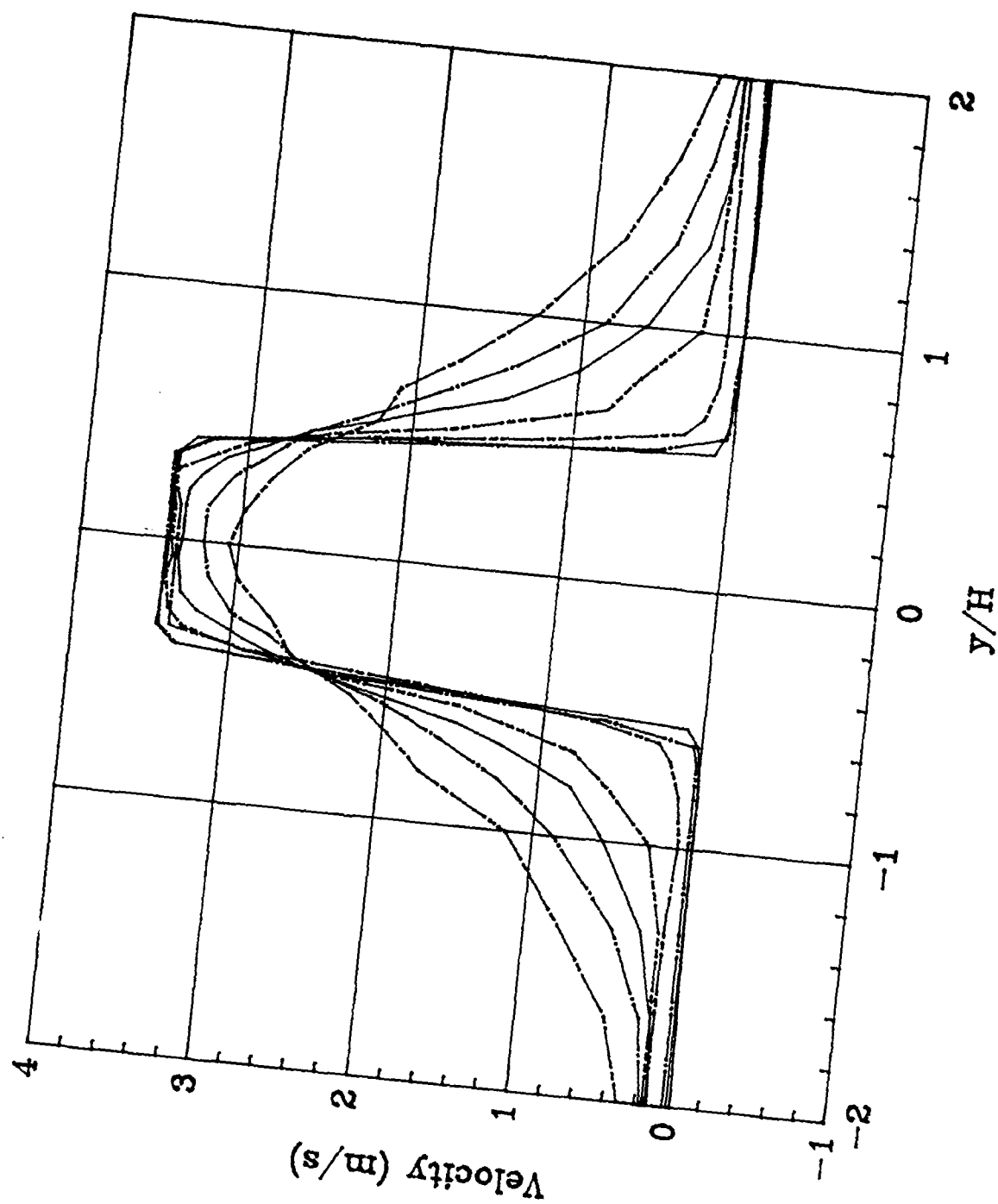
Figure 15 $\bar{V}(y)$ at $z/H=0$, $x/H=0,1,2,3,4,6,8$. $q=0.75$ mmH_2O, $S=1$.

49
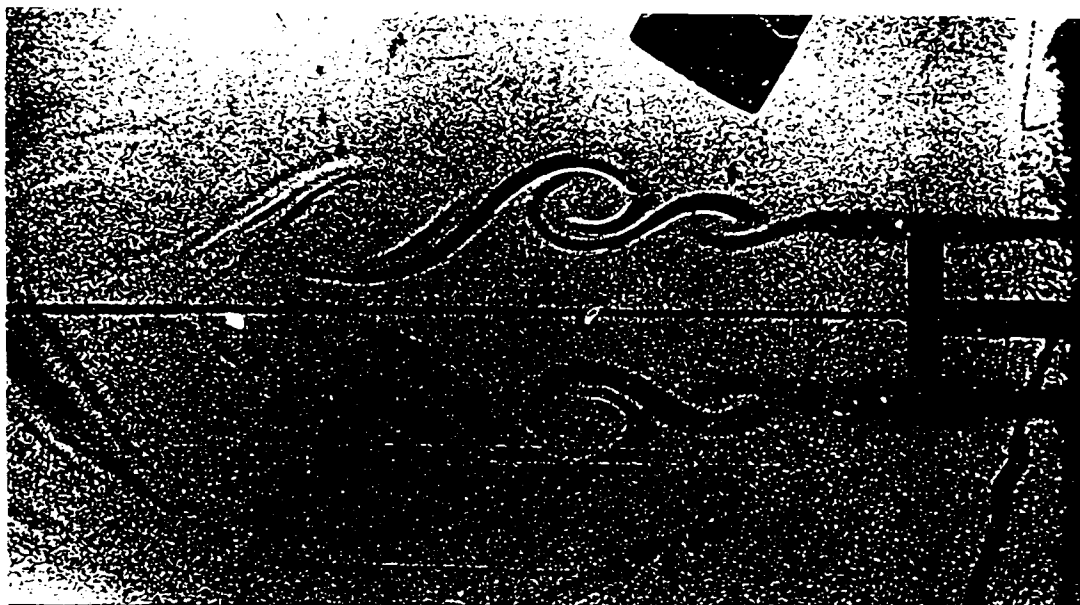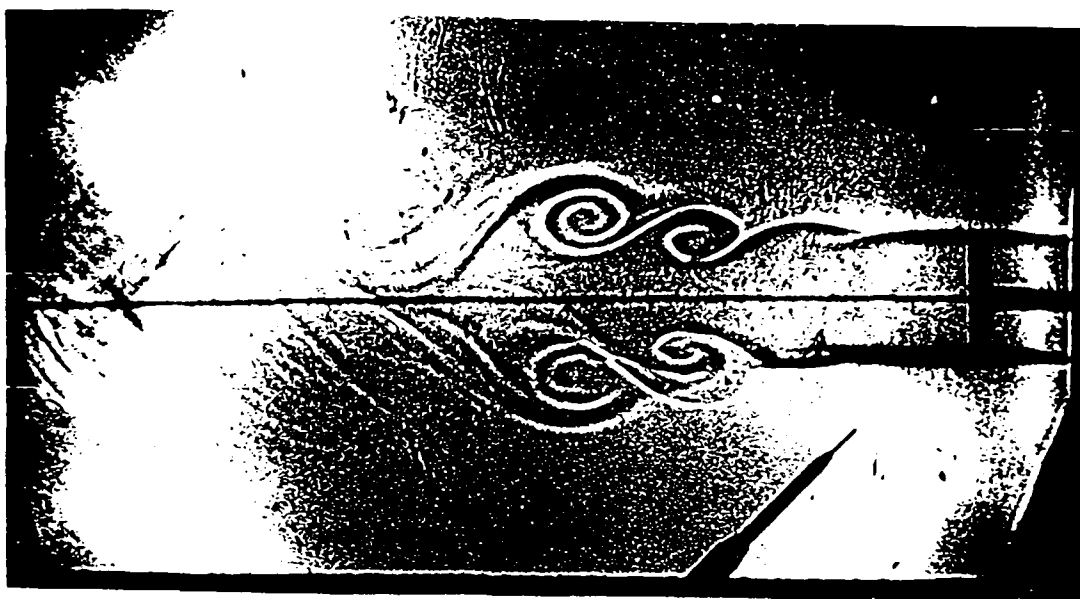
Figure 16(a)

Figure 16(b)

Figure 16   Spark Schlieren views of the slightly heated jet and
self-excited hot jet (20 ns exposure time; length of 'T'
mark = jet width) (a)   Slightly heated jet with S= ρ/ρ_∞
=0.90 ($T = 42\,C$). q=1.04 mmH_2O (b)   Slightly heated jet with
S=0.90 ($T = 42\,C$). q=1.31 mmH_2O (c)   Hot jet with S=0.73
($T = 133\,C$) , q=1.04 mmH_2O (d) (e) and (f) Hot jet with
S=0.73 ($T = 133\,C$) , q=1.31 mmH_2O

Figure 16(c)

Figure 16(d)

51
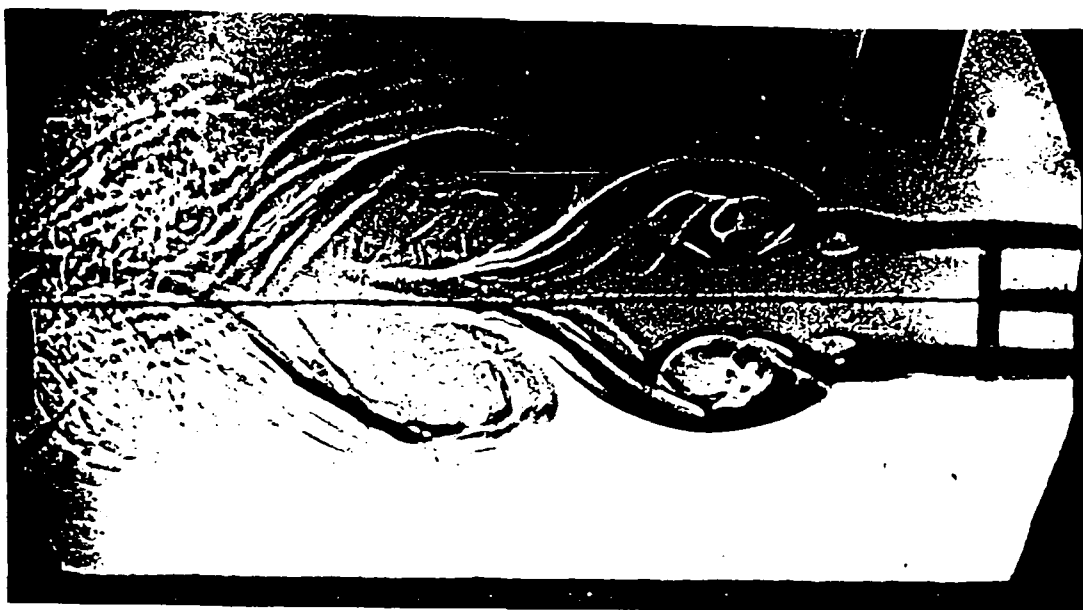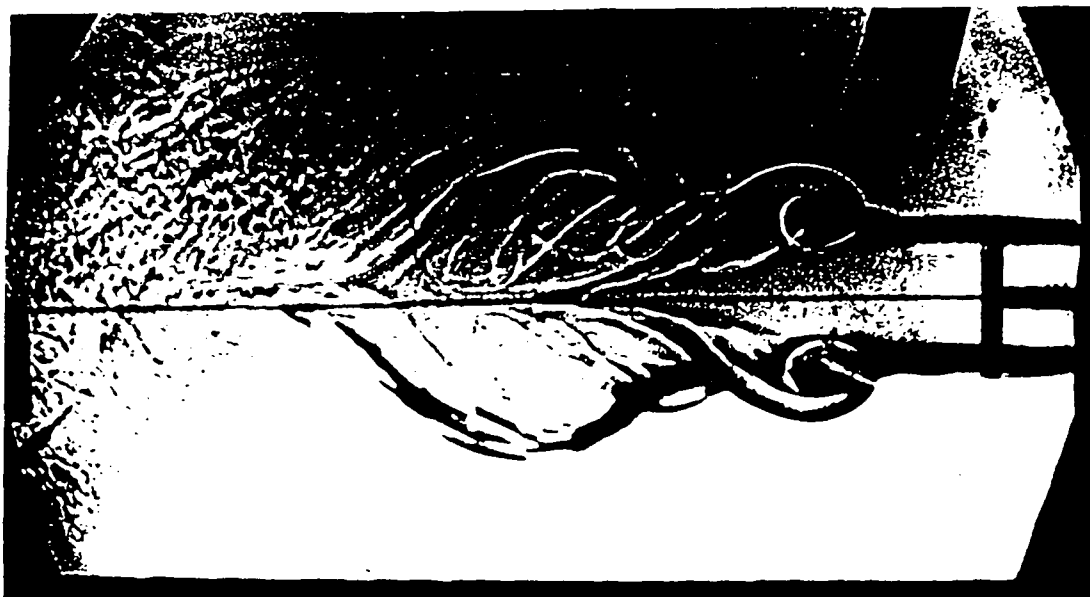
Figure 16(e)

Figure 16(f)
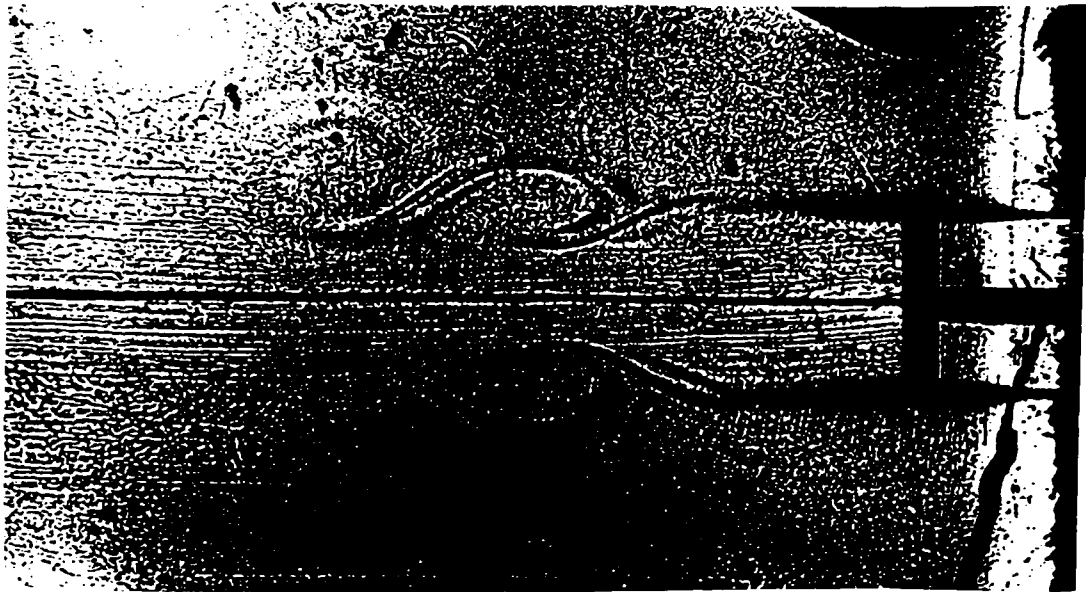
Figure 17(a)
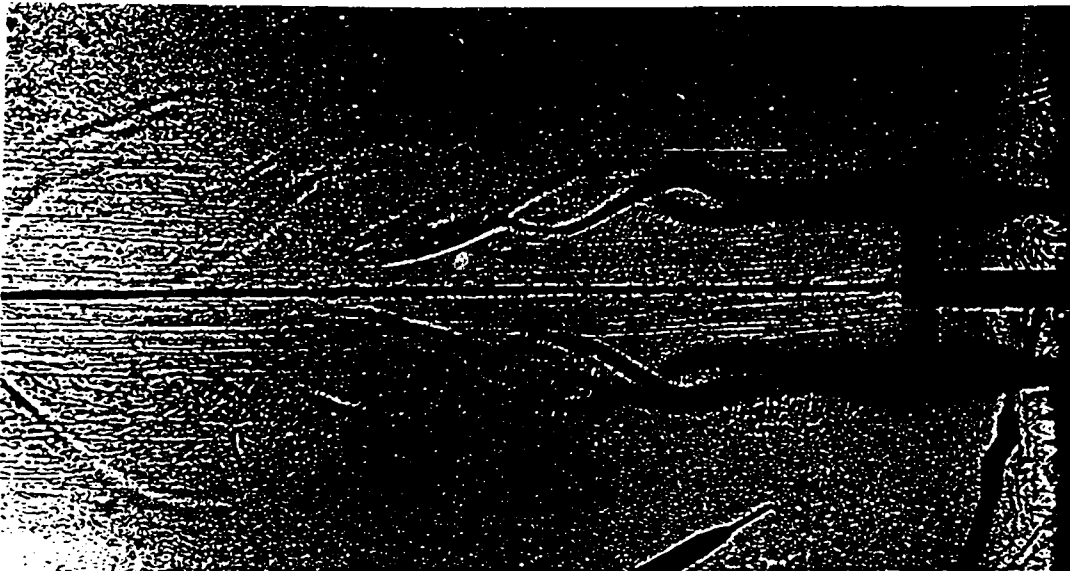
Figure 17(b)

Figure 17   Schlieren images of the heated jet at different density
            ratio
                    (a)   S=0.95, q=0.76 mmH_2O
                    (b)   S=0.89, q=0.83 mmH_2O
                    (c)   S=0.81, q=0.75 mmH_2O
                    (d)   S=0.81, q=0.75 mmH_2O
                    (e)   S=0.81, q=0.75 mmH_2O
                    (f)   S=0.79, q=0.75 mmH_2O

53

Figure 17(c)

Figure 17(d)

54
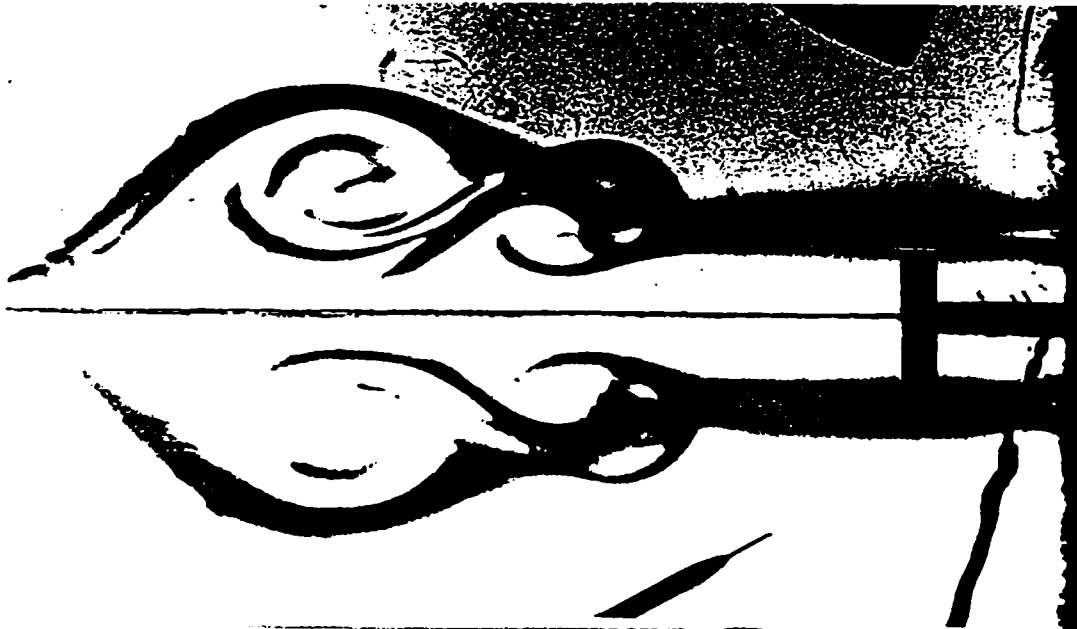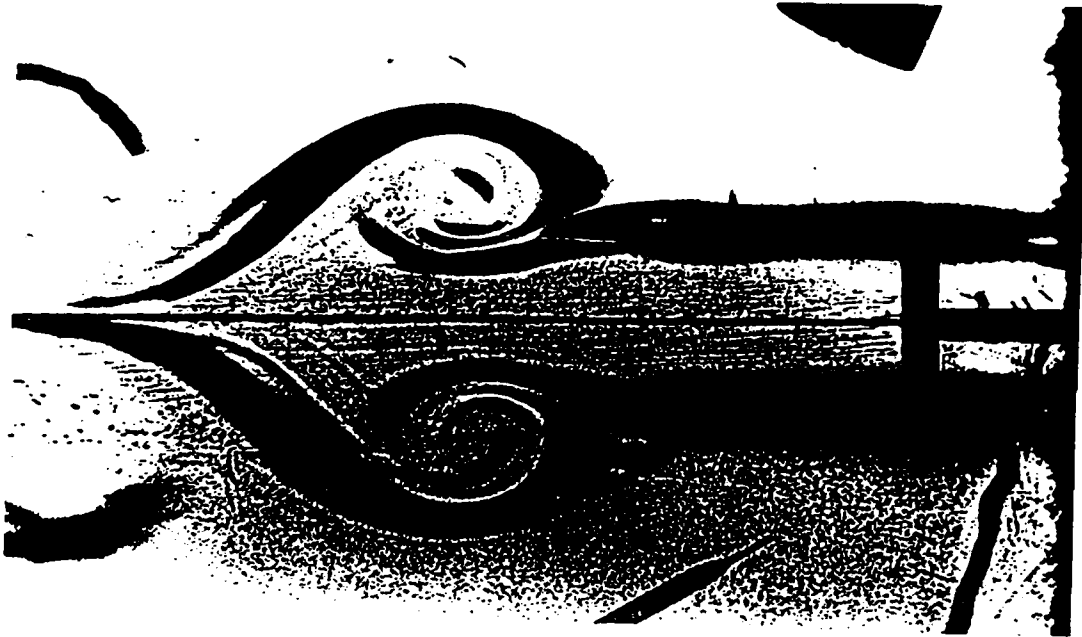
Figure 17(e)

Figure 17(f)
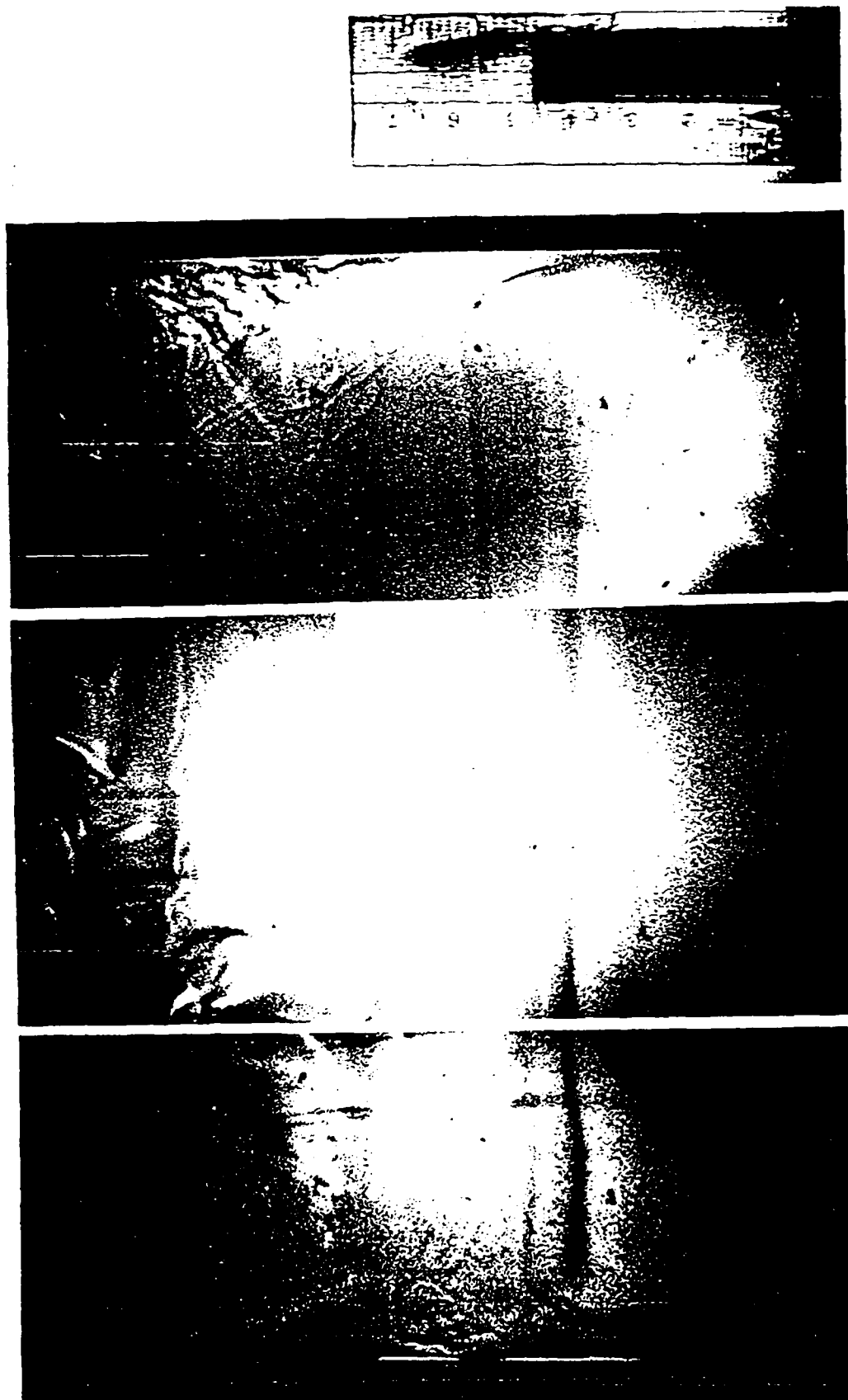
Figure 18   Side view of the heated jet with S=0.75, for q=1.30 mmH_2O
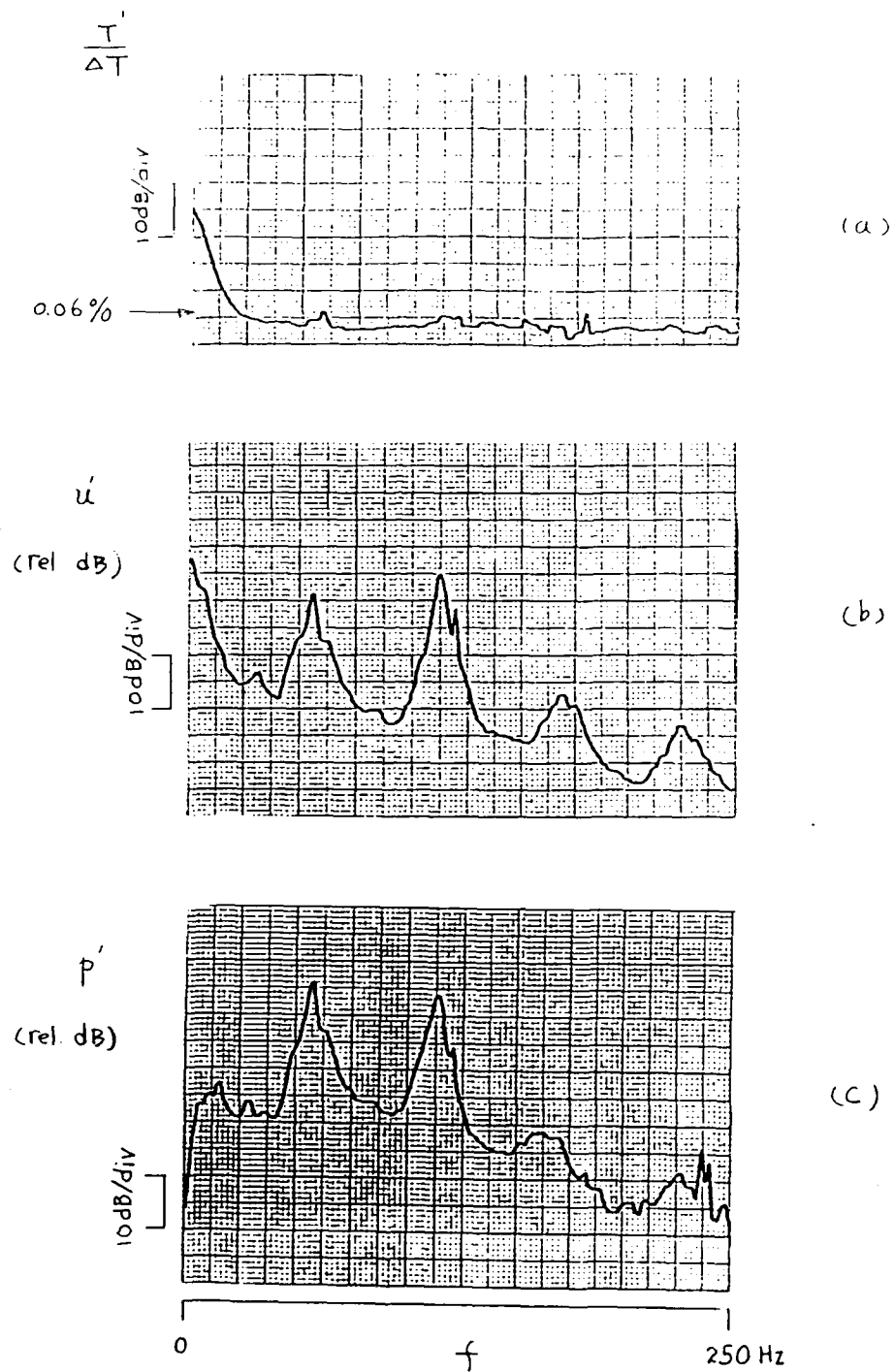
Figure 19 Temperature, velocity, pressure spectra of hot jet in the entrainment region, x/H=1.67, y/H=1, for q=1.30 mmH_2O, T = 120°C
  (a) Temperature spectra
  (b) Velocity spectra, the first two peaks occur at 56, 113 Hz
  (c) Pressure spectra, the first two peaks occur at 56, 113 Hz
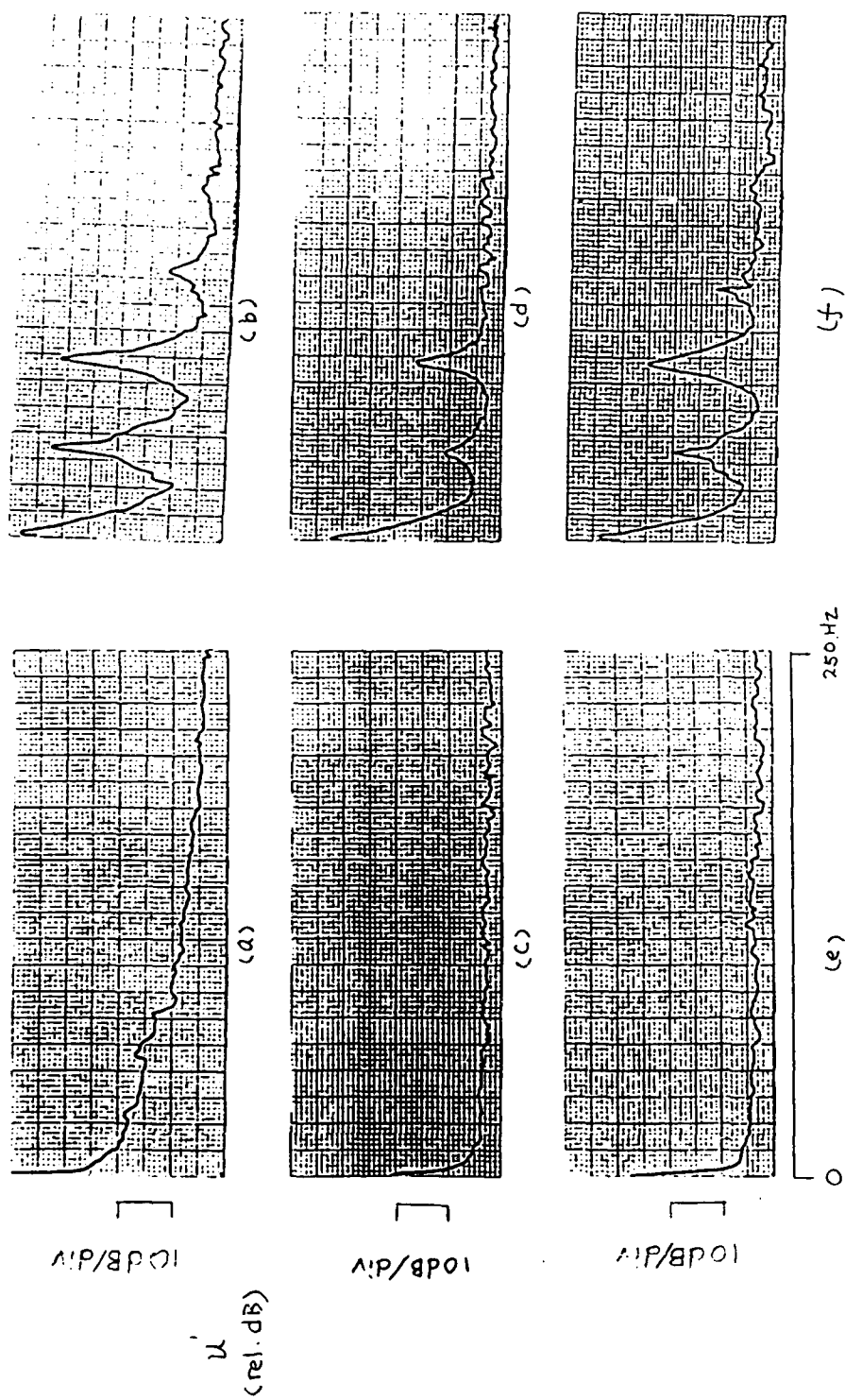
Figure 20 Velocity spectra of the cold jet (S=1) and the hot jet with
S=0.76 at different locations in the entrainment region
for q=0.85 mmH_2O

(a) S=1 and (b) S=0.76   at x/H=2.00, y/H=1.33
(c) S=1 and (d) S=0.76   at x/H=1.00, y/H=1.00
(e) S=1 and (f) S=0.76   at x/H=1.00, y/H=0.67

58

T'

$(rel.\ dB)$

$10dB/div$

$0 \qquad f \qquad 250\ Hz$
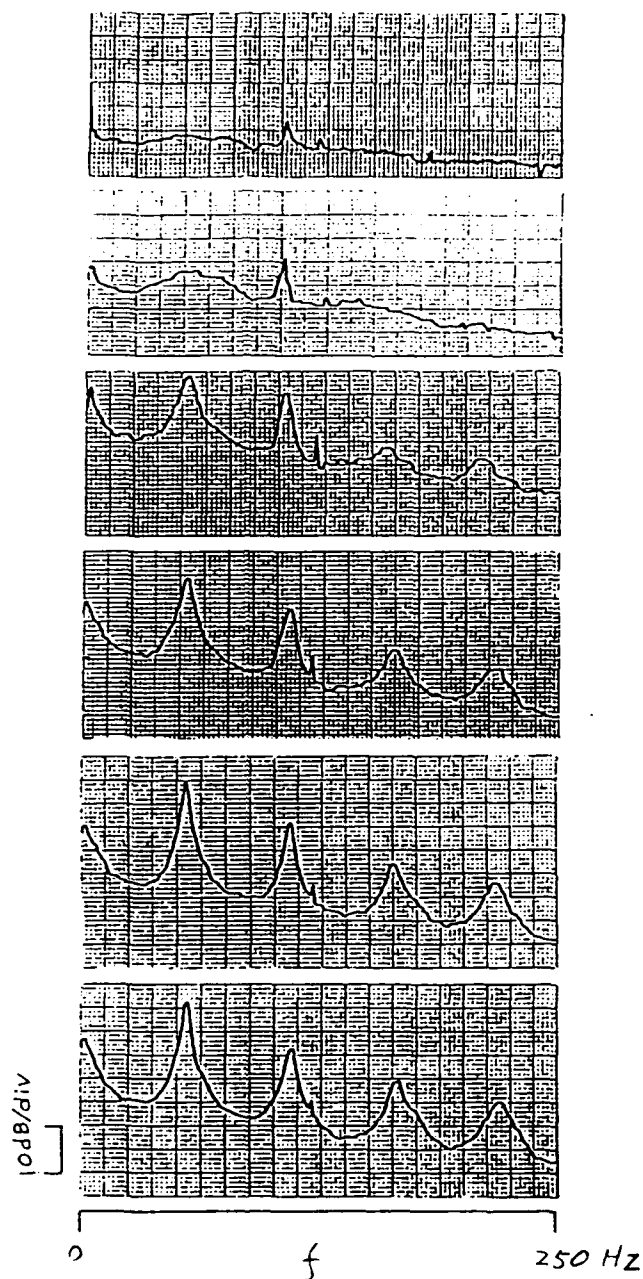
Figure 21   Temperature spectra as function of density ratio for
constant total head $q = 1.26mmH_2O$, hot wire probe at x/H=3
and y/H where the maximum amplitude of dominant frequency
mode was obtained.
(a) At maximum amplitude of the first peak (frequency
$f_o \simeq$ 54 Hz). Spectra were obtained at approximately y/H=0.9
for each case. From top to bottom S=0.97,0.94,
0.88,0.85,0.82,0.75.

T'

$(rel. dB)$

$10 dB/div$

0 f $250 Hz$
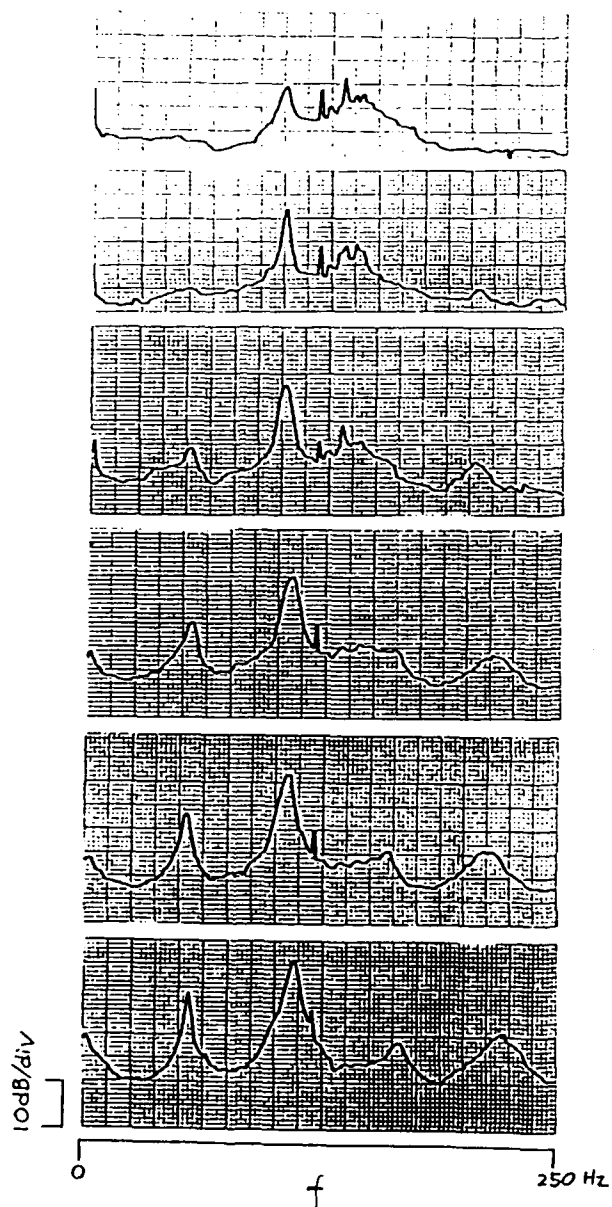
Figure 21   (b)   At maximum amplitude of the second peak with
frequency $2f_o$. Spectra were obtained at approximately
y/H=0.4 for each case. From top to bottom
S=0.97,0.94,0.89.0.85, 0.82,0.75.

60
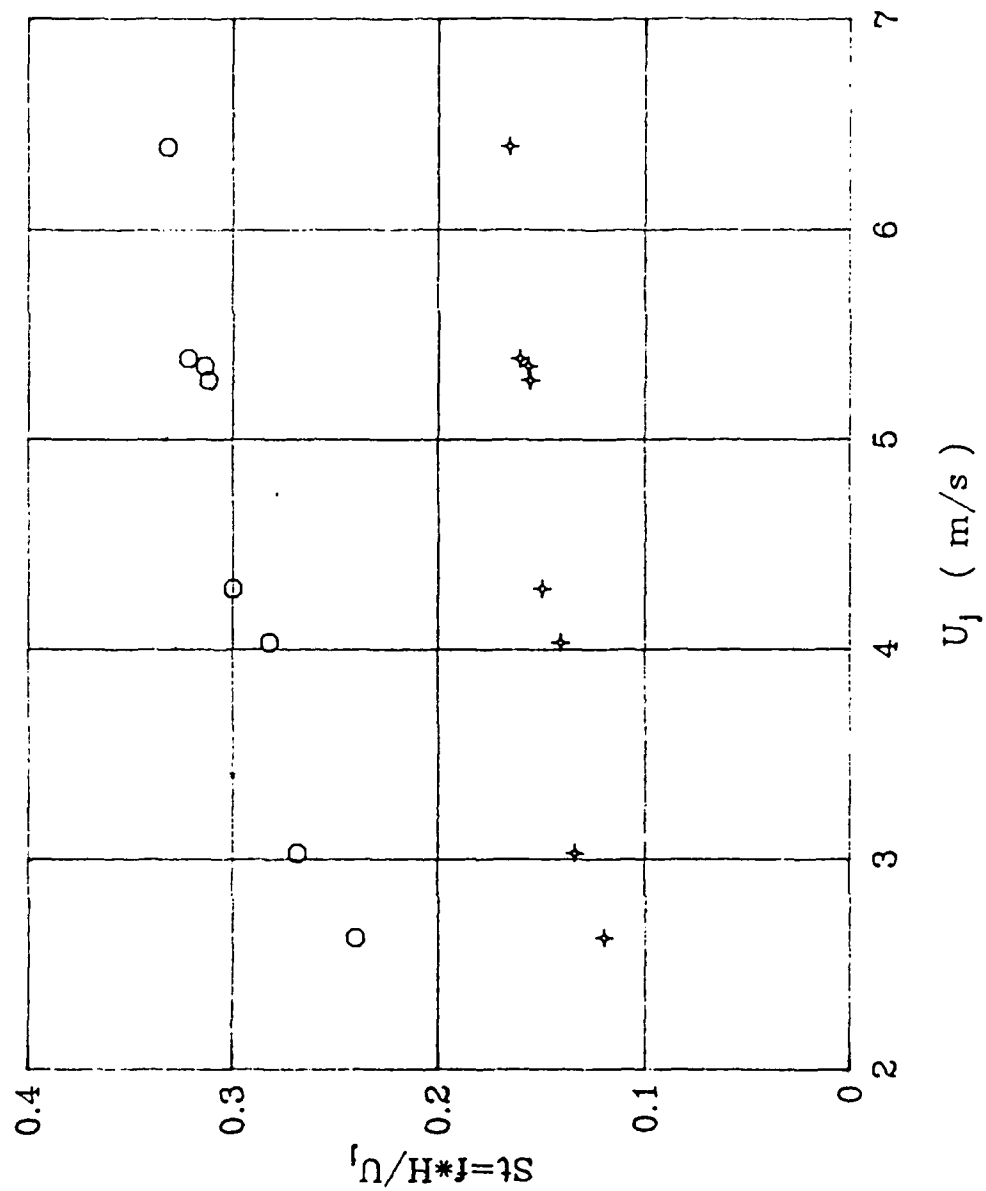
Figure 22   Dominant Strouhal numbers in the line-dominated spectra
for the lowest frequency peak f_o (+), and for the frequency
$2f_o$ (O).   S=0.76
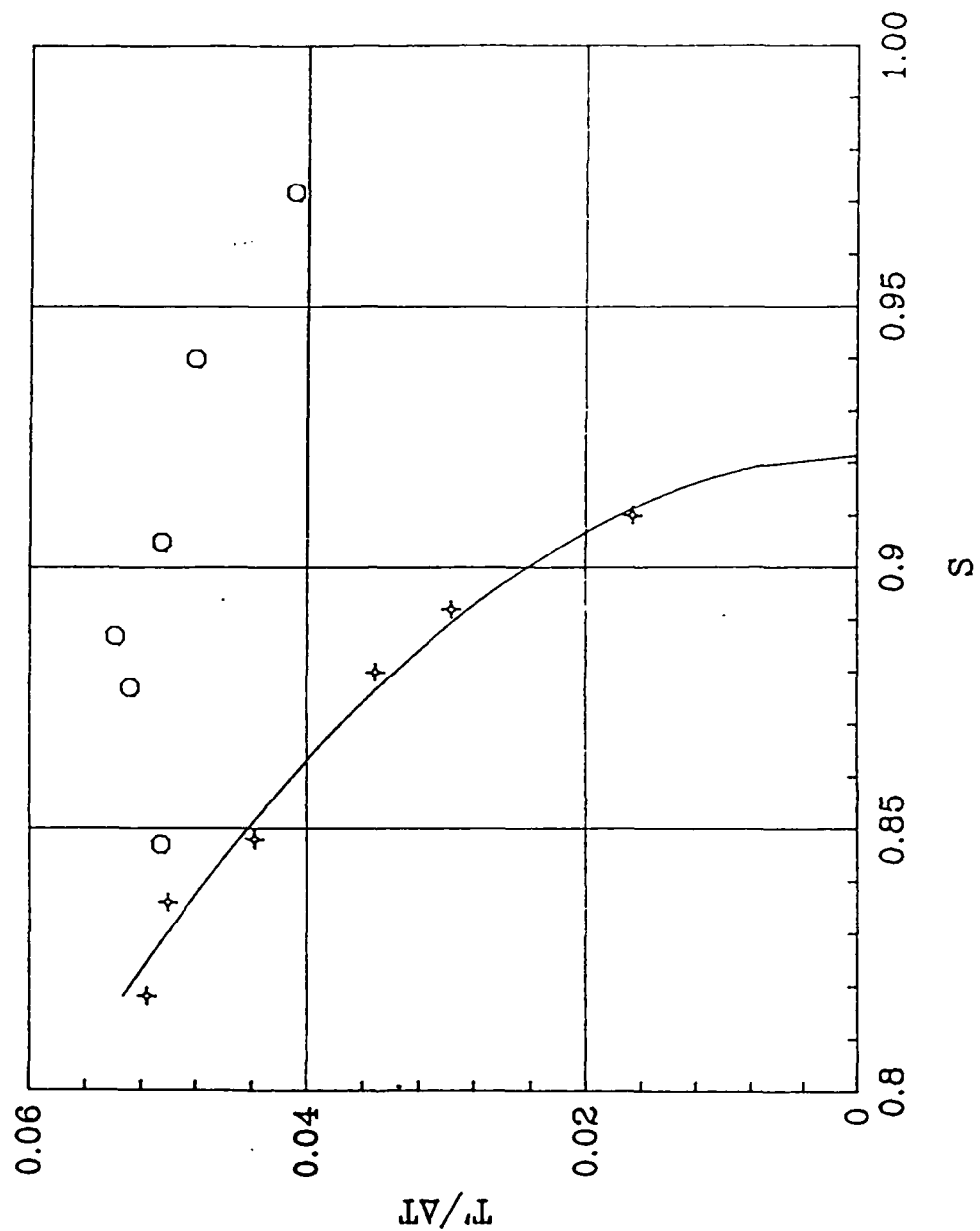
Figure 23   Amplitude of the dominant near-field temperature oscil-
lation, normalized by the mean temperature difference
$\Delta T = T_j - T_{ambient}$, versus density ratio S. $+$: peak at
$f_o \simeq 54 Hz$; $\bigcirc$: peak at 2 f_o .   q=1.26 mmH_2O , probe at
x/H=3.0.   Solid curve is given by $T'/\Delta T \propto (S_{crit} - S)^{1/2}$, fitted
to the data.
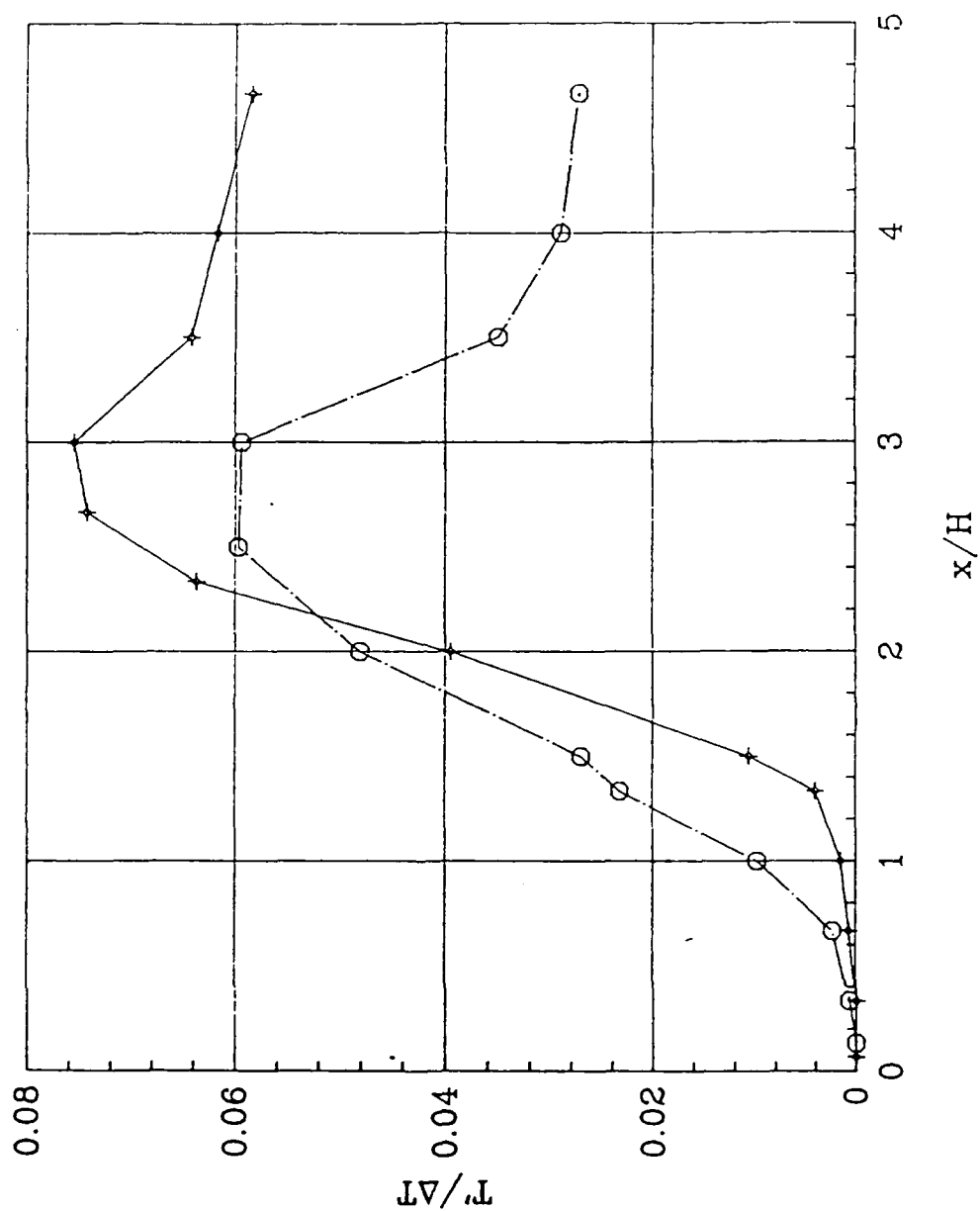
Figure 24   Amplitude of dominant spectral components versus streamwise
coordinate x/H.   St=0.157 (——),   and St=0.314 (− · −).
$q = 1.25 mmH_2O$,   S=0.75.
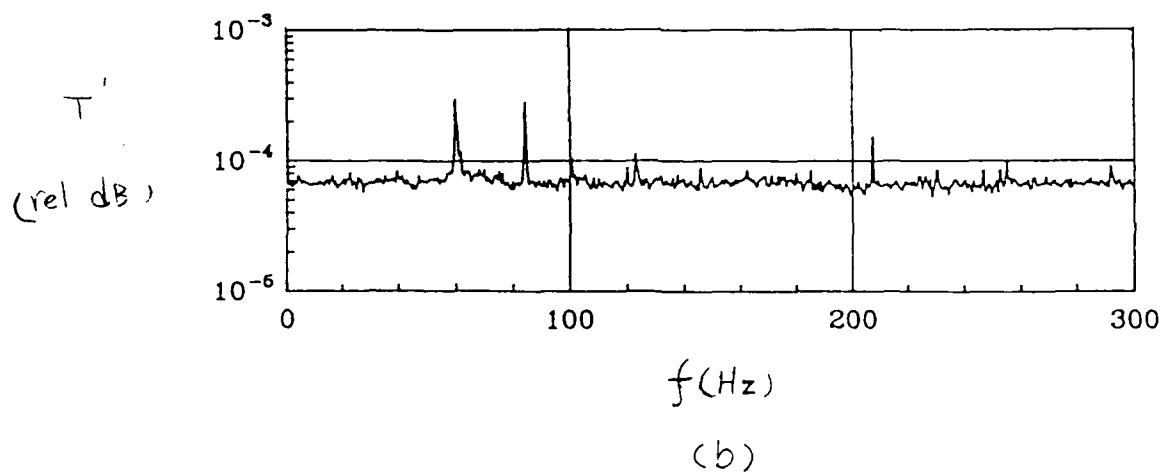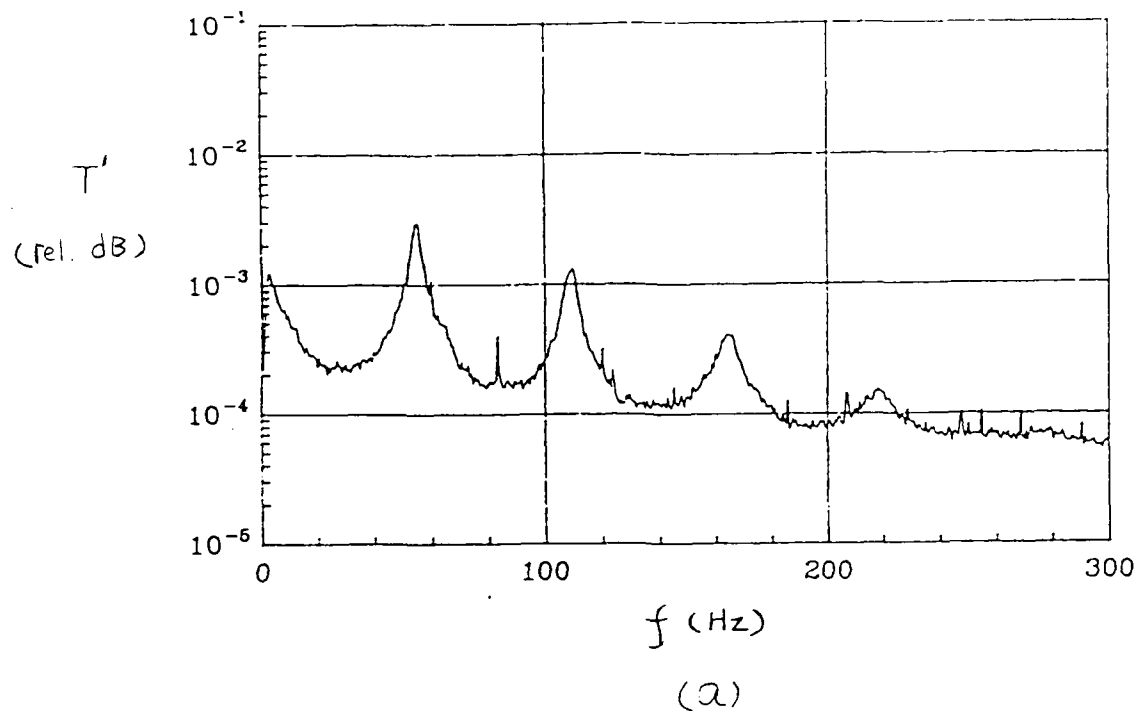
Figure 25   (a) Amplitude spectrum of temperature fluctuation in a hot
jet by FFT with S=0.77, q=1.26 mmH_2O,   at x/H=3.0, y/H=0.9
(b) Amplitude spectrum of temperature fluctuation in a
slightly heated jet with S=0.95, q= $1.26mmH_2O$ at the same
location as in (a).
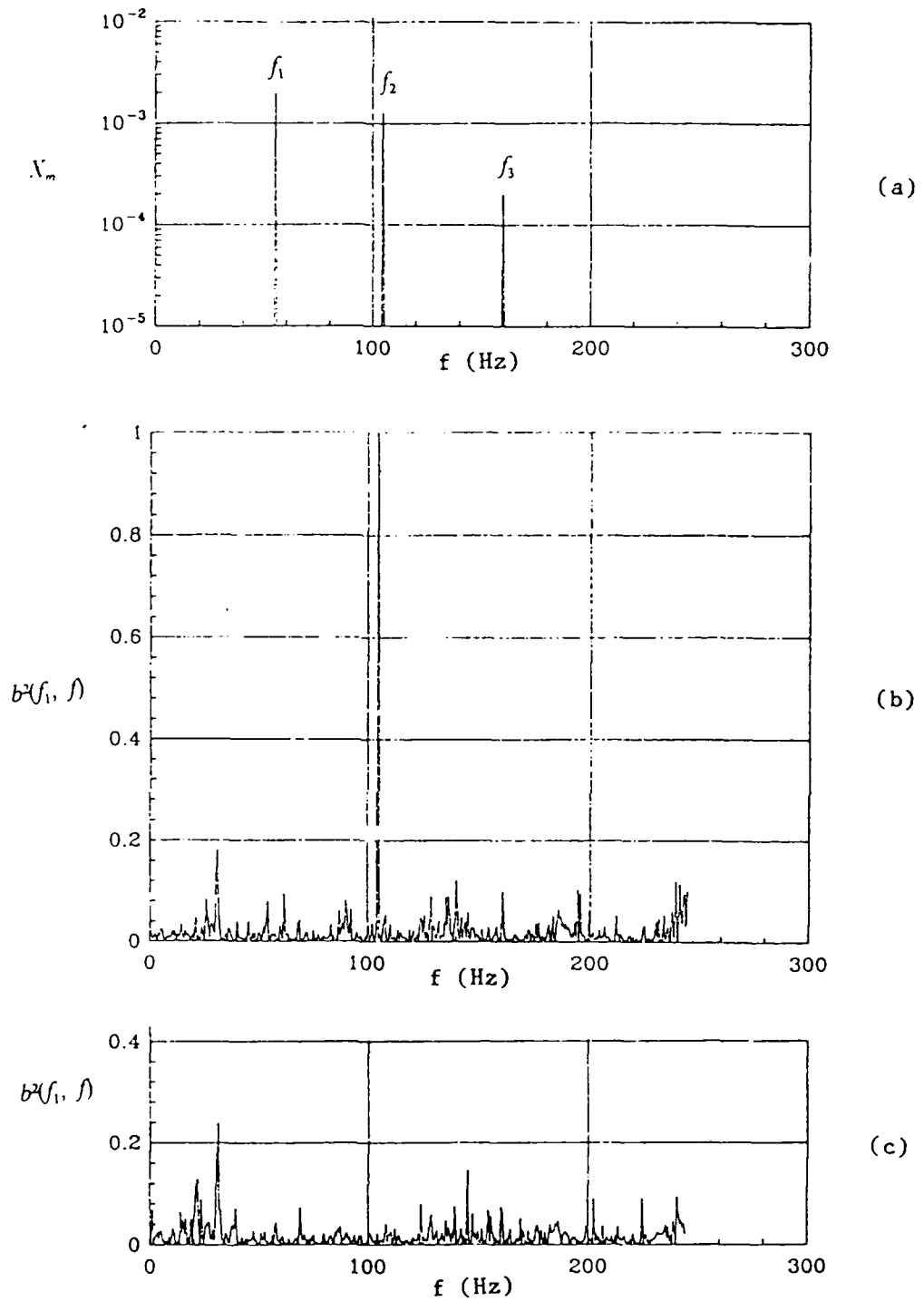
Figure 26   (a) Amplitude   spectrum of test signal (3.4) with
$f_1 = 55Hz$, $f_2 = 104Hz$, $f_3 = f_1 + f_2$. (b) Bicoherence $b^2(f_1, f)$ with
θ_1, θ_2 arbitrary and $\theta_3 = \theta_1 + \theta_2$ (c) Same but all phases
θ_1, θ_2, θ_3 random.
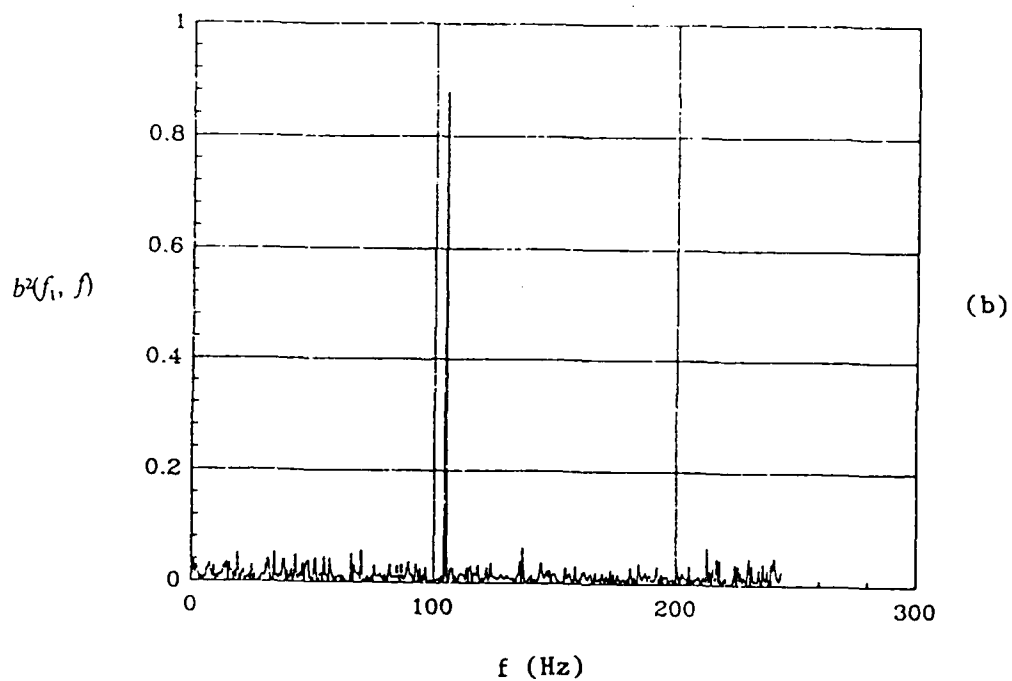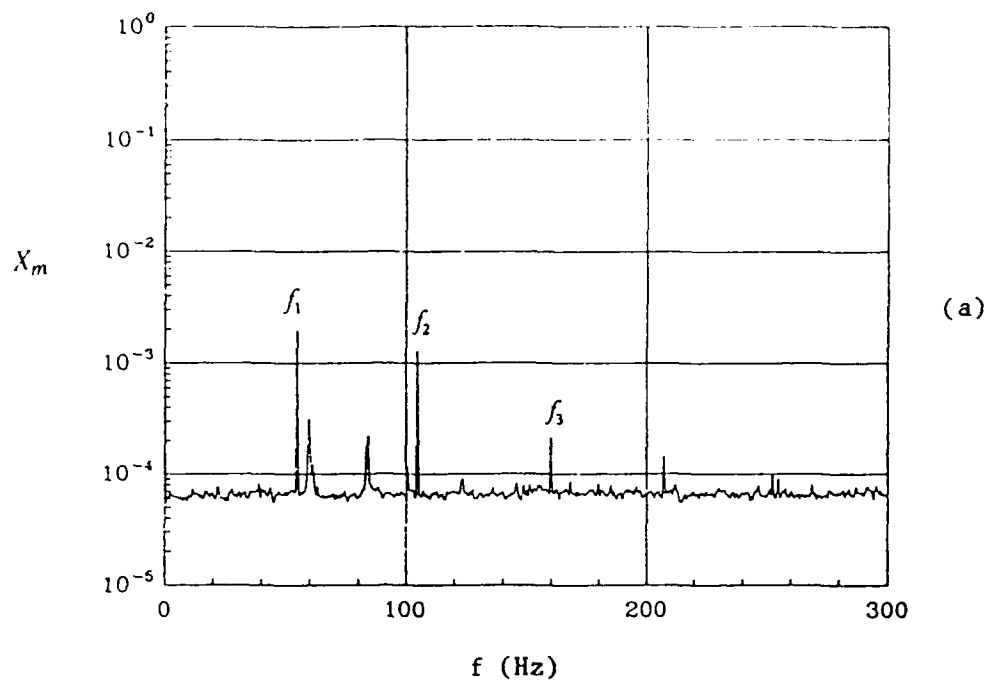
Figure 27   (a) Amplitude spectrum of the test signal (3.4) as in Figure
26 superimposed on the noisy spectrum of Figure 25(a).
(b) $b^2(f_1, f)$ with $\theta_3 = \theta_1 + \theta_2$.
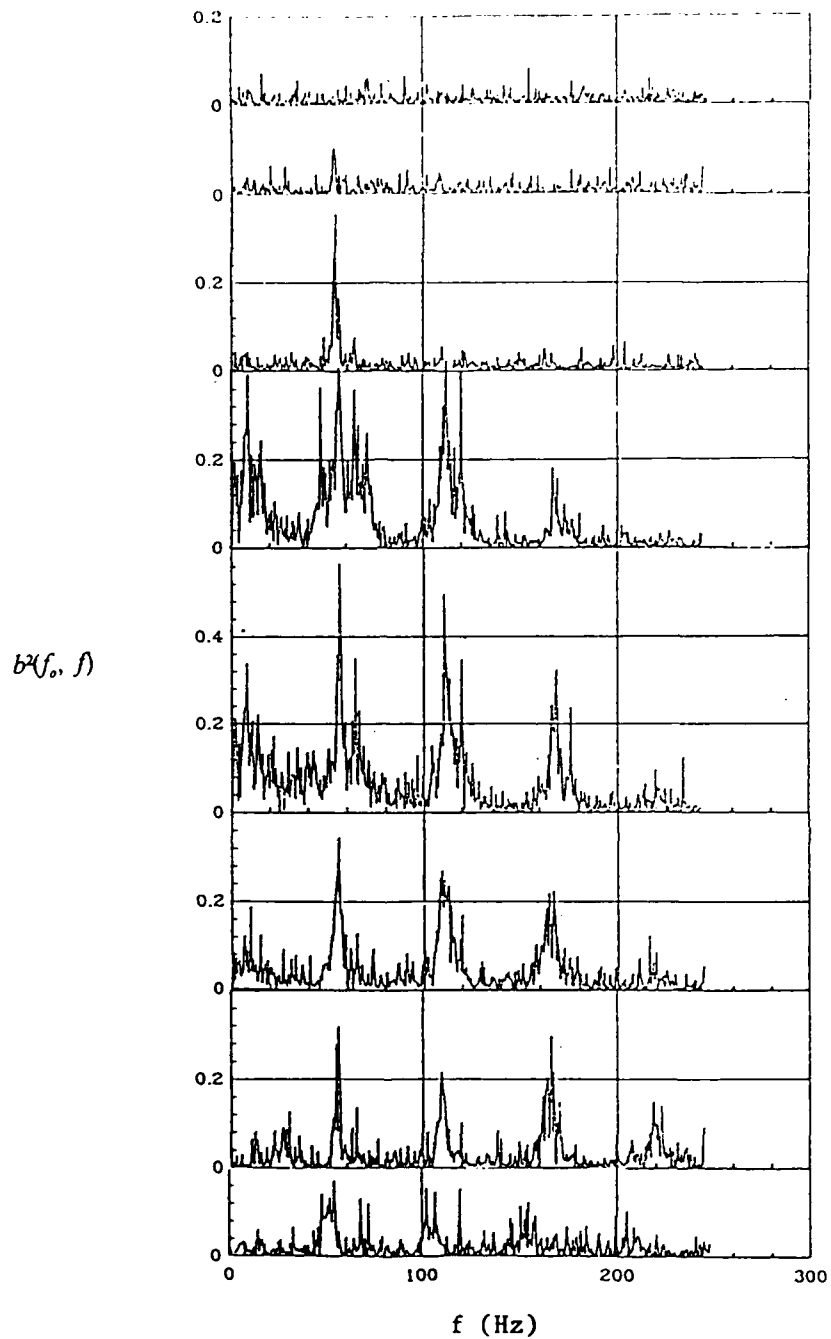
Figure 28   Bicoherence $b^2(f_0, f)$ of temperature in the hot jet with S=0.77
            and q= 1.26 *mm/l$_2$O* at different streamwise location and
            corresponding y/H, where maximum amplitude of the dominant
            frequency f_0 was obtained. From top to bottom, x/H=0.5,
            1.0, 1.5, 2.0, 2.5, 3.0, 4.0, and 5.0
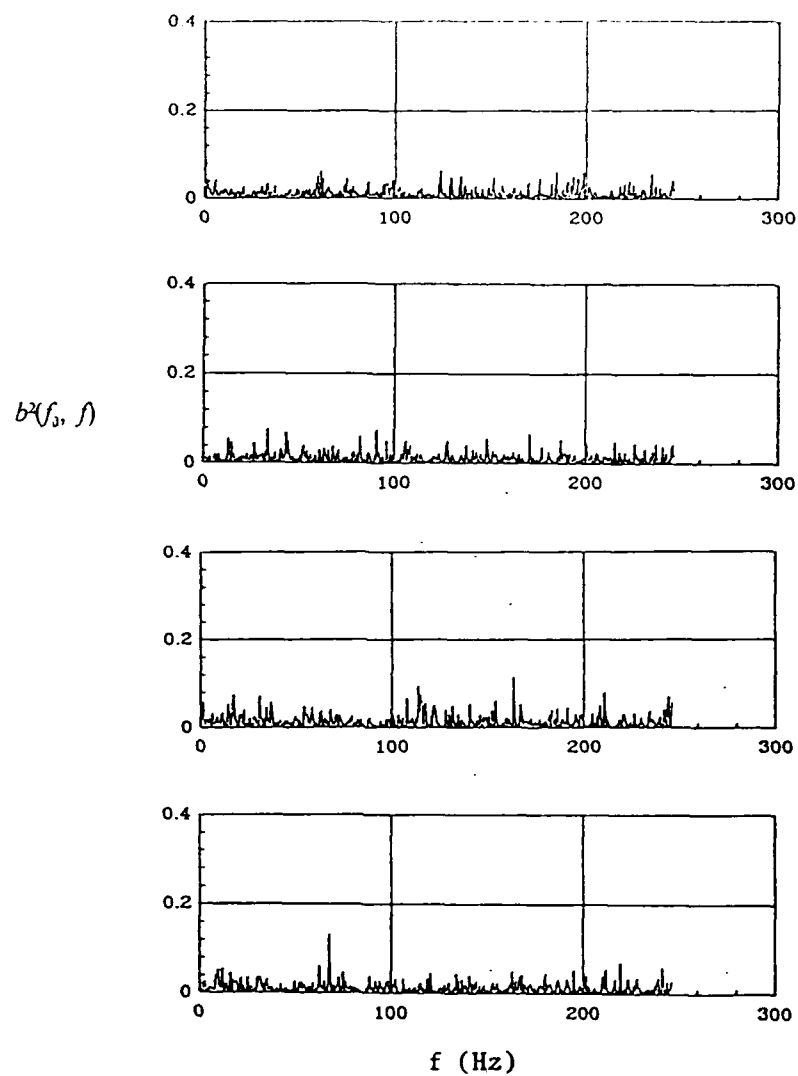
Figure 29   Bicoherence $b^2(f_0, f)$ of temperature in a slightly heated jet with S=0.95, q=1.26 mmH_2O at x/H=2.0 ,2.5, 3.0, and 4.0 and corresponding y/H, being the same as in Figure 28. f_0 is the dominant frequency found in the hot jet.

68
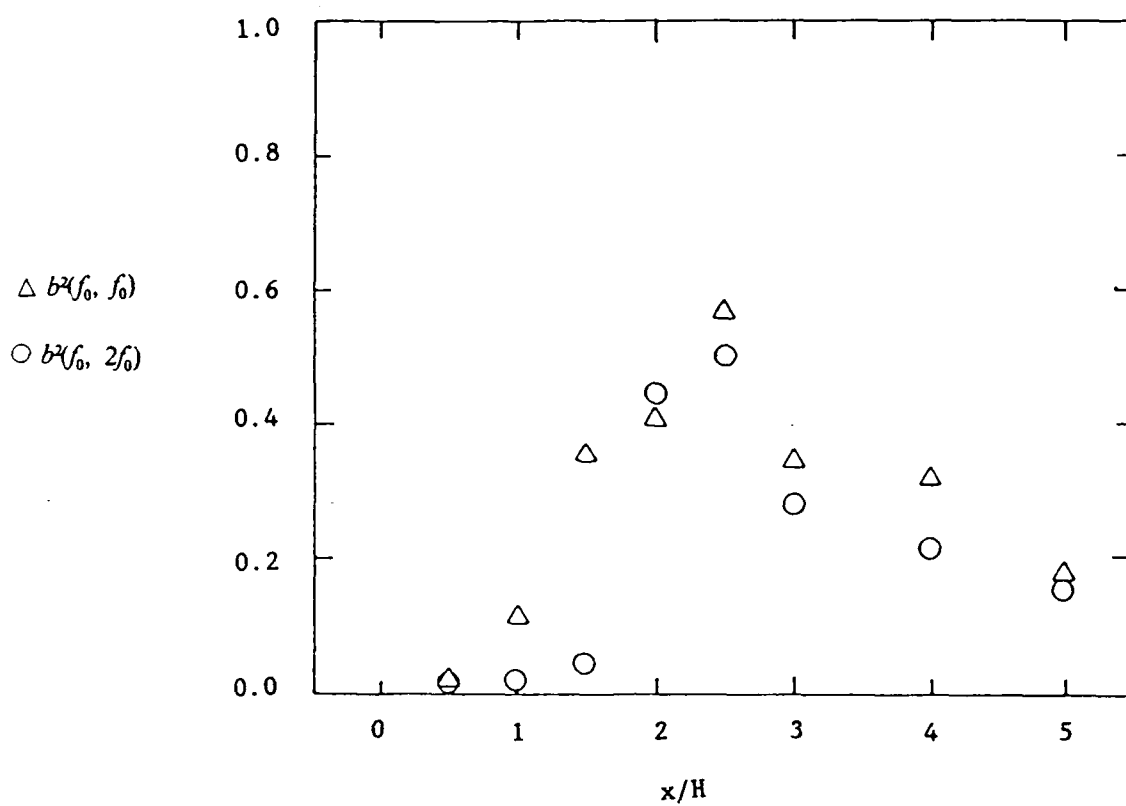
Figure 30 $b^2(f_0, f_0)$, $b^2(f_0, 2f_0)$ vs x/H of the hot jet with S=0.77 and q = $1.26mmH_2O$, $\triangle$ $b^2(f_0, f_0)$, $\bigcirc$ $b^2(f_0, 2f_0)$.
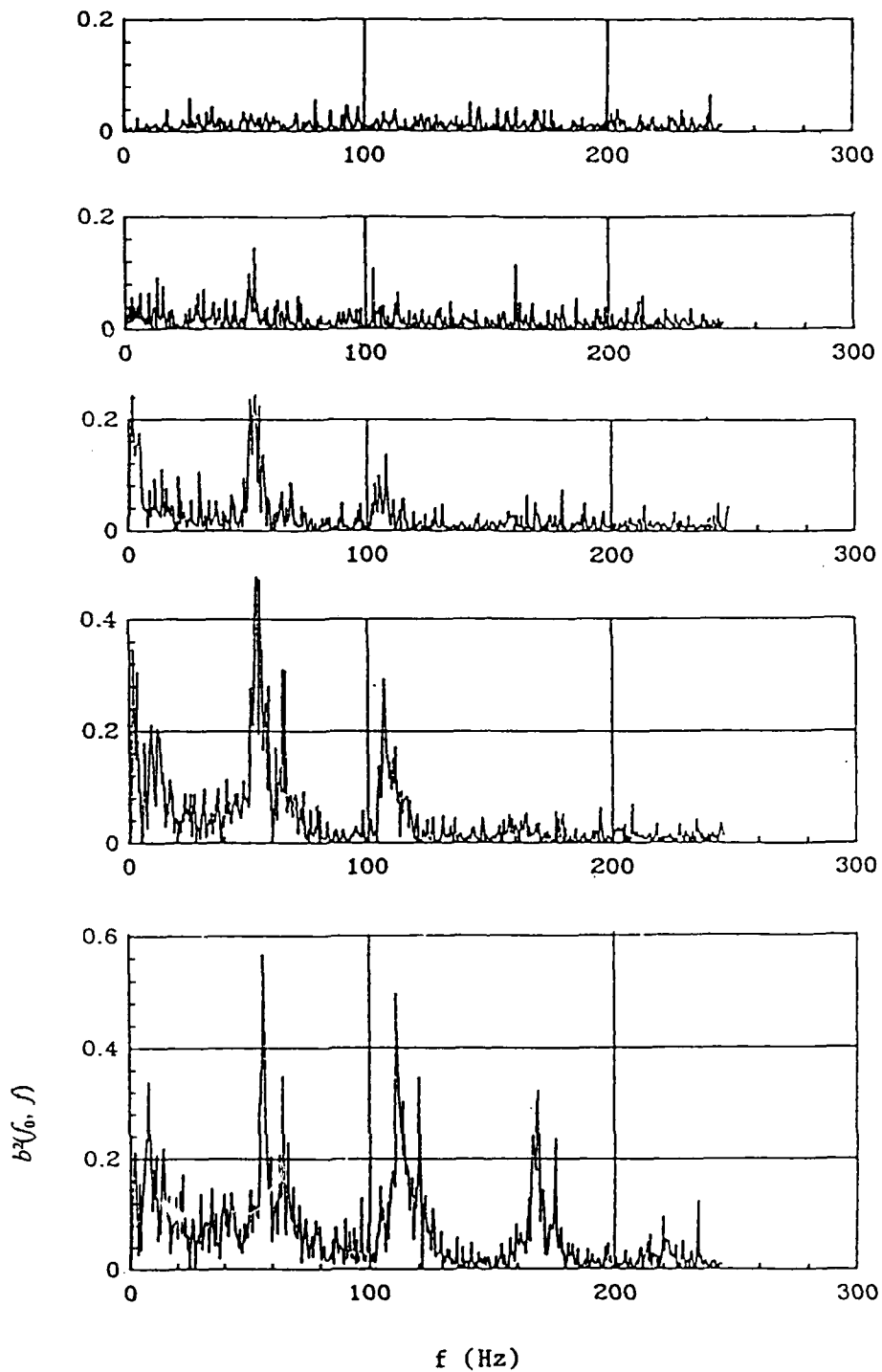
Figure 31 $b^2(f_0, f)$ of the temperature disturbance at x/H =2.5 y/H=0.87.
Jet with q=1.26 mmH_2O and, from bottom to top, S=0.77,
0.86, 0.87, 0.89 and 0.92.
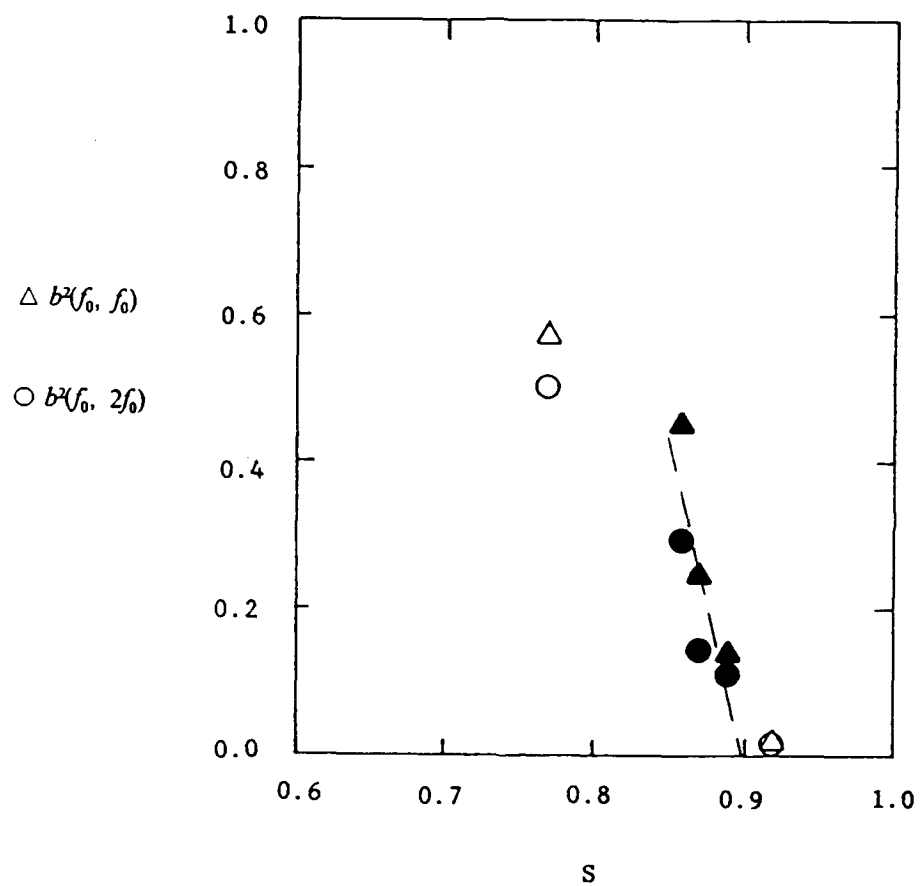
Figure 32 $b^2(f_0, 2f_0)$, $b^2(f_0, f_0)$ vs density ratio S, △ $b^2(f_0, f_0)$, ○ $b^2(f_0, 2f_0)$. — — : least square fit through solid symbols. x/H=2.5, y/H=0.87.
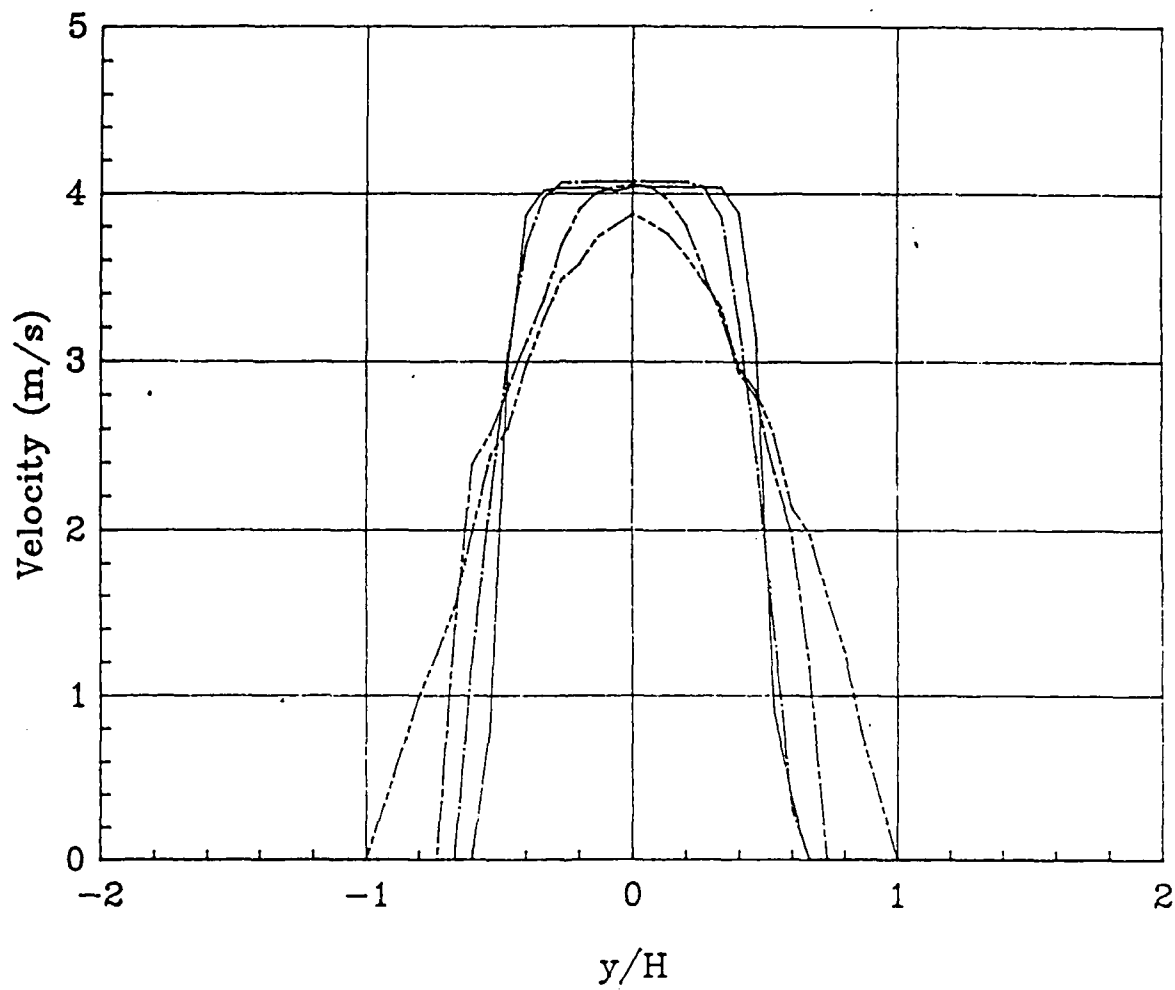
Figure 33   Mean velocity profiles of the heated jet with S=0.78 for
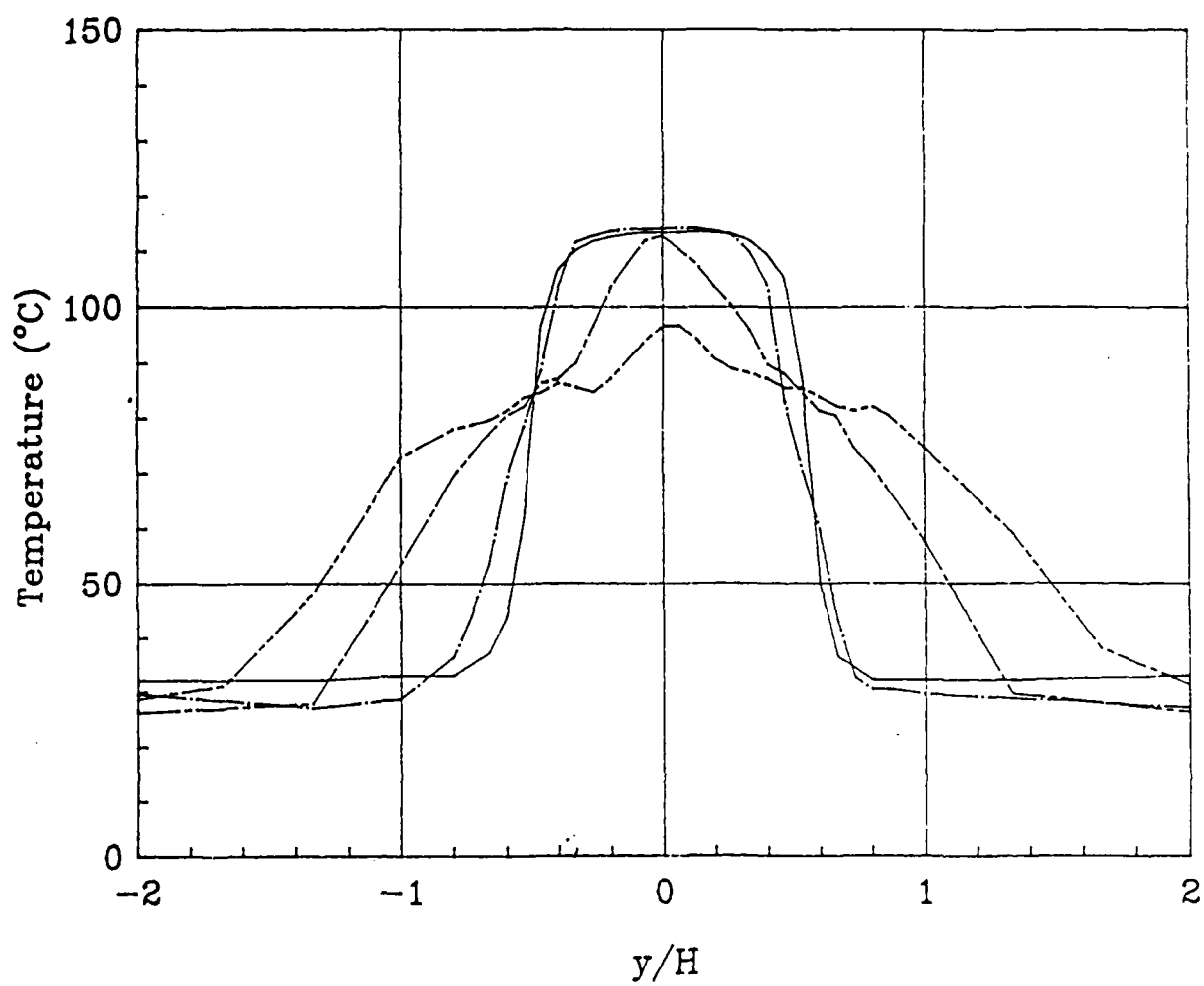q=0.75mmH₂O , at x/H=0,2,4,6

Figure 34   Mean temperature profiles of the heated jet with S=0.76
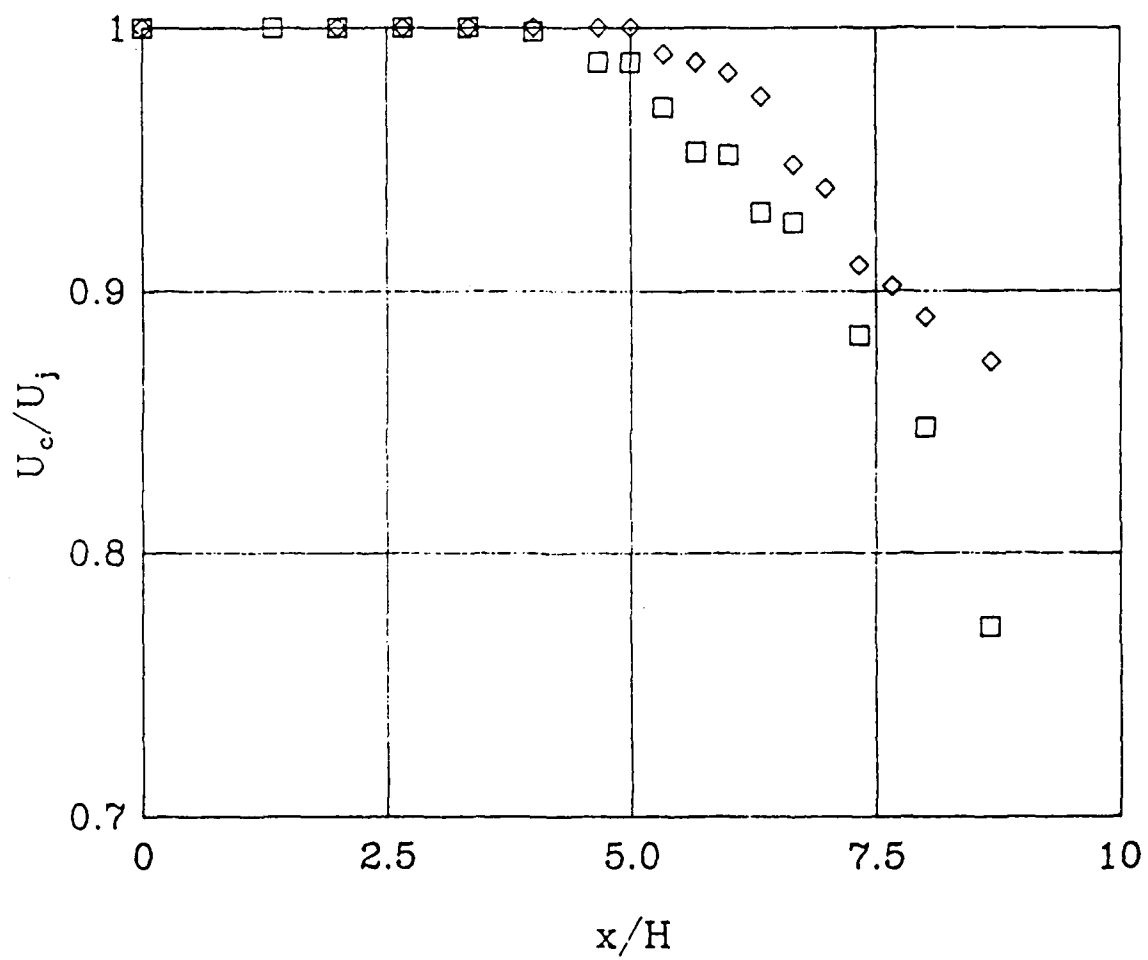   for q=0.75mmH₂O , at x/H=0,2,4,6

73

Figure 35   Centerline velocity versus x/H for S=1 and S= 0.78 at
$R_e = 3000$

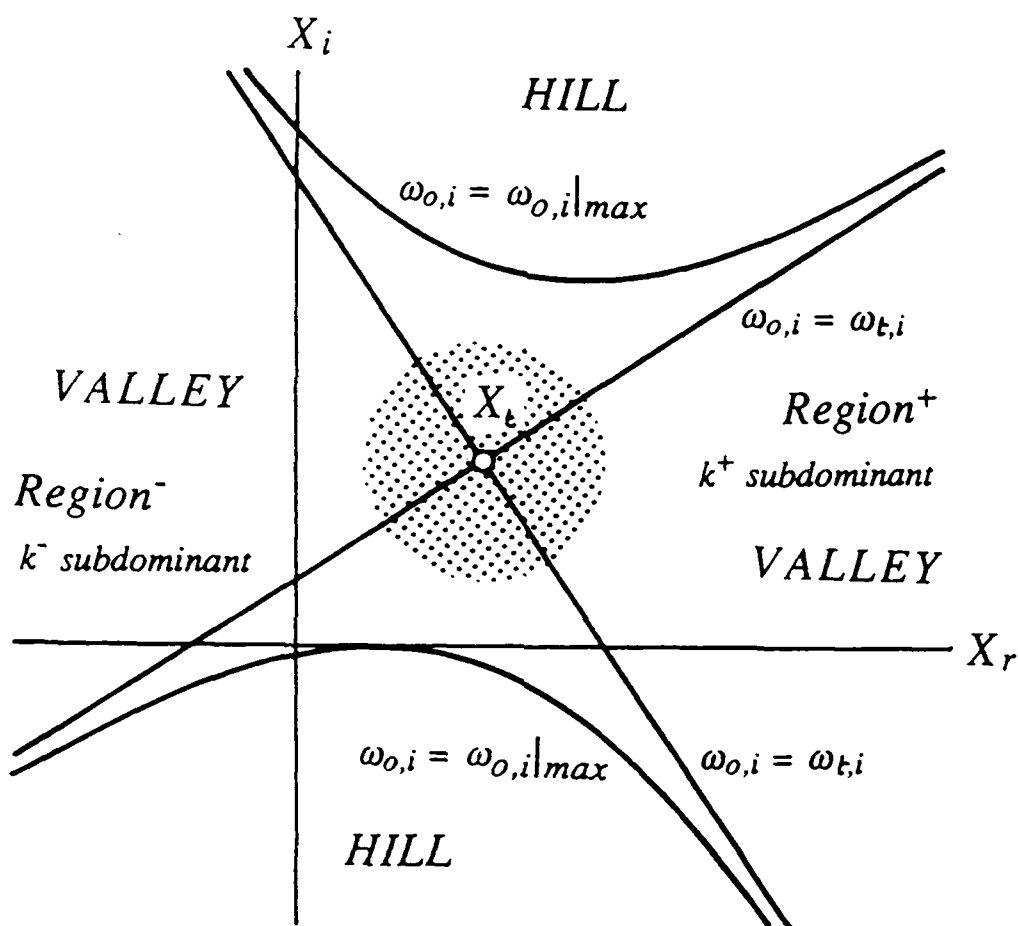Figure 36. Sketch of different regions in the complex X-plane. The curves represent contours $\omega_{o,i}(X)=$const in the vicinity of the saddle point X_t, with $\omega_{o,i}|_{max}$ denoting the maximum absolute growth rate on the real (physical) X-axis. Shaded area denotes the inner turning point region.